CHAPTER 1

Structural–Functional Relationships in the Kidney

Wilhelm Kriz • Astrid Weins • Ruth Ellen Bulger

STRUCTURE–FUNCTION CORRELATIONS ALONG THE RENAL STRUCTURE

The kidney functions as it does, in large part, because of its architecture. In no instance is this more evident than in the urinary concentrating mechanism, where the complex nephron and vascular interrelationships permit the coordinated function of different nephron and vascular elements into countercurrent multiplication and exchange processes. A recent proliferation of detailed structural, biochemical, and functional information has led to an appreciation of other structural–functional relationships that are relevant to solute and water handling by the kidney. Moreover, it has become evident that an understanding of the pathologic developments in kidney diseases is only possible on the basis of a thorough knowledge of kidney structure.

The purpose of this chapter is to review some of the recent findings, with special emphasis on structural–functional relationships, to enhance our understanding of overall renal function; therefore, this chapter is divided into two parts. The first part considers the structural and functional interrelationships of each morphologic segment of the urinary tubule, stressing the unique characteristics of each segment. The second part discusses structure and function in terms of more general mechanisms used by several segments of the renal tubule to accomplish specific functions, such as ion or water transport.

FORM OF THE HUMAN KIDNEY

Human kidneys are paired, bean-shaped organs situated in a retroperitoneal position on the posterior aspect of the abdominal cavity, on either side of the vertebral column against the psoas major muscle. A fibrous capsule located within the perirenal adipose tissue and surrounded by perirenal fascia surrounds each kidney. The lateral border of each kidney is convex. The kidneys of an adult man weigh approximately 120 to 170 g each and measure roughly 11 × 6 × 2.5 cm; those of an adult woman weigh slightly less and are somewhat smaller. In both men and women, total kidney mass best correlates with body surface area.

The concave medial margin has a slitlike aperture, called the renal hilum. Branches of the renal artery, vein, nerves, lymphatics, and the expanded pelvis of the ureter pass through the hilum. The hilum communicates with a flattened space within the kidney called the renal sinus. Within this space, the renal pelvis branches into major and minor calyces.

Sections through the kidney reveal the cortex and medulla (Fig. 1.1). The human kidney is a multilobar organ containing 4 to 18 (average, 8) pyramids of medullary substance[1] and is situated so that their bases are adjacent to the cortex. The darker red cortical substance covers the base of each medullary pyramid like the cap of an acorn. During fetal life, the kidney surface is demarcated by clefts that gradually disappear in the normal adult kidney. The apex of each medullary pyramid (called the papilla) extends into the renal sinus and is capped by a funnel-shaped, minor calyx. The minor calyces receive the urine that is released from the kidney into the extrarenal collecting system. A lobe of the kidney is composed of the conical medullary pyramid and the surrounding cortical substance. During fetal development, some lobes may fuse and calyces are remodeled so that the mature kidney has fewer calyces and papillae than the original number of papilla anlagen[1]; one calyx may drain a fused papilla developed from up to four anlagen, predominantly at the kidney poles. Striated elements called medullary rays extend peripherally at intervals from the bases of the medullary pyramids and penetrate into the cortex. These rays resemble the medulla in structure and although they extend deeply into the cortex, they are part of the cortex. The rest of the cortex is called the cortical labyrinth.

The medulla can be subdivided further either grossly or microscopically (Fig. 1.2). The medulla has an outer zone that is adjacent to the cortex and an inner zone that includes the papilla. The outer zone is subdivided into an inner and outer stripe. This zonation is important because it represents the location and orientation of the various segments of the renal tubules within the kidney.

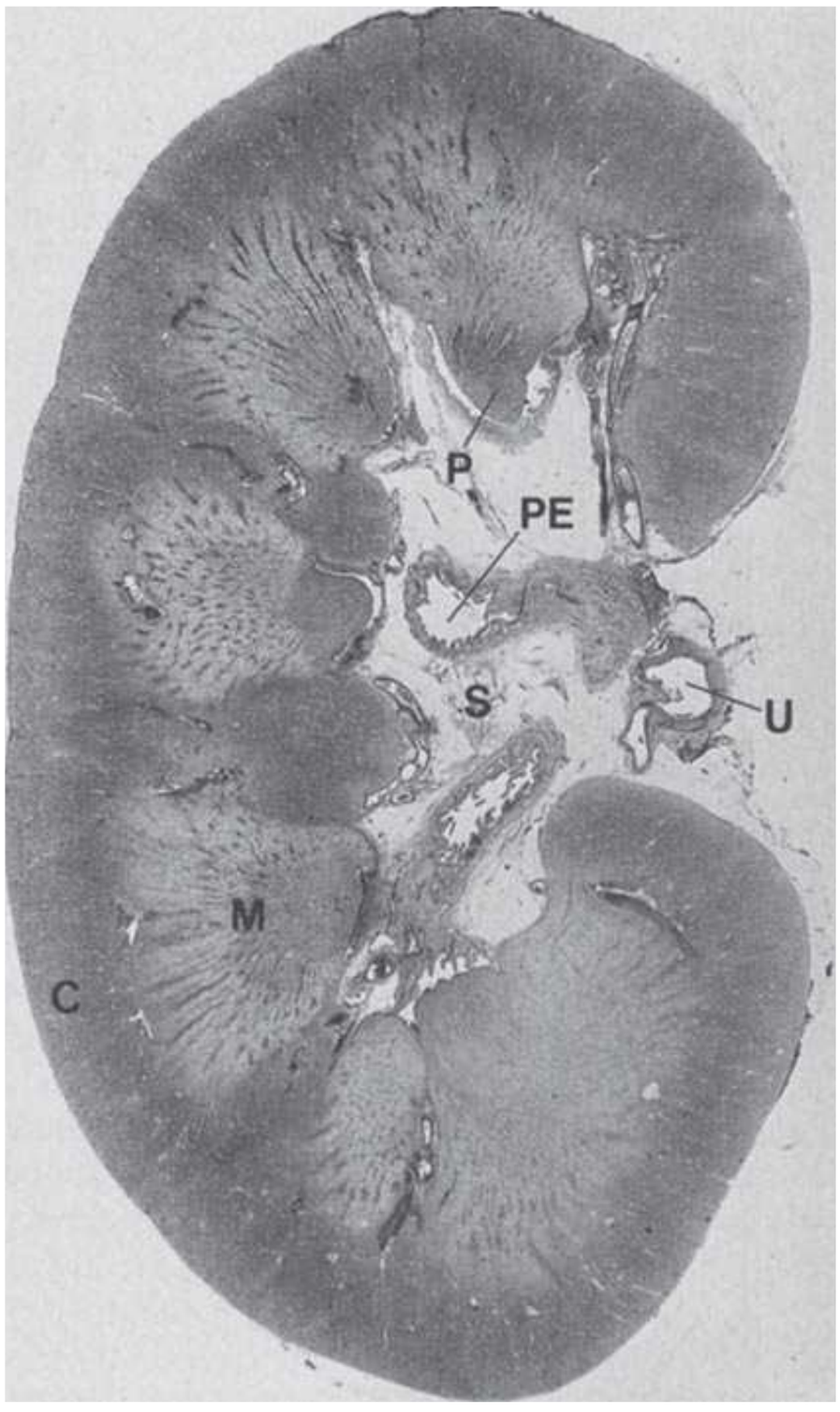

FIGURE 1.1 Gross anatomic appearance of a human kidney. A paraffin section through the whole kidney shows elements of the internal structure: *C*, cortex; *M*, medulla; *P*, papilla projecting into a minor renal calyx; *PE*, pelvis; *S*, sinus; *U*, ureter.

The relative volumes occupied by the cortex, outer medulla, and inner medulla are 70%, 27%, and 3%, respectively,[2] in humans. The relative thicknesses vary considerably among mammalian species.

RENAL (URINIFEROUS) TUBULES

Human renal morphology resulted from a long evolutionary process in which animals adapted to many changing environmental conditions. The three sequential types of kidneys that evolved were the pronephros, mesonephros, and metanephros. The urogenital system of each human embryo repeats this evolutionary process. The pronephros develops first, but degenerates before attaining any functional capacity.

The mesonephric kidney functions for a short period in utero, but it also degenerates, with the notable exception of the part of the mesonephric tubules that form a portion of the excurrent duct system of the male reproductive tract. The metanephric kidney forms last and eventually becomes the functional kidney of the human. The metanephric kidney is well suited to the human condition because of its efficient filtering device and its complex tubule, which allows for the production of not only dilute urine but also concentrated urine. This process occurs only in mammals and birds. Although it is well suited for maintaining homeostasis, the mammalian kidney is an inefficient organ for the elimination of salt and water. In humans, 180 L of fluid are filtered into the tubular lumen every 24 hours, of which approximately 178 L must be returned to the blood.

Each human kidney contains approximately 1 million functional units, called nephrons (with considerable interindividual variation).[3] Each nephron is made up of a renal corpuscle (glomerulus) and a complex tubular portion, which drain into a unifying tubular system called the collecting duct system. Both kinds of tubules represent the renal (or uriniferous) tubules.

The nephrons are derived from the metanephric blastema, the collecting ducts from the urethral bud. A connecting tubule lies between the nephron and collecting ducts. At present, there is controversy as to whether the connecting tubule is derived from the metanephric blastema[4–6] or the ureteric bud.[7] As is discussed in the next section, the connecting tubule has marked morphologic similarities to the cortical collecting duct (CCD).

The segmentation of the renal tubule then includes the following regions.[8]

The Nephron

I. Renal corpuscle (most of which is called glomerulus)
- A. Bowman's capsule
- B. Glomerular tuft

II. Proximal tubule
- A. Convoluted part (pars convoluta) consists of P_1 and the first part of P_2 (PCT)
- B. Straight part (pars recta) consists of the last part of P_2 and all of P_3 (PST)

III. Thin limbs of the loop of Henle (intermediate tubule)
- A. Thin descending part of short-looped nephrons (SDTL)
- B. Upper thin descending part of long-looped nephrons (LDTL up)
- C. Lower thin descending part of long-looped nephrons (LDTL lp)
- D. Ascending thin part of long-looped nephrons (ATL)

IV. Distal tubule
- A. Straight part (pars recta)
  1. Medullary thick ascending limb (MTAL), which includes regions located within the inner stripe and outer stripe of the medulla
  2. Cortical thick ascending limb (CTAL), which includes the part ascending through the cortex, the macula densa (MD), and the post macula densa segment
- B. Convoluted part (pars convoluta) (DCT)

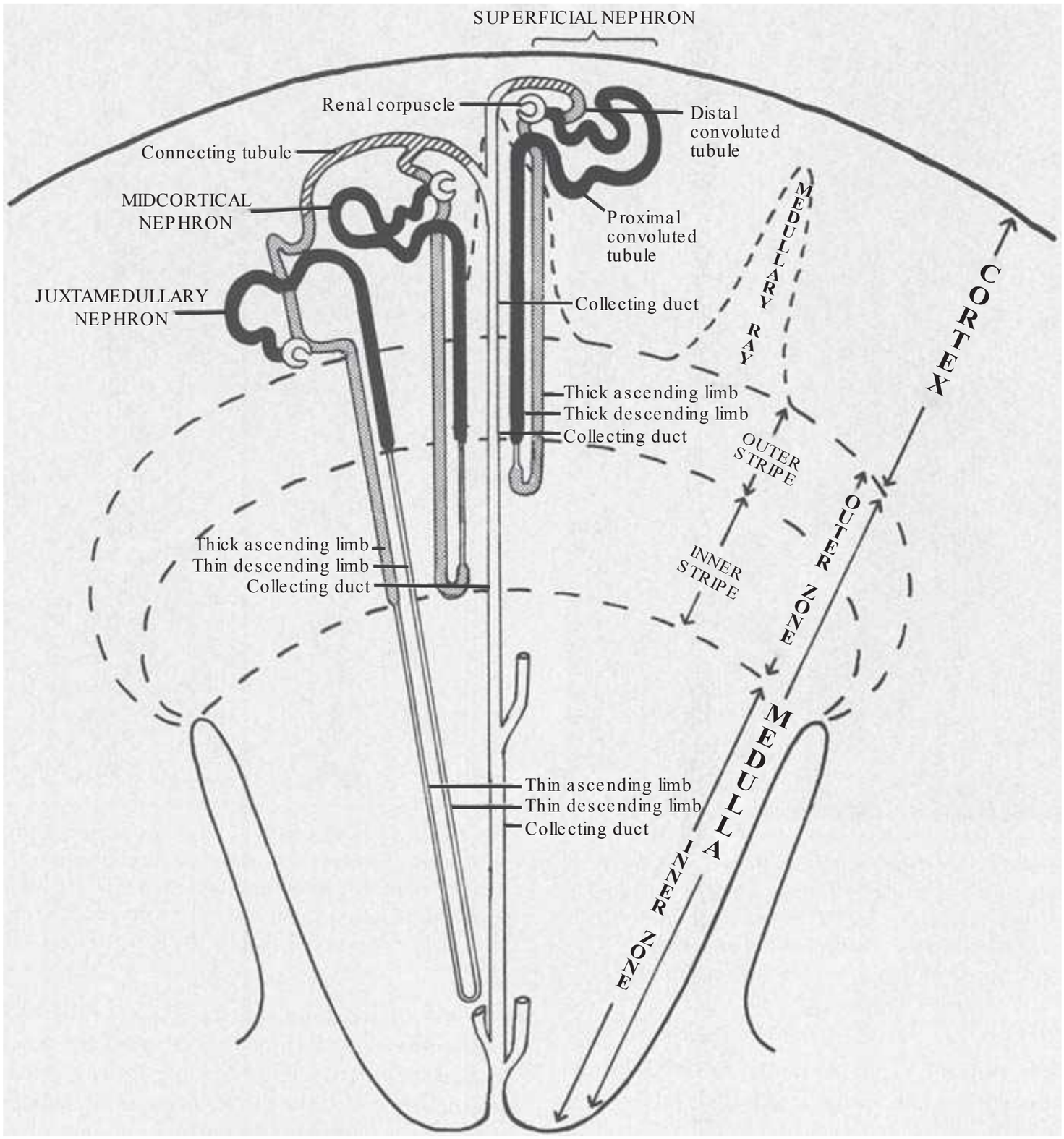

FIGURE 1.2 The relationship of nephron segments to zones of the kidney.

The Collecting Duct System

I. Connecting tubule (CNT)
II. Cortical collecting duct (or tubule) (CCD)
III. Outer medullary-collecting duct (or tubule) (OMCD)
IV. Inner medullary-collecting duct (or tubule) including the papillary collecting ducts (also called the ducts of Bellini; IMCD)

Nephrons lie in characteristic positions (Fig. 1.2), with the renal corpuscles and proximal convoluted segments in the cortex (Figs. 1.3 and 1.4). The straight part of the proximal tubule, the thin limb segments, and the straight part of the distal tubule form the loop of Henle, which enters a medullary ray of the cortex and extends into the medulla, where it bends, returning to the cortex by means of the same medullary ray. The loops of juxtamedullary nephrons directly connect the outer stripe of the medulla without ever being contained in a medullary ray. As the straight part of the distal tubule returns to the cortex, it passes by the renal corpuscle from which the nephron originated, forming the macula densa; then, after a short postmacula densa segment, it continues as the distal convoluted tubule within the cortex.

The morphology of the nephron varies with the position of the renal corpuscle in the cortex. Each nephron is classified as superficial, midcortical, or juxtamedullary, according to the position of its renal corpuscle within the respective regions of the cortex (Fig. 1.2) and the pattern of efferent vessel formation.[9–11] A given segment tends to occupy a specific region of the kidney, which gives rise to the gross zonation referred to in the preceding text. In the human kidney, superficial nephrons empty singly into a terminal collecting duct, whereas several juxtamedullary nephrons empty into an arched tubular portion (arcade) that courses peripherally in the cortex before it turns to enter a medullary ray. Most midcortical nephrons from humans empty individually as well.[5,12] As known from the study of several species (rats and rabbits), an arcade is established by the connecting tubule epithelium (data from studies in humans are not available).

Nephrons also are classified as short or long looped according to the location of the position where their loops of Henle turn within the kidney. Short-looped nephrons arise from renal corpuscles located in superficial and midcortical regions and have loops of Henle that turn within the outer medulla. In humans, some superficial nephrons may have loops within the cortex itself. Short-looped nephrons have

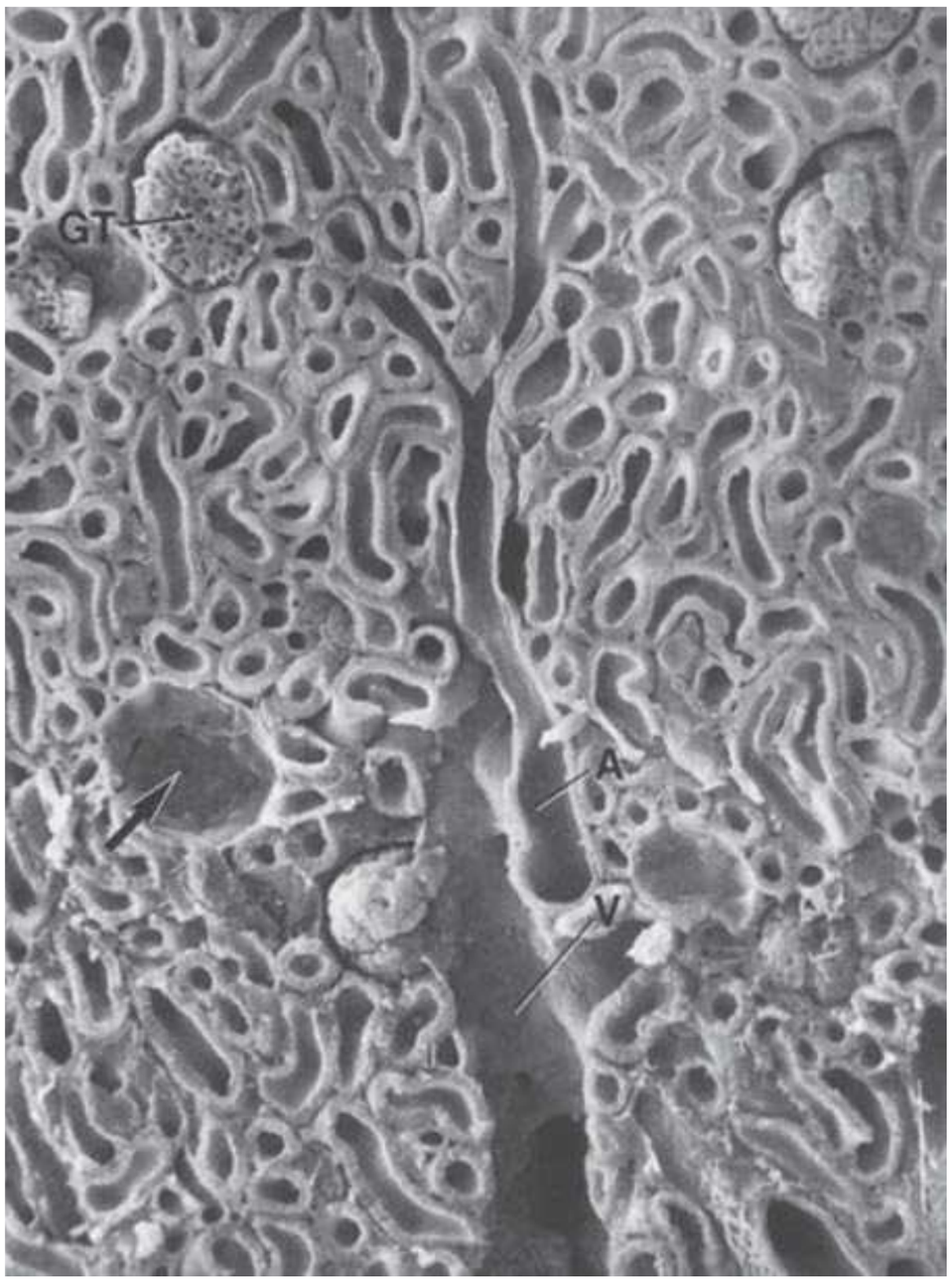

FIGURE 1.3 Scanning electron micrograph of the cortex. Convoluted tubules are shown, along with renal corpuscles, some of which contain a glomerular tuft (*GT*) and some from which the tuft is removed (*arrow*). A cortical radial artery (*A*) and vein (*V*) are also apparent. Note the thin wall of the vein. (Magnification ×140.)

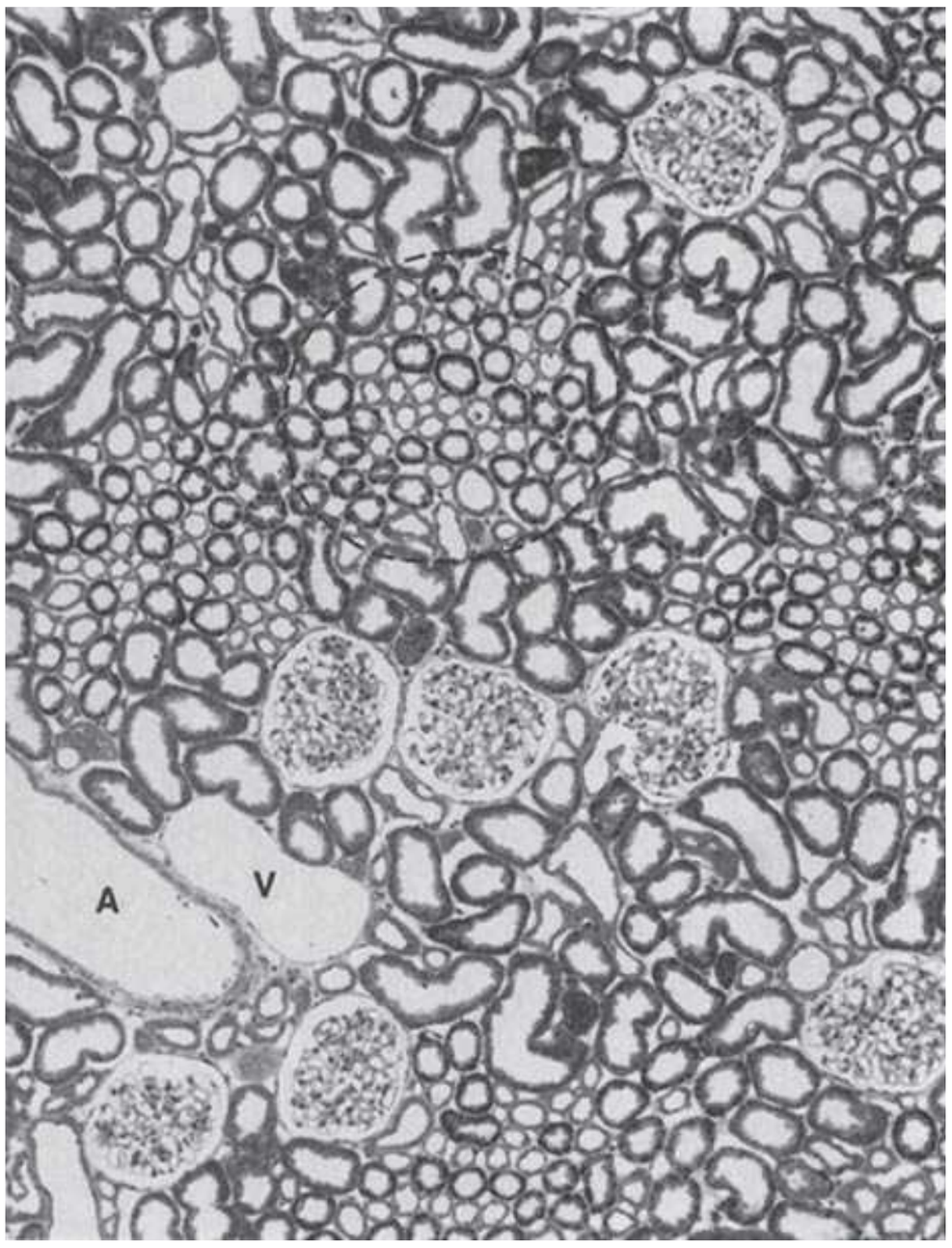

FIGURE 1.4 Light micrograph of renal cortex (rat). Cortical radial vessels (*A*, artery; *V*, vein), glomeruli, and convoluted tubules make up the cortical labyrinth. The straight tubular portions are found in the medullary rays of the cortex (one medullary ray is delineated by the *hatched line*). (Magnification ×80.)

short, thin limb segments that occur only along the descending limb. Long-looped nephrons have loops of Henle that turn within the inner medulla and have thin limb segments in both descending and ascending limbs. Although most species have both long- and short-looped nephrons, some species, such as dogs and cats, have only long ones,[13] whereas other species, such as beavers, have only short ones.[14,15] In human kidneys, the ratio of short- to long-looped nephrons is 6:1 to 7:1.

THE RENAL CORPUSCLE

The renal corpuscle (first segment of the nephron) is the site at which an ultrafiltrate of the blood is produced (Fig. 1.5). The filtrate moves from the capillary lumen into Bowman's space. This flow is influenced by the following factors: renal blood flow; the oncotic and hydrostatic pressures in the capillaries and in Bowman's space; the size, shape, and charge of plasma molecules; and the various morphologic components of the wall separating the capillary lumen from Bowman's space. The filtrate contains only barely detectable quantities of plasma proteins.[16] The filtration barrier increasingly restricts the passage of larger molecules, with very little filtration of molecules larger than albumin (70 kDa).[17]

The renal corpuscle consists of Bowman's capsule and the glomerular tuft. The latter is made up of capillaries, derived from the afferent arteriole, their supporting cells, and an envelope consisting of the glomerular basement membrane (GBM) and the visceral (podocyte) layer of Bowman's capsule (Fig. 1.5). At the vascular pole, the visceral epithelium becomes the parietal epithelium, which then transforms into the proximal tubule epithelium at the urinary pole (Fig. 1.5). The space between both layers is the urinary space (Bowman's space).

The human renal corpuscle is roughly ovoid and approximately 150 to 240 μm in diameter. The term glomerulus is widely used to refer to the entire renal corpuscle. The renal corpuscle without the parietal epithelial cells is referred to as the glomerular tuft. The afferent arteriole enters the renal corpuscle at the vascular pole, where it divides into several primary branches that each ramify to form a network of anastomosing capillaries, called a lobule. The lobule has a supporting region called the mesangium (Figs. 1.6 and 1.7). All lobules together establish the tuft; the converging mesangial regions are called the glomerular stalk, by which the tuft is connected to the extraglomerular mesangium (see Juxtaglomerular Apparatus). The capillaries coalesce toward the center of the capillary tuft to form

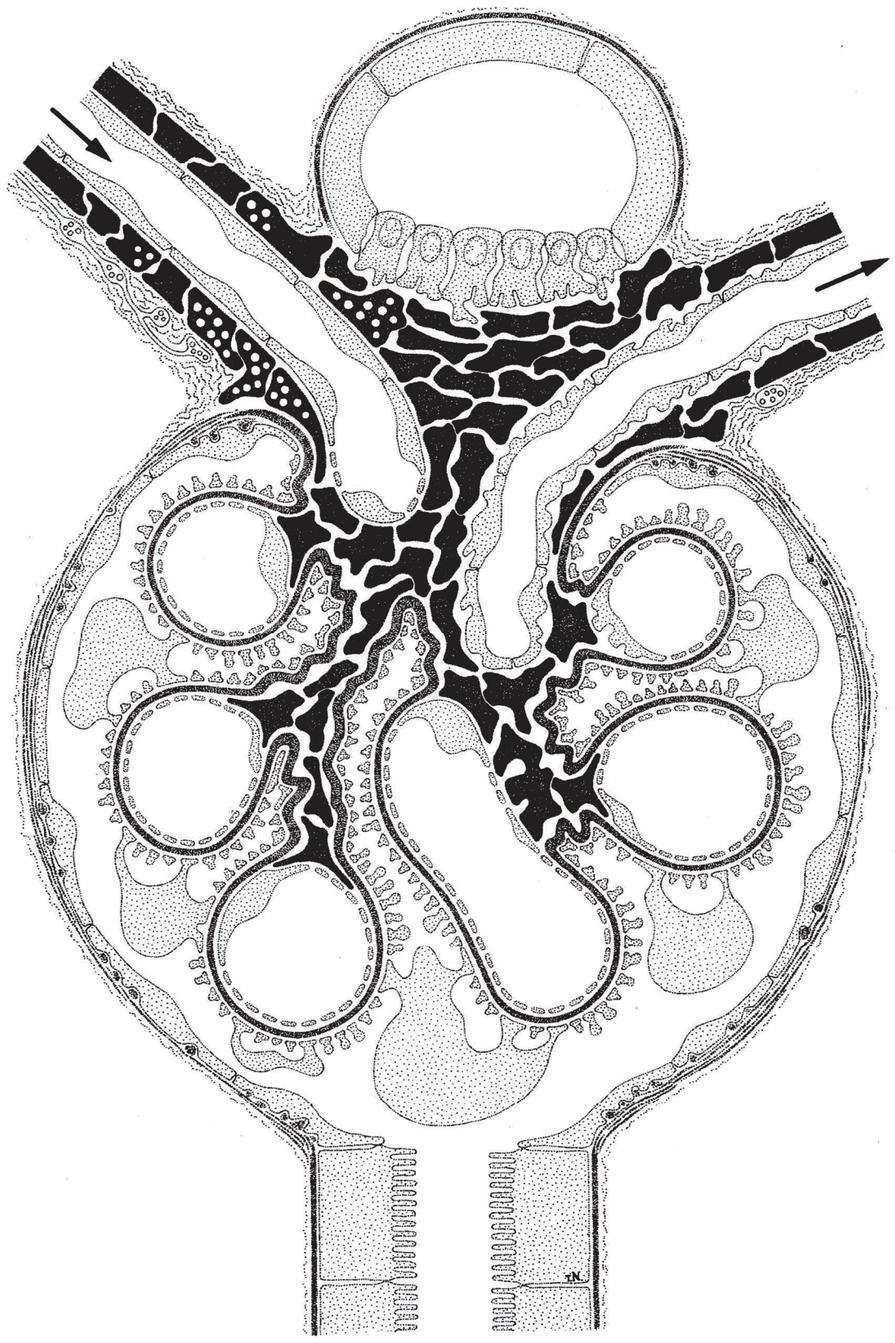

FIGURE 1.5 Schematic of a longitudinal section through a glomerulus and juxtaglomerular apparatus (*JGA*). The direction of blood flow in the glomerular arterioles is indicated by arrows. The capillary network, together with the mesangium, is enclosed in a common compartment bounded by the glomerular basement membrane (*GBM*) (shown in *dark gray*). The outer aspect of the GBM is covered by the glomerular visceral epithelium (podocytes). Note that there is no basement membrane at the interface between the capillary endothelium and the mesangium. At the vascular pole, the visceral epithelium, together with the GBM, is reflected into the parietal epithelium of Bowman's capsule, which, at the urinary pole, passes over into the epithelium of the proximal tubule. The JGA consists of the macula densa of the distal tubule, the extraglomerular mesangium (which is continuous between both arterioles and continues via the glomerular stalk into the intraglomerular mesangium), and the granular cells within the afferent arterioles. All cells that have been suggested to be of smooth muscle origin are shown in black. Note the sympathetic nerve terminals at the afferent arteriole. (From Kriz W, Sakai T, Hosser H. Morphological aspects of glomerular function. In: Davison AM, ed. *Nephrology*, Vol. 1. Proceedings of X International Congress of Nephrology, London, 1987. London: Bailliere Tindall; 1988:3, with permission.)

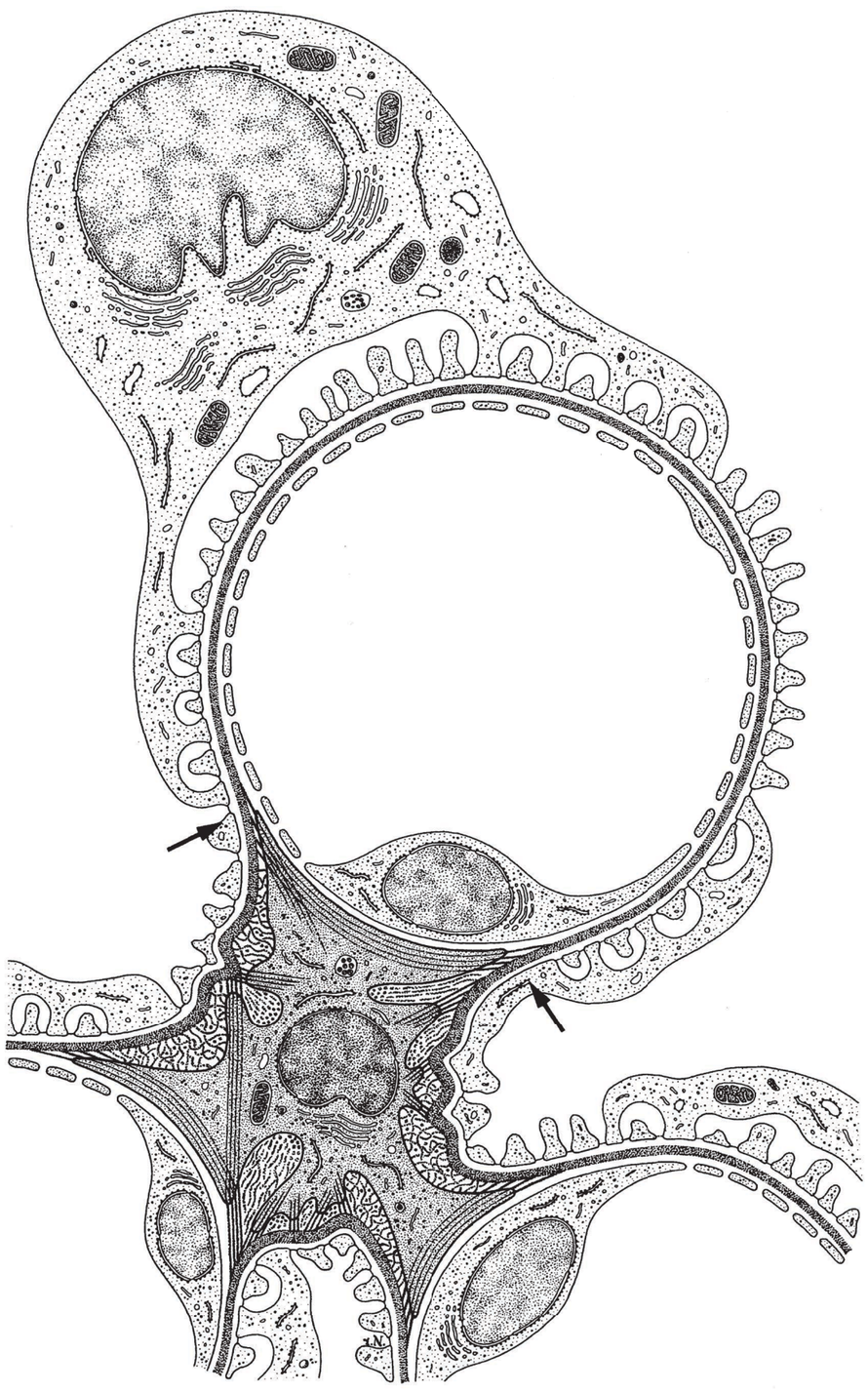

FIGURE 1.6 Schematic of a cross-section of a glomerular capillary and its relationships to the mesangium. The capillary is made up of a fenestrated epithelium. The peripheral part of the endothelium tubule is surrounded by the glomerular basement membrane (GBM; shown in *dark gray*), which, at mesangial angles (*arrows*), deviates from a pericapillary course and covers the mesangium. The outer aspect of the GBM is covered by the interdigitating pattern of podocyte foot processes. In the center, a mesangial cell is shown; its many processes contain microfilament bundles and extend toward the GBM, to which they are connected. The mesangial matrix contains an interwoven network of microfibrils. (From Venkatachalam MA, Kriz W. Anatomy of the kidney. In: Heptinstall R, ed. *Pathology of the Kidney*, 4th ed. Boston: Little, Brown; 1991, with permission.)

the efferent arteriole, which runs through the stalk and exits from the vascular pole. The efferent arteriole again breaks up to form a second capillary network, which surrounds the tubules and is called the peritubular capillary network.

The renal corpuscle, therefore, consists of the following parts: (a) the parietal epithelium, (b) the visceral epithelium (podocytes), (c) the endothelial cells lining the capillaries, (d) the glomerular basement membrane (GBM), and (e) the intraglomerular mesangial cells and matrix. In the rat, the ratio of the number of endothelial cells to mesangial cells to visceral epithelial cells is 3:2:1.[18]

The Visceral Epithelium of Bowman's Capsule

The visceral epithelial cells (nowadays generally called podocytes) are octopus-shaped cells that reside in Bowman's space and attach to the GBM only by way of their processes (see below). This shape was well described by Zimmermann[19] and is seen to advantage in scanning electron micrographs (SEM) (see later, Fig. 1.10). The exact details of cell shape differ depending

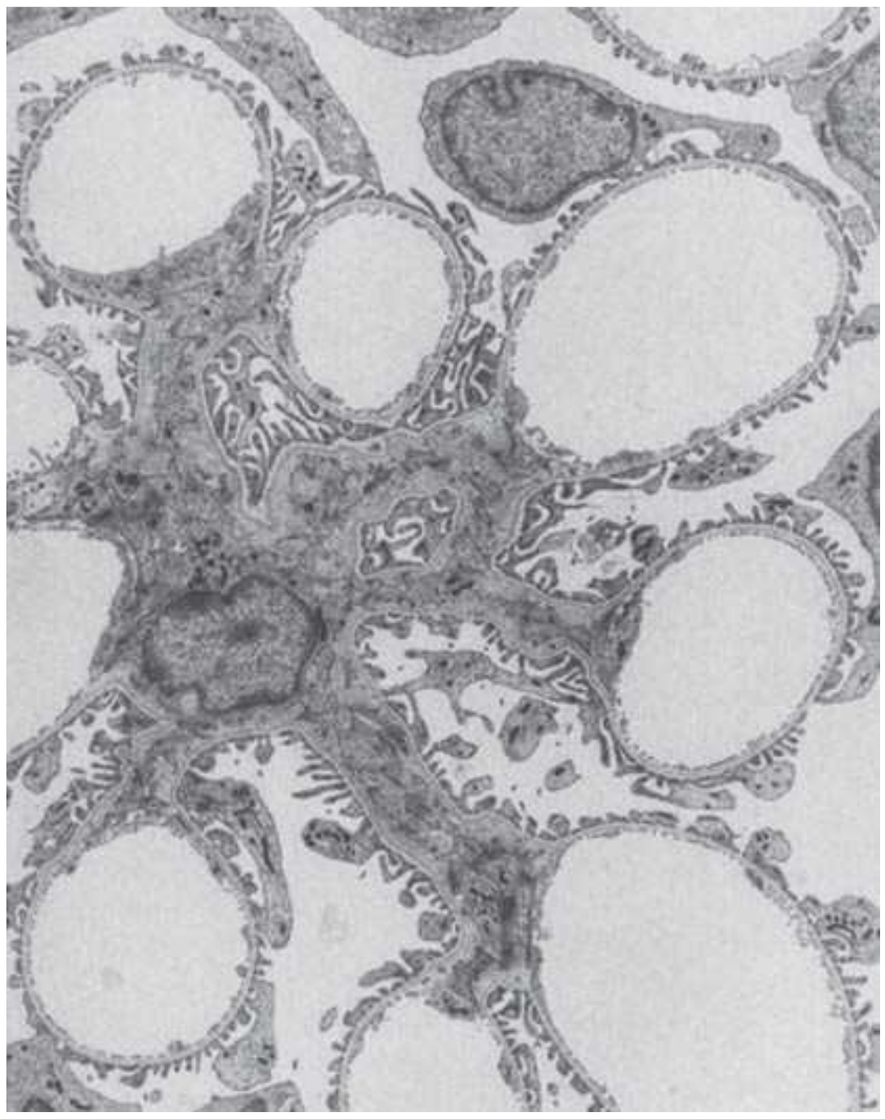

FIGURE 1.7 Transmission electron micrograph of a rat glomerular lobule. Glomerular capillaries and the glomerular mesangium occupy a common compartment enclosed by the glomerular basement membrane (GBM). The mesangial cell body (*in the center*) gives rise to many processes that fill (together with the mesangial matrix) radial arms that extend to the peripherally located capillaries. The outer aspect of the GBM is covered by podocytes. (Magnification ×3,500.)

on the species being studied.[20,21] As a consequence of the high degree of differentiation, podocytes, like neurons, are incapable of regenerative cell replication in the adult. Thus, podocytes that were lost, for any reason, cannot be replaced by new ones.[22–24] On the other hand, in glomerular diseases based on dedifferentiation of podocytes (collapsing glomerulopathy), a vivid proliferation of the dedifferentiated cells accompanies the disease.[25]

Recent observations in parietal epithelial cells question this view. First, it has been proposed that a niche of glomerular epithelial stem cells resides within the parietal epithelium at the transition to the proximal tubule.[26,27] It is an intriguing hypothesis that proliferating stem cells from this locus may transform into podocytes and may reach the tuft via the transitions of the epithelia at the glomerular vascular pole. Migration of parietal cells onto the the vascular pole and subsequent transition into podocytes have been shown to occur in the newborn mouse.[28] However, evidence that such a process may be of any relevance in the adult has so far not been presented.[28] Moreover in the adult mouse, it has been shown that proliferating parietal epithelial cells may reach the glomerular tuft via tuft–capsule bridges; there they replace podocytes causing the collapse of the concerned tuft area obviously by bringing the local cross talk between podocytes and the endocapillary compartment to an end.[29]

The cell bodies give rise to large primary processes that may branch another time, finally splitting apart into terminal processes, called foot processes (as seen from SEM pictures, "finger processes" would be a better word) or pedicels (Figs. 1.6, 1.8 to 1.11, and see Fig. 1.13). The foot processes are anchored within the GBM to a depth of about

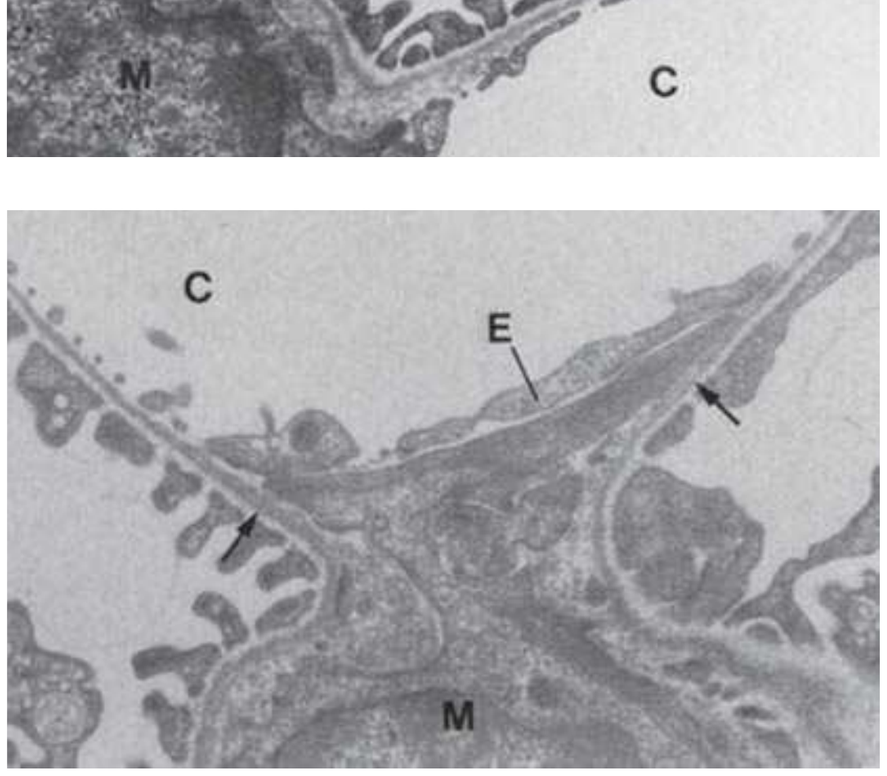

A

B

FIGURE 1.8 Transmission electron micrographs of glomerular capillaries (*C*) and associated mesangium. **A:** A mesangial cell body (*M*) gives rise to cell processes that extend to peripherally located capillaries. Note that there is no basement membrane at the interface between the capillary endothelium and the mesangium. (Magnification × 13,000.) **B:** Capillary mesangium interface. Beneath the endothelium (*E*), tonguelike mesangial cell processes run toward both opposing turning points of the GBM (*arrows*). They contain microfilament bundles that obviously interconnect the GBM of both mesangial angles. (Magnification ×24,000.)

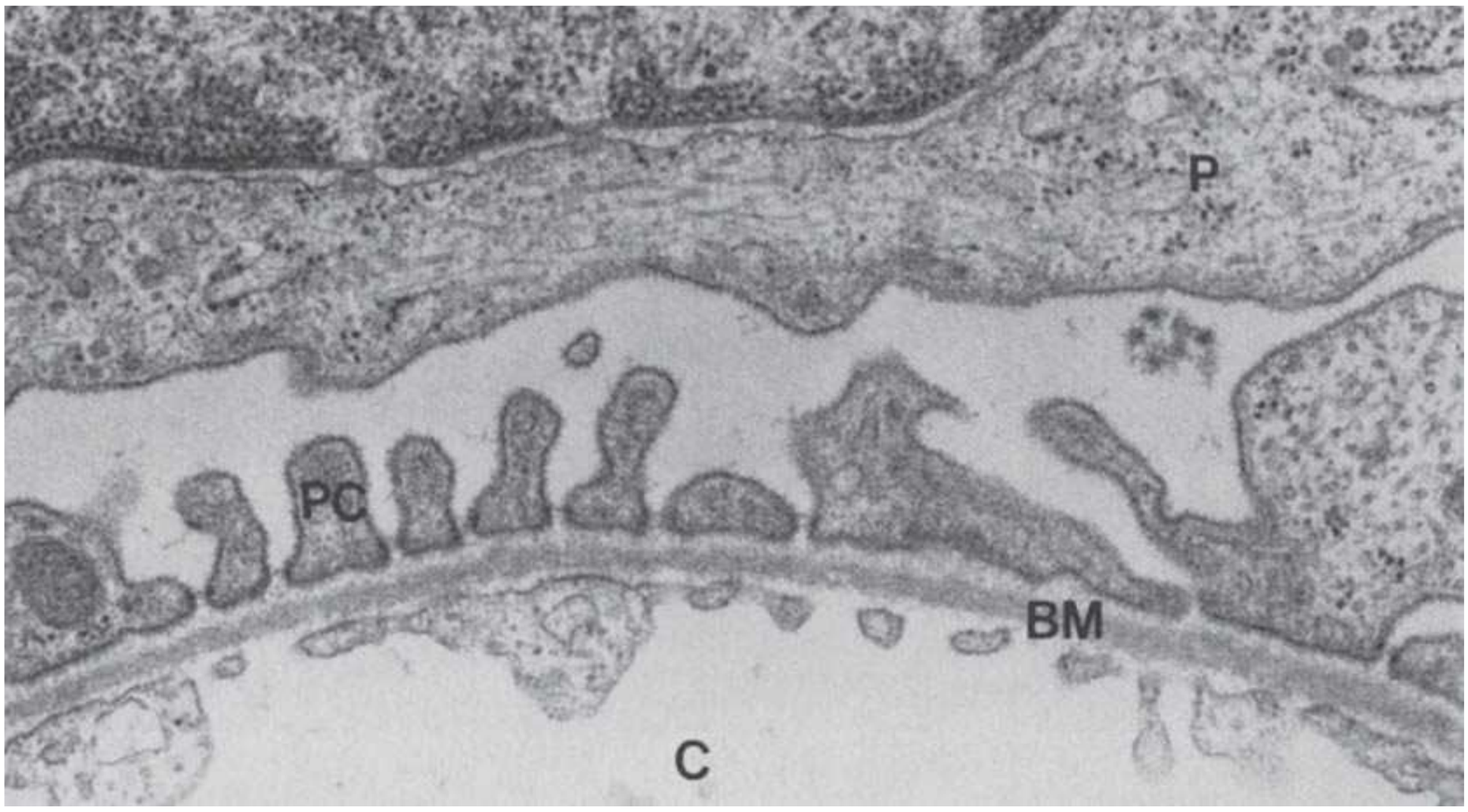

FIGURE 1.9 Transmission electron micrograph showing the podocyte (*P*), pedicels (*PC*) near the basement membrane (*BM*), and the endothelial cells lining the capillary (*C*). (Magnification ×34,000.)

40 to 60 nm. The foot processes interdigitate in a complicated manner with those from adjacent cells to form an elaborate layer of small processes along the glomerular basement membrane. This interdigitation results in the formation of an extensive series of narrow slits between the foot processes, which provide a long extracellular path for filtration of water and solutes (Fig. 1.10). In transmission electron micrographs, these slits are bridged by a layer of extracellular material (4 to 6 nm thick) called the *filtration-slit membrane* (see Figs. 1.9 and 1.13). If tannic acid is added to the fixative solution, a highly ordered isoporous substructure is revealed in en face views of the filtration-slit membrane.[30] Staggered rodlike units project from the podocyte plasmalemma and connect to a central linear bar. These rodlike units delineate rectangular pores 4 × 14 nm within the slit membrane (i.e., which approximate the size of an albumin molecule).

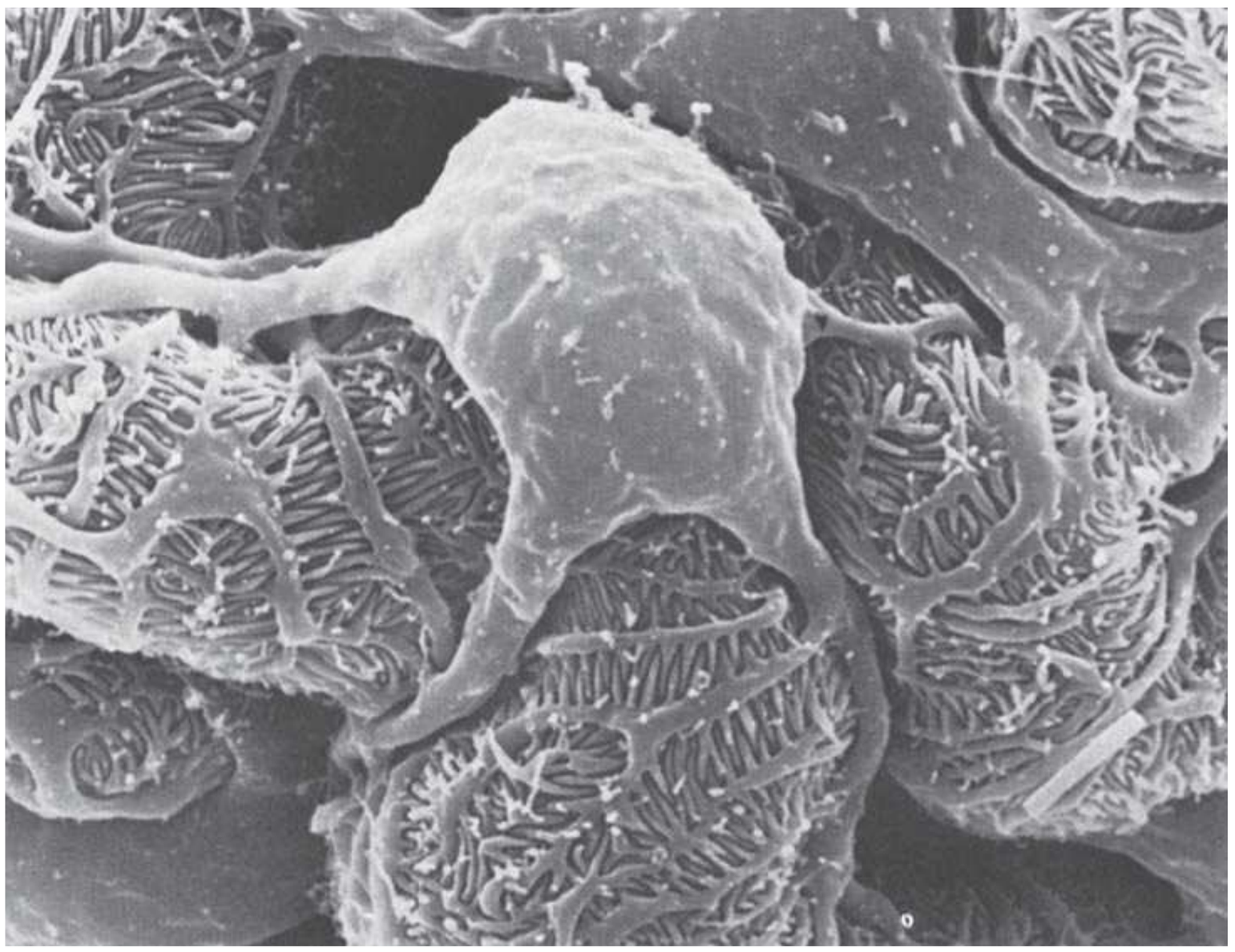

FIGURE 1.10 Scanning electron micrograph showing the elaborate cell shape of rat podocytes. (Magnification ×5,900.)

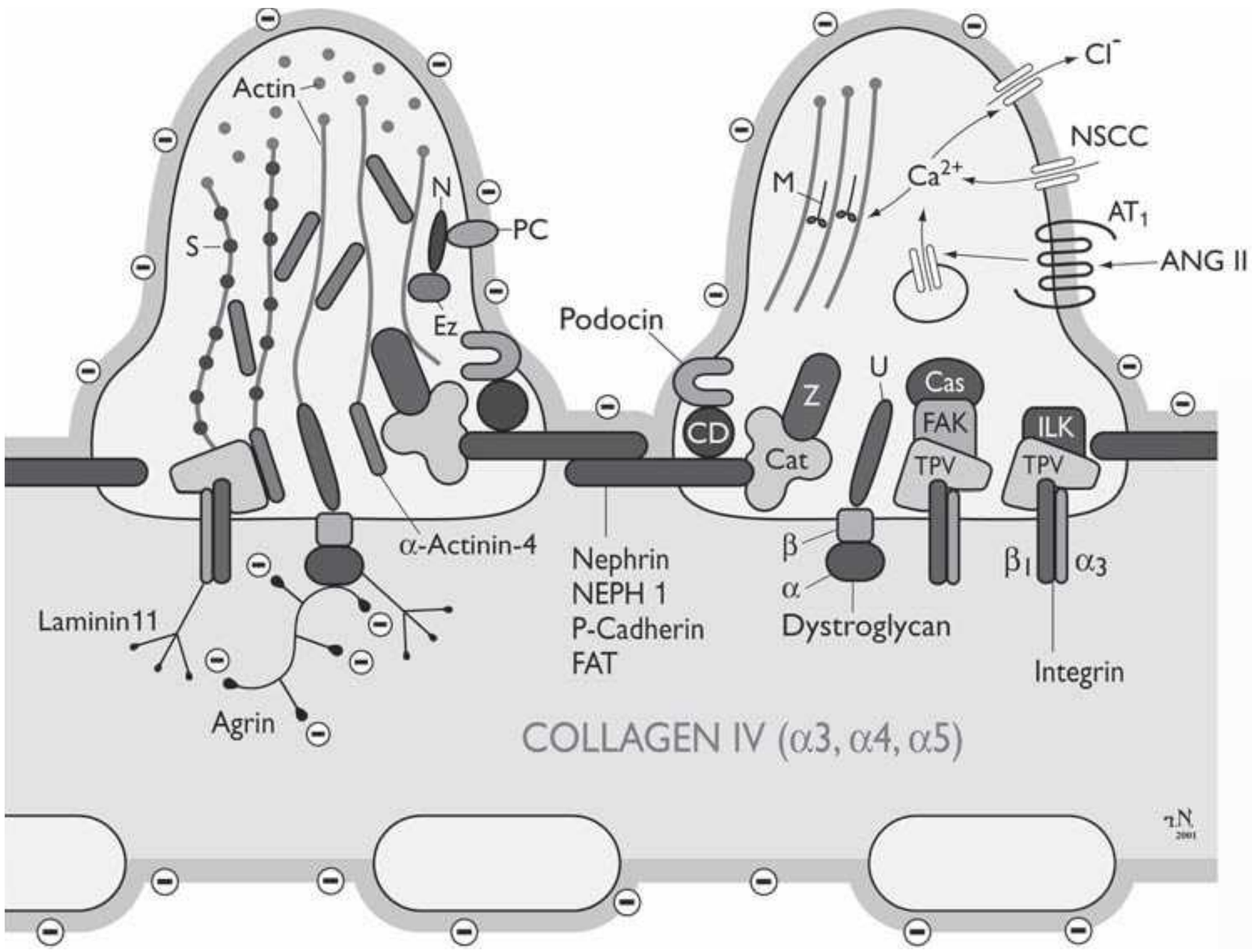

FIGURE 1.11 Schematic drawing of the molecular equipment of podocyte foot processes. *Cas*, p130Cas; *Cat*, catenins; *CD*, CD2-associated protein; *Ez*, ezrin; *FAK*, focal adhesion kinase; *ILK*, integrin-linked kinase; *M*, myosin; *N*, NHERF2; *NSCC*, nonselective cation channel; *PC*, podocalyxin; *S*, synaptopodin; *TPV*, talin-paxilinvinculin; *U*, utrophin; *Z*, ZO-1. See text for further explanations. (From Endlich K, Kriz W, Witzgall R. Update in podocyte biology. *Curr Opin Nephrol Hypertens*. 2001;10:331, with permission.)

Generally, the slit diaphragm is considered as an adherenslike intercellular junction.[31] Intensive research in recent years has uncovered several transmembrane proteins that participate in the formation of the slit membrane (Fig. 1.11)—including P-cadherin,[31] nephrin,[32] Neph1,[33] and FAT.[34] Other molecules, such as ZO1,[35] Podocin,[36] CD2AP,[37] and catenins mediate the connection to the actin cytoskeleton (see below). Nephrin is a member of the immunoglobin superfamily (IgCAM); its gene, NPHS1, has been identified as the gene whose mutations cause congenital nephrotic syndrome of the Finnish type.[32] In addition to its role as a structural component, nephrin acts as a signaling molecule that can activate MAP kinase cascades.[38] Neph1 is considered as a ligand for nephrin. Podocin belongs to the raft-associated stomatin family, whose gene, NPHS2, is mutated in a subgroup of patients with autosomal recessive steroid-resistent nephrotic syndrome.[36] These patients show disease onset in early childhood and rapid progression to end-stage renal failure. Podocin interacts with nephrin and CD2AP.[39] FAT is a novel member of the cadherin superfamily with 34 tandem cadherinlike extracellular repeats and a molecular weight of 516 KDa.[40] Because FAT has a huge extracellular domain, it is speculated that it dominates the molecular structure of the slit membrane[34]; the FAT mutant mouse fails to develop a slit membrane.[41] P-cadherin[31] is thought to mediate with its intracellular domain the linkage to β- and γ-catenin, a complex which then connects to the actin cytoskeleton via α-catenin and α-actinin. Taken together, many components of the slit membrane are known, but an integrative model of its substructure including all components is thus far lacking.

The cell body of podocytes contains a large nucleus that tends to be indented in the region of the large Golgi apparatus. Furthermore, it houses abundant rough-surface endoplasmic reticulum; individual cisternae, generally arranged in one complex per cell, are widened and filled with fine granular material of varying electrondensity—their relevance is unknown. In addition to the synthesis of membrane proteins necessary to supply the huge surface of their processes, podocytes in the adult synthesize and secrete all components of the GBM[42] (see below). On the other hand, abundant multivesicular bodies (predominantly found in the large cell processes) demonstrate strong catabolic activity in podocytes.

Podocytes contain a well-developed cytoskeleton that accounts for the unique shape of the cells and the maintenance of the processes. In the cell body and the primary processes, microtubules and intermediate filaments, such as vimentin and desmin, dominate, whereas microfilaments are densely accumulated in the foot processes. Here, they are part of a complex contractile apparatus.[43] The microfilaments form loop-shaped bundles, with their limbs running along the longitudinal axis of the foot processes. The bends of these loops are located centrally at the transition to the primary processes and are probably connected to the microtubules by the microtubule-associated protein τ.[44] Peripherally, the actin bundles appear to be anchored in the dense cytoplasm associated with the cell membrane of the soles of foot processes, and are dynamically linked to the slit diaphragm complex (discussed earlier). The importance of the podocyte actin cytoskeleton is emphasized by the discovery of inherited forms of focal segmental glomerulosclerosis (FSGS) caused by

mutations in actin-binding proteins: α-actinin-4 is a widely expressed homodimeric protein that bundles and crosslinks actin, and is highly expressed within podocyte foot processes. It interacts with a variety of other adhesion and signalling molecules. Several mutations in the ACTN4 gene encoding this protein cause a late-onset, autosomal dominant form of kidney failure.[45,46] More recently, nine independent missense mutations in INF2, which encodes a member of the formin family of actin-regulating proteins, were shown to segregate with FSGS in 11 unrelated families.[47]

Specific transmembrane matrix receptors anchor the podocyte foot processes to the GBM. Two systems are so far known. The first is a specific integrin heterodimer consisting of $\alpha_3\beta_1$ integrins. Within the GBM, these integrins bind to collagen type IV, fibronectin, and laminin 11.[48,49] Second, a dystroglycan complex connects the intracellular molecule utrophin to laminin 11, agrin, and perlecan in the GBM.[50,51] Both integrins and dystroglycans are coupled via adapter molecules (paxillin, vinculin, α-actinin, etc.) to the podocyte cytoskeleton, allowing outside-in and inside-out signaling as well as transmission of mechanical force in both directions.

In addition to the actin cytoskeleton within the foot processes, a subplasmalemmal actin system is found in podocytes.[43] This actin network is connected to the transmembrane sialoprotein podocalyxin, which represents the major protein of the negatively charged surface coat of podocytes.[52,53] The cell coat has the characteristics of a glycocalyx that contains sialic acid. A decrease in the content of sialic acid is associated with a podocyte foot process effacement and results in protein leakage through the filter, which has been shown under a great variety of circumstances.[54–58]

A huge body of data has been accumulated in recent years concerning the inventory of receptors and signaling processes starting from them in podocytes. cGMP signaling (stimulated by atrial natriuretic peptide [ANP], brain natriuretic peptide [BNP], and C-type natriuretic peptide [CNP], as well as by nitric oxide [NO]), cAMP signaling (stimulated by prostaglandin E_2, dopamine, isoproterenol, parathyroid hormone [PTH]/PTH-related peptide [PTHrP]), and Ca^{2+} signaling (stimulated by a huge number of ligands, including angiotensin II, acetylcholine, prostaglandin F_2 (PGF_2), arginine vasopressin [AVP], adenosine triophosphate [ATP], endothelin, histamine, etc.) have been identified.[59] An example of an ion channel of particular importance in podocytes is transient receptor potential canonical 6 (TRPC6), a nonselective cation channel, which is activated by diacylglycerol in a protein kinase C-dependent manner.[60] Mutations in TRPC6 were found to cause autosomal dominant, late adult-onset proteinuria, with a similar clinical phenotype as seen in ACTN4-mediated FSGS.[37] The major target of this signaling orchestra is the cytoskeleton, the concrete effects of which, however, are poorly understood. Other receptors, such as for C3b,[61] Heymann's antigen,[62] transforming growth factor β (TGFβ),[63,64] fibroblast growth factor 2 (FGF2),[65] and various other cytokines and chemokines have been shown to be involved in the development of podocyte diseases.[59]

Endothelium

The endothelium consists of a simple squamous layer of fenestrated (porous) cells with the cell nuclei generally located near the axial region of the capillary loop (Fig. 1.6). The fenestrated regions (Fig. 1.12), which compose roughly 55% of the surface area,[66] have a thin layer of cytoplasm (about 50 nm thick) penetrated by numerous fenestrae of round, oval, or irregular shape and varying sizes. The total area occupied by fenestrae accounts for 13% of the capillary surface. The fenestrated regions outline the pericapillary portions of the glomerular basement membrane, but also may be found adjacent to the mesangium (Fig. 1.8). The fenestrae have a diameter of 50 to 100 nm (thus they are larger than endothelial fenestrae elsewhere in the body) and are not bridged by diaphragms. Thus, this kind of a porous endothelium is unique for glomerular capillaries. Fenestrae with diaphragms are found only in the outflow segment of the efferent arteriole.[67] Nonfenestrated regions are generally seen over nuclei and mesangial cell regions. Human glomerular endothelial cells also are fenestrated.[68,69] A cell coat that is rich with polyanionic glycoproteins, including podocalyxin, covers the endothelial surface[70–72] and appears to fill the fenstraelike "sieve plugs."[73] In addition, above this "classic" glycocalix a 200-nm thick endothelial surface layer has been revealed consisting of loosely attached plasma compounds.[74]

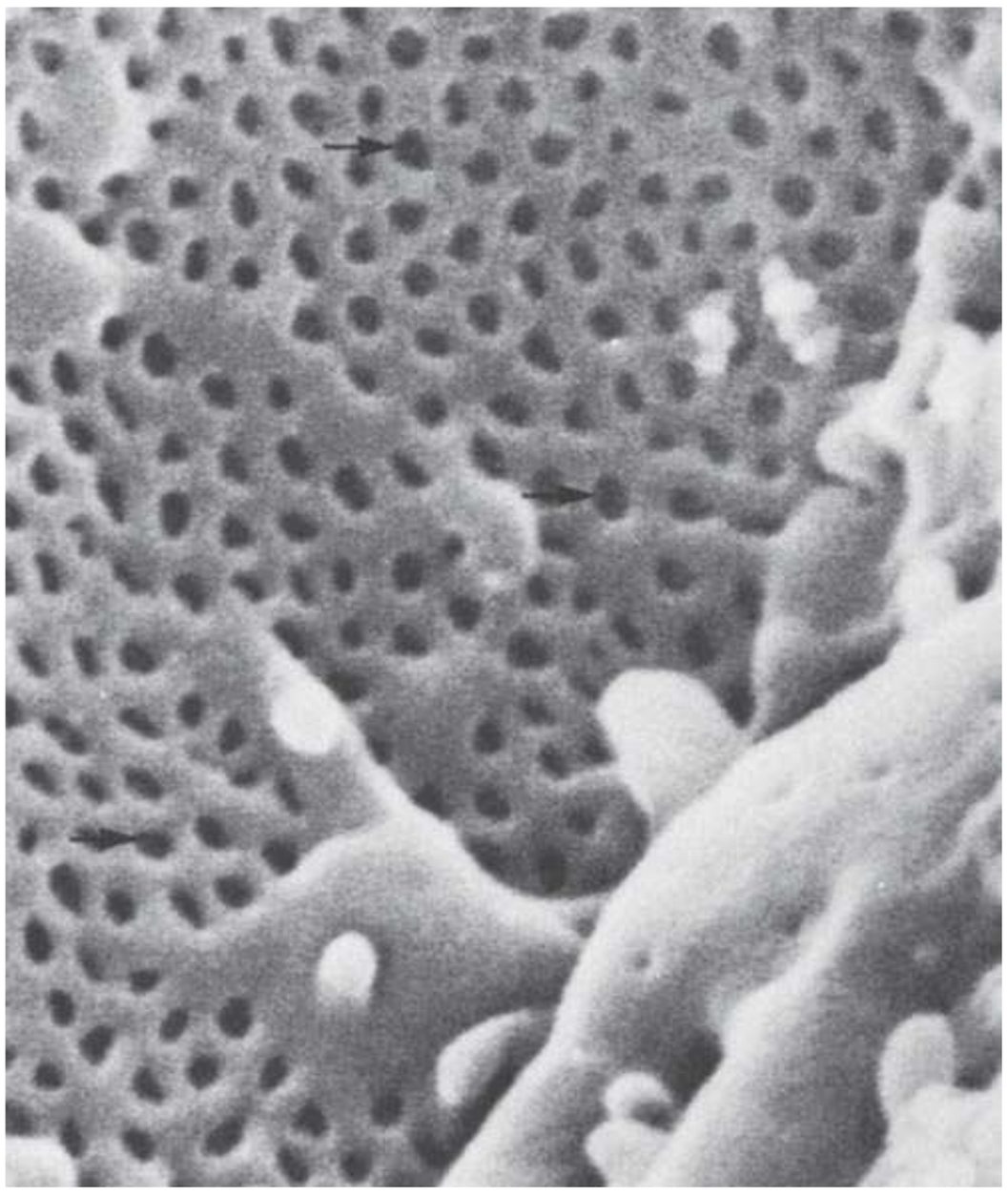

FIGURE 1.12 Scanning electron micrograph of a sectioned capillary loop showing the pores (*arrows*) of the endothelium. (Magnification ×50,400.)

As elsewhere in the body, glomerular endothelial cells are active participants in processes controlling coagulation, inflammation, and immune processes. Renal endothelial cells express surface antigens of the class 2 histocompatibility complex. Like platelets, glomerular endothelial cells contain components of the coagulation pathway and are capable of binding factors IXa and Xa and synthesize, release, and bind von Willebrand factor (factor VIII).[69] Glomerular endothelial cells synthesize and release endothelin-1 and endothelium-derived relaxing factor (EDRF).[75] Glomerular endothelial cells have receptors for vascular endothelial growth factor (VEGF) and angiopoetin I that are produced by podocytes.[76,77] The signaling axis via VEGF appears to have a major relevance for the maintenance of the glomerular tuft. Glomerular endothelial cells, in turn, synthesize and secrete platelet-derived growth factor β (PDGFβ) that acts on adjacent mesangial cells.[78]

Glomerular Basement Membrane

The GBM covers the capillary loops except in the axial region, where it is reflected over the mesangium to the next capillary loop, accompanied by the layer of foot processes (Figs. 1.6 to 1.8). The endothelial cells do not have a separate basement membrane; thus, the endothelial cells directly abut the mesangium toward axial regions. In adult humans, the basement membrane has a mean diameter of 320 to 340 μm.[79] It is thinner in young children and most laboratory animals.[80]

The basement membrane is composed of three layers: an outer, less dense subepithelial layer, the lamina rara externa; a central, electron-dense layer, the lamina densa; and an inner subendothelial layer, the lamina rara interna, which is continuous with the mesangial matrix (see Figs. 1.9 and 1.13).

During glomerulogenesis, the GBM is generated as two separate layers produced by glomerular endothelial and epithelial cells. The two sheets are fused together to form the mature GBM.[81–84] In the adult, the GBM is subject to a continuous turnover,[85–88] but few details are known so far about these processes. Podocytes appear to be the dominant cell type to synthesize and probably to degrade the GBM. Podocytes are alone capable to synthesize all the components of the GBM[42,89,90]; glomerular endothelial cells and also mesangial cells may contribute to the formation of the GBM.[91] It is less clear how the GBM degrades. In recent years, several extracellular matrix degrading enzymes have been described being produced by podocytes and mesangial cells.[92–94] The relevance of these enzymes for the turnover of the GBM remains to be established.

The GBM is generally considered as a hydrated meshwork consisting of collagen type IV, laminin, entactin/nidogen, and sulfated proteoglycans including agrin and perlecan.[42,95–99] Models of the ultramicroscopic structure of the basement membrane picture the GBM as a mat of collagen type IV. Monomers of type IV collagen consist of a 400-μm triple helix that, at its carboxy-terminal end, has a large noncollagenous globular domain called NC 1. At the amino-terminus the helix possesses a 60-μm triple helical rod, the 7S domain. Interactions between the 7S domain and the NC1 domain allow collagen type IV monomers to form tetramers that, by lateral association of triple helical strands, assemble into a three-dimensional network.[100,101] Laminin forms a second network that is superimposed to the collagenous network. Laminin is a noncollagenous glycoprotein consisting of three polypeptide chains, two of which are glycosylated and cross-linked by disulfide bridges.[95,102,103] Laminin binds to specific sites on the polymerized network of type IV collagen as well as the basal endothelial and epithelial integrins (see the preceding). The α-5-, β-2-, γ-1-laminin chains are assembled to form the GBM-specific heterotrimeric laminin 11.[48] This combined network of collagen type IV and laminin provides mechanical stability to the basement membrane and serves as a basic structure on which other matrix components attach.

The proteoglycans of the basement membrane consist of core proteins and covalently bound glycosaminoglycans, which are concentrated in the laminae rarae internae and externae, where they have been referred to as anionic sites and can be localized with cationic probes.[104] The major proteoglycans of the GBM are of the heparan sulfate type—the most prominent is agrin,[96] but perlecan also has been shown to occur in the GBM.[42] Digestion of these molecules with heparinase leads to a dramatic increase in the permeability of the basement membrane to anionic native ferritin used as a probe.[70]

Mesangium

The mesangium consists of mesangial cells that are embedded in a mesangial matrix. The term mesangium was introduced by Zimmermann in 1929[19] to describe the cells that form the stalk of the glomerulus and the axes of its lobules. Glomerular capillaries pursue a tortuous, highly anastomosing course around the mesangial axes. Together with the capillaries, the mesangium occupies the space inside the GBM, frequently termed the "endocapillary region." Topographically, the mesangium can be subdivided into a juxtacapillary region, where it abuts the capillary endothelium, and more centrally located axial regions, which are bound by the perimesangial GBM (Figs. 1.5 to 1.7).[105] The glomerular mesangium is continuous with the extraglomerular mesangium (Polkissen or lacis cells) along the glomerular stalk (Fig. 1.5). Both intraglomerular and extraglomerular mesangial cells have many similarities.

Mesangial cells are quite irregular in shape, with many cytoplasmic processes extending from the cell body toward the GBM. They have structural characteristics similar to those of smooth muscle cells in that they contain many bundles of microfilaments (especially within the cell processes) and peripheral dense bodies. Actin, myosin, and α-actin have been shown by immunocytochemistry to be contained in mesangial cells.[106,107] The relevance of mesangial cell contractility is discussed in the following text.

The processes of mesangial cells extend toward the GBM, to which they are attached either directly or by the interposition of extracellular bundles of microfibrils (Figs. 1.6 and 1.9). The GBM has to be considered as the effector structure of mesangial contractility.[105,108] Connections between mesangial cells and the GBM are especially prominent in the juxtacapillary region. At this site, tonguelike mesangial cell processes (packed with microfilament bundles) run underneath the capillary endothelium toward the turning points (mesangial angles) of the GBM, where they are anchored. Generally, two of these processes interconnect the GBM from two opposing mesangial angles (Fig. 1.8). In the axial mesangial region, contractile filament bundles are predominantly found within the numerous fingerlike projections of mesangial cells. These microprojections also run toward the GBM and are anchored to it. As in the juxtacapillary region, these microfilament bundles interconnect opposing parts of the GBM.[105]

The mesangial matrix fills the highly irregular spaces between mesangial cells and the perimesangial part of the GBM. In immunocytochemical studies, collagen types IV and V, heparan sulfate proteoglycan, fibronectin, laminin, and entactin have been localized within the mesangial matrix.[99,109,110] Among these components, fibronectin is the most abundant and has been shown to be associated with microfibrils.[109,111] Fibrillin 1 and other specific elastic fiber proteins have been detected in the glomerular mesangium and have been shown to be produced by mesangial cells.[112,113]

In specimens prepared for transmission electron microscopy according to routine methods, the mesangial matrix appears as basement membranelike material, albeit more fibrillar in character than the basement membrane proper.[114] In specimens prepared by a technique that avoids osmium tetroxide and uses tannic acid for staining, the mesangial matrix is seen to contain a dense network of microfibrils.[105,115] Microfibrils are noncollagenous, nonbranching, hollow structures of indeterminate length that are about 15 μm thick.[116] Within the mesangium, microfibrils form a three-dimensional network that establishes a solid base of contact between mesangial cells and the GBM, fettering the GBM to mesangial cells. Distinct bundles of microfibrils may be regarded as "microtendons" that allow the transmission of contractile force of mesangial cells to specific sites of the GBM.[105,115] The functional relevance of this system is discussed later.

The relevance of mesangial cells in phagocytosis is well documented. Mesangial cells are able to ingest particular tracers as well as macromolecules, such as thorotrast,[117] ferritin,[114] and aggregated proteins, as well as immune complexes.[118] An increased uptake of such materials by mesangial cells has been noted in proteinuric states.[114,119] It appears, however, that mesangial cells proper (i.e., mesangial cells that have contractile properties) are not primarily phagocytotic. A small subpopulation (3% to 7%) of cells in this region has been recognized as bone marrow-derived—they represent macrophages that have taken up residence in the mesangium.[120]

Supportive Functions of the Mesangium and Podocytes

The glomerular tuft is constantly exposed to comparably high intraglomerular pressures within glomerular capillaries and mesangium. The high intraglomerular pressures challenge not only the glomerular capillaries themselves but also the folding pattern of the glomerular tuft. Increased pressures lead to the loss of the folding pattern and to dilation of the glomerular capillaries. Therefore, we have to ask: what are the specific structures and mechanisms that counteract the expansile forces in the glomerular tuft? To answer this question we have to distinguish between the structures and mechanisms maintaining (1) the folding pattern of the glomerular tuft and those maintaining (2) the width of glomerular capillaries.

The folding pattern of the glomerular tuft is primarily sustained by the mesangium.[105,108,121] Mesangial cells are connected to the GBM by their contractile processes—they maintain the infoldings of the GBM by centripetal contractions, thereby allowing for the capillaries to arrange in the peripheral expansion of the GBM. This supporting role of mesangial cells is best illustrated under circumstances with loss of mesangial cells, such as Thy-1 nephritis.[122] Under those circumstances the folding pattern of the GBM is progressively lost, finally resulting in mesangial aneurysms. Podocytes clearly contribute to maintenance of the folding pattern by specific cell processes that interconnect opposing parts of the GBM from outside within the niches of the infoldings. This function is also best illustrated under circumstances with loss of mesangial support: podocytes are capable of maintaining a high degree of the GBM folding pattern for 2 to 4 days after which they obviously fail, and mesangial aneurysms become prominent.[122]

The width of glomerular capillaries, in the long run, is probably controlled by growth processes accounting for differently sized capillaries. The width of a given capillary, in an acute situation being exposed to changes in blood pressure, appears to be stabilized by the GBM, which is a strong elastic structure[123] and, together with the mesangial cell bridges (see previous text), capable of developing wall tension.[121,124] In addition, the tensile strength of the GBM is reinforced by podocytes. Podocytes are a kind of pericyte; their foot processes represent a unique type of pericyte process which, like elsewhere in the body, counteract the dilation of the vessel. Podocyte processes are firmly attached to the underlying GBM (see previous text); their cytoskeletal tonus counteracts the elastic extension of the GBM. In this function, podocytes cannot be replaced by any other cell—failure in this function will lead to capillary dilation.

Glomerular Filtration Barrier

The essential components of the glomerular filtration barrier are the endothelium (Fig. 1.13), which is perforated by large open pores, the extracellular matrix feltwork of the GBM membrane, and the slit diaphragms between the podocyte

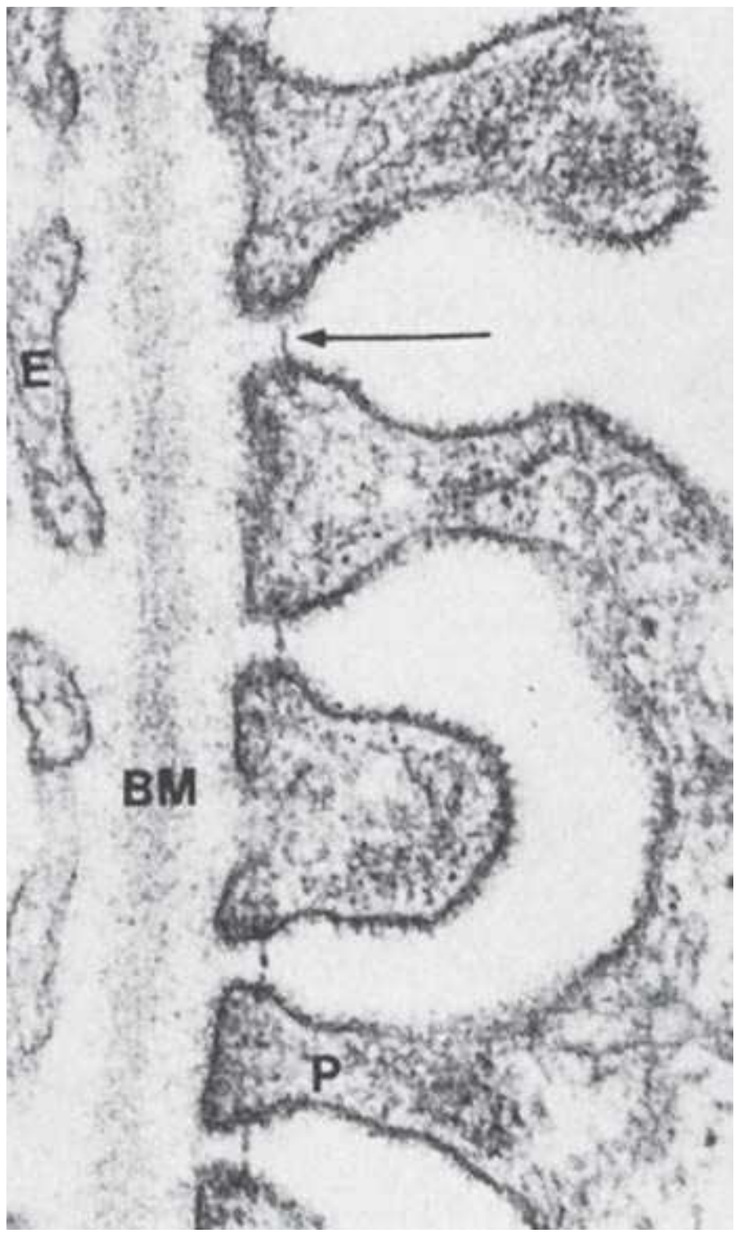

FIGURE 1.13 Transmission electron micrograph from a rat renal corpuscle showing the endothelial lining (*E*), the basement membrane (*BM*), and the pedicels (*P*). The filtration-slit membrane (*arrow*) bridges the pedicels. (Magnification ×23,600.)

foot processes. When compared with the barrier established in capillaries elsewhere in the body, a glomerular filtration barrier is quite different in two respects: its permeability to water, small solutes, and ions is extremely high, whereas its permeability to plasma proteins the size of albumin and larger is very low.

The high hydraulic permeability is rooted in the fact that filtration occurs along extracellular routes. All components of this route—the endothelial pores, the highly hydrated GBM, and the slit membrane—can be expected to be quite permeable to water and small solutes. Drummond and Deen[125] have calculated the hydraulic conductance of the individual layers. According to this calculation, the hydraulic resistance of the endothelium is negligible. The GBM and the filtration slits each make up roughly one-half of the total hydraulic resistance of the filtration barrier.

Any decrease in the length of the filtration slit, and thus in slit area, as in experimental and clinical glomerulopathies along with footprocess effacement, correlates with the decrease in the ultrafiltration coefficient K_f.[126,127] A model simulating those conditions showed, along with a decrease in slit area, its relevance in determining increases in flow resistance. The decrease in filtration slit area caused the average path length for the filtrate, through the basement membrane, to increase, thereby explaining the overall decreased hydraulic permeability.[128]

On the basis of evidence of contractility of mesangial cells exposed to vasoconstrictor stimuli in culture,[129,130] of dimensional changes observed in intact glomeruli ex vivo,[131,132] and of changes in ultrafiltration coefficient K_f found in vivo in response to vasoactive substances,[133,134] some researchers have concluded that mesangial cells contract in situ and that this contraction alters glomerular filtration dynamics by decreasing filtration surface area.

Other considerations speak against this possibility. The geometric arrangement of the mesangial contractile apparatus (Fig. 1.6), however, does not seem to be compatible with the previously mentioned sequence of actions. Shortening of the mesangial cell processes connecting opposing angles would only bring the angles closer together, compressing the mesangial capillary interface, but leaving peripheral capillary wall area (filtration area) unaltered. In addition, with regard to the contractility of mesangial cells ex vivo (in culture as well as preparations of whole glomeruli), it should be remembered that mesangial contraction in these cases is not opposed by intercapillary hydrostatic pressure as it is in situ. These considerations, together with the absence of measurable changes in glomerular tuft dimensions in morphometric studies,[135,136] as well as in response to vasoactive substances in vivo,[137] have led to the suggestion[121] that the mechanical action of the mesangial cell contraction is essentially static in nature, developing tension that serves to counteract expansile forces on the tuft without inducing significant changes in capillary dimension. If mesangial contractility acutely alters the glomerular ultrafiltration coefficient K_f, it is, therefore, probably not because of an acute change in filtration surface area.

The low permeability of the glomerular filtration barrier to plasma proteins is still poorly understood. Several points seem to be relevant. First, there is no vesicular transport of proteins through this barrier as in most other capillaries elsewhere in the body. The barrier function of the glomerular filter for macromolecules is quite specific and is selective for size, shape, and charge.[138–140]

In early extensive studies, Farquhar and associates,[138,141,142] as well as Rennke and associates,[143] used tracers, such as ferritin and dextrans of different sizes and charge, to elucidate the role of the various layers in determining the selectivity of this filtration barrier. When their results are summarized, it appears that the basement membrane may be the major barrier to anionic substances, whereas the most restrictive part for uncharged and cationic substances may be the slit diaphragm. Uncharged macromolecules up to an effective radius of 1.8 μm pass freely through the filter. Larger compounds are more and more restricted (indicated by their fractional clearances, which progressively decrease) and are totally restricted at effective radii of more than 4.0 μm. The effective radius is an empiric value, measured in artificial membranes, that takes into account the shape of micromolecules and also attributes a radius to nonspherical molecules. Plasma albumin has an effective radius of 3.6 μm; without the repulsion because

of the negative charge, plasma albumin would pass through the filter in considerable amounts.[144]

Thus, since these early studies, the glomerular barrier has been generally suggested to contain a size- and a charge-restrictive element. Despite more than 40 years of intensive research, the principles of the glomerular barrier function are still controversial and poorly understood—a situation that gives room even to hypotheses claiming that the glomerular barrier itself does not have any restrictive properties to macromolecules, such as albumin.[145–147] A more realistic and elegant recent barrier hypothesis is based on the observation that filtration—the flow of filtrate through the barrier—creates a potential difference of 0.02 to 0.05 mV negative in Bowman's space and that this potential difference is sufficient to hinder the negatively charged macromolecules like albumin from passing the filter.[148]

Summarizing the present status of knowledge, accumulating evidence suggest that the GBM has little relevance in size restriction, but the slit membrane is the decisive size-restrictive element within the glomerular barrier.[149] The current strong engagement in elucidating the molecular architecture of the slit membrane promises to enlighten the porous pattern of the slit membrane and, hopefully, explain its size-restrictive property. Regarding the charge selectivity, it appears that the proximal portion of the barrier, above all the endothelium, are most important.[73,150–152] Furthermore, prevention of albumin from entering the filter is also dependant on normal hemodynamic conditions in glomerular capillaries, as first shown by Ryan and Karnovsky.[153]

PROXIMAL TUBULE

At the urinary pole of the glomerulus, the flat parietal epithelium of Bowman's capsule transforms abruptly into the high epithelium of the proximal tubule. In some species (rabbits),[154] a neck segment is found interposed between the glomerulus and the proximal tubule—short neck segments also may be seen in humans.[80] In contrast, in mice, the proximal tubule epithelium generally begins deep within the Bowman's capsule.

The proximal tubule is composed of segments that have differing morphology, functional relevance, and vulnerability to toxins (Figs. 1.14 to 1.18). The two segments most frequently identified are the proximal convoluted portion (pars convoluta) occupying the cortical labyrinth (Figs. 1.14 to 1.17), and the straight portion (pars recta) in the medullary rays of the cortex and the outer stripe of the outer medulla (Fig. 1.18). Further subdivision on structural criteria results in the three segments of P_1, P_2, and P_3 according to Jacobsen and Jorgensen,[155] and S_1, S_2, and S_3 according to Maunsbach.[156,157] S_1, or P_1, corresponds to the first segment of the pars convoluta and lies exclusively in the cortical labyrinth; S_2, or P_2, corresponds to the remainder of the convoluted segment and the beginning of the pars recta, with the first part occupying the cortical labyrinth and the remainder

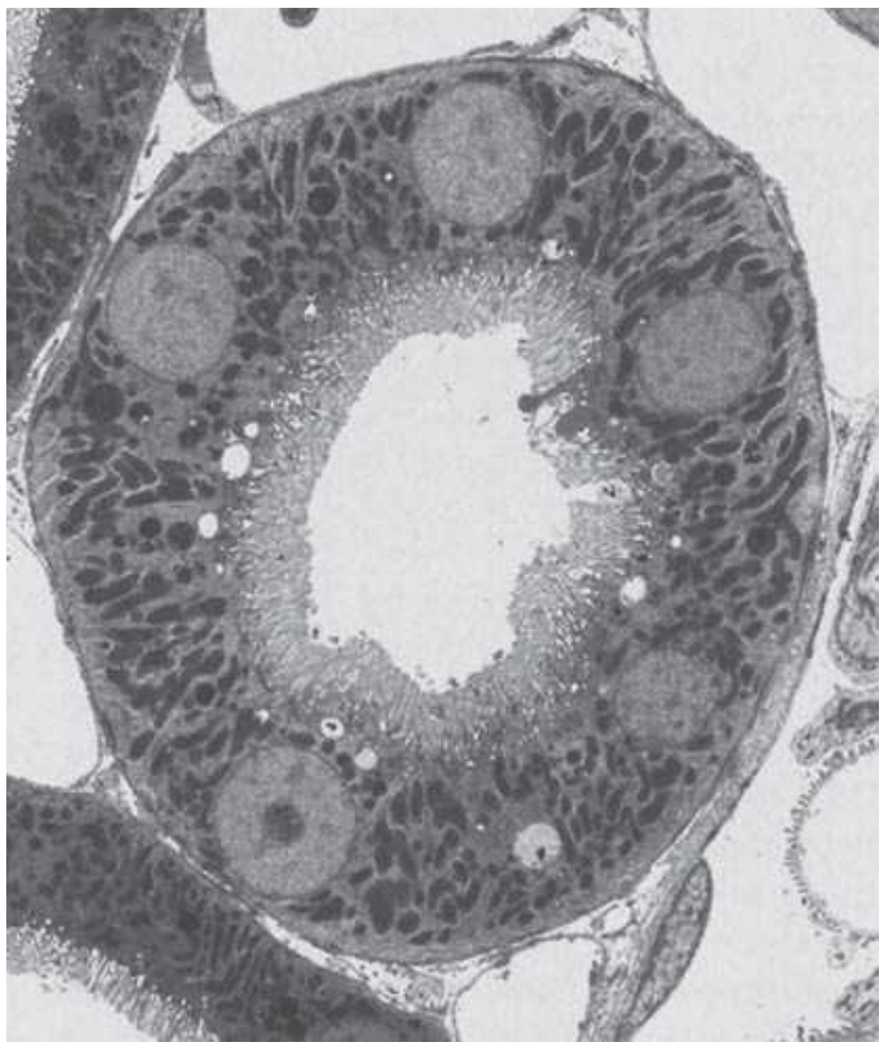

FIGURE 1.14 Transmission electron micrograph of a proximal tubule (P1 segment) of the rat. Note the apical brush border, the vesicular zone of the apical cytoplasm, and the basal zone of interdigitating cell processes filled with mitochondria. (Magnification ×2,300.)

occupying the medullary ray; and S_3, or P_3, corresponds to the remaining part of the pars recta located primarily in the outer stripe of the outer zone of the renal medulla. The transition from P_1 to P_2 is gradual, whereas the transition from P_2 to P_3 is generally abrupt, except in rabbits.[158]

To confuse matters further, the morphology of the subdivisions differs not only from each other but also among species, including mice,[159] rats,[156] rhesus monkeys,[160] rabbits,[158] and dogs.[161] For a detailed description of a particular species, the reader should consult the original studies. Segmentation of human proximal tubules has not been studied as recently or thoroughly because of a lack of availability of well-fixed normal human kidney and, therefore, has been divided only into convoluted and straight regions.[162]

In general, cells of the P_1 region are tall, have a well-developed apical microvillus border, an elaborate cell shape with well-developed lateral interdigitating processes containing abundant, large mitochondria, and a well-developed endocytic apparatus (Fig. 1.16). P_2 cells decrease in cell height from those seen in P_1, have a shorter microvillus border, and are less elaborately shaped cells with smaller mitochondria (Fig. 1.17). The P_3 cells are more cuboidal in shape (less elaborate) and their microvillus border is generally less elaborate. The cells of rats are an exception and have a well-developed brush border of very long microvilli (Fig. 1.18).[156] This cytologic segmentation of the proximal tubule is maintained in superficial, midcortical, and juxtamedullary nephrons.

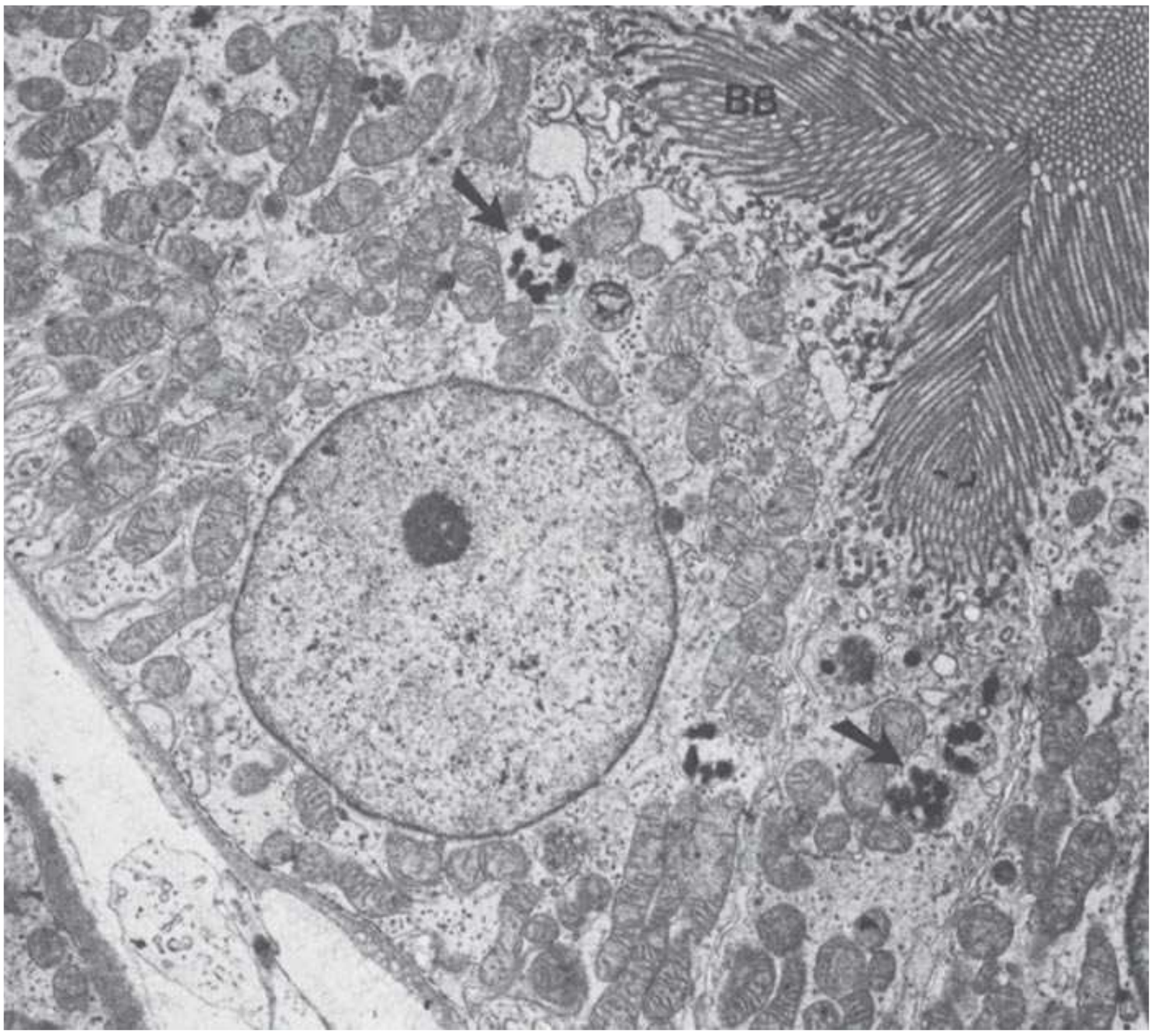

FIGURE 1.15 Transmission electron micrograph of a human proximal convoluted tubule showing the brush border (*BB*) and apical condensing vacuoles containing small dense bodies (*arrows*). (Magnification ×7,800.)

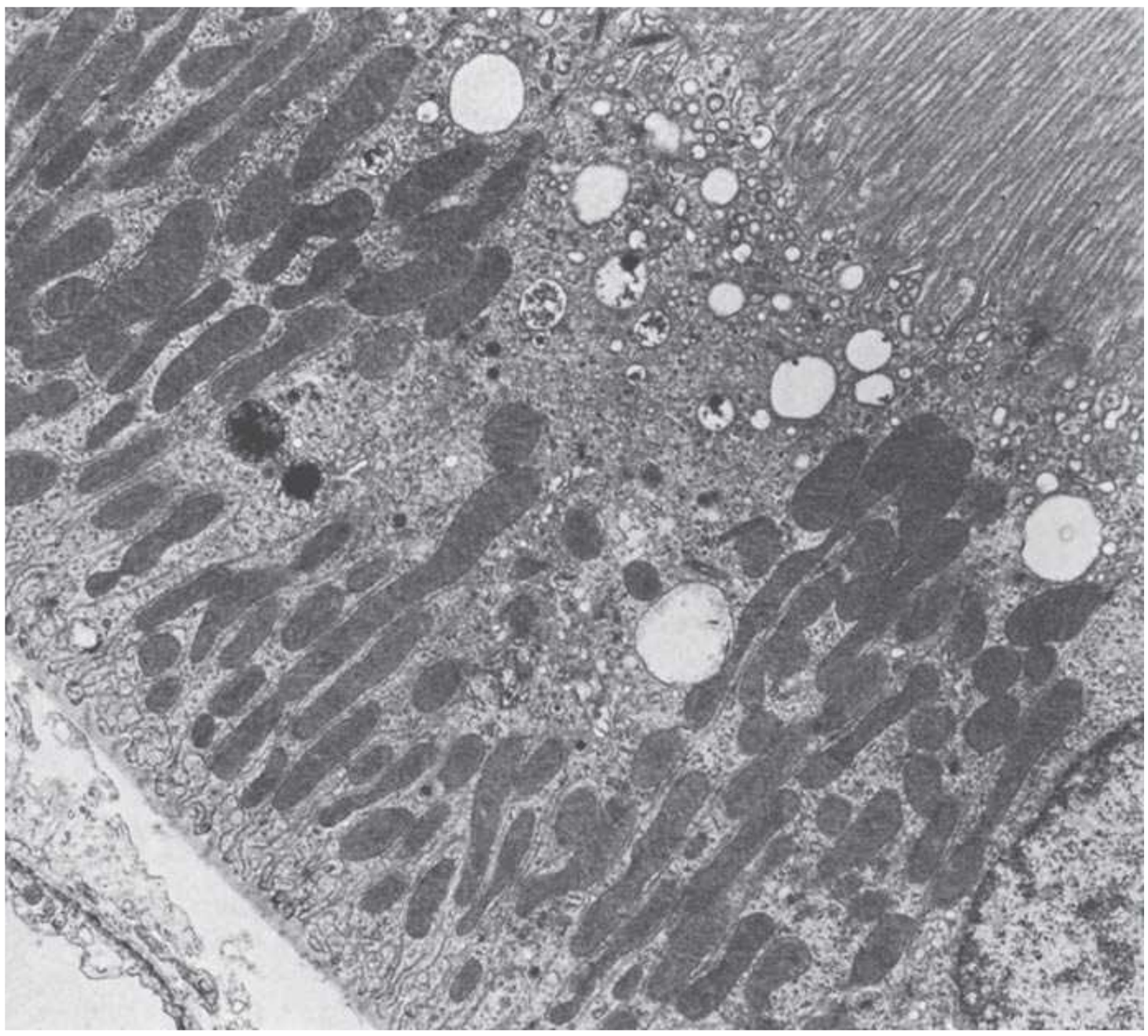

FIGURE 1.16 Transmission electron micrograph of a P1 segment from a rat kidney. (Magnification ×8,000.)

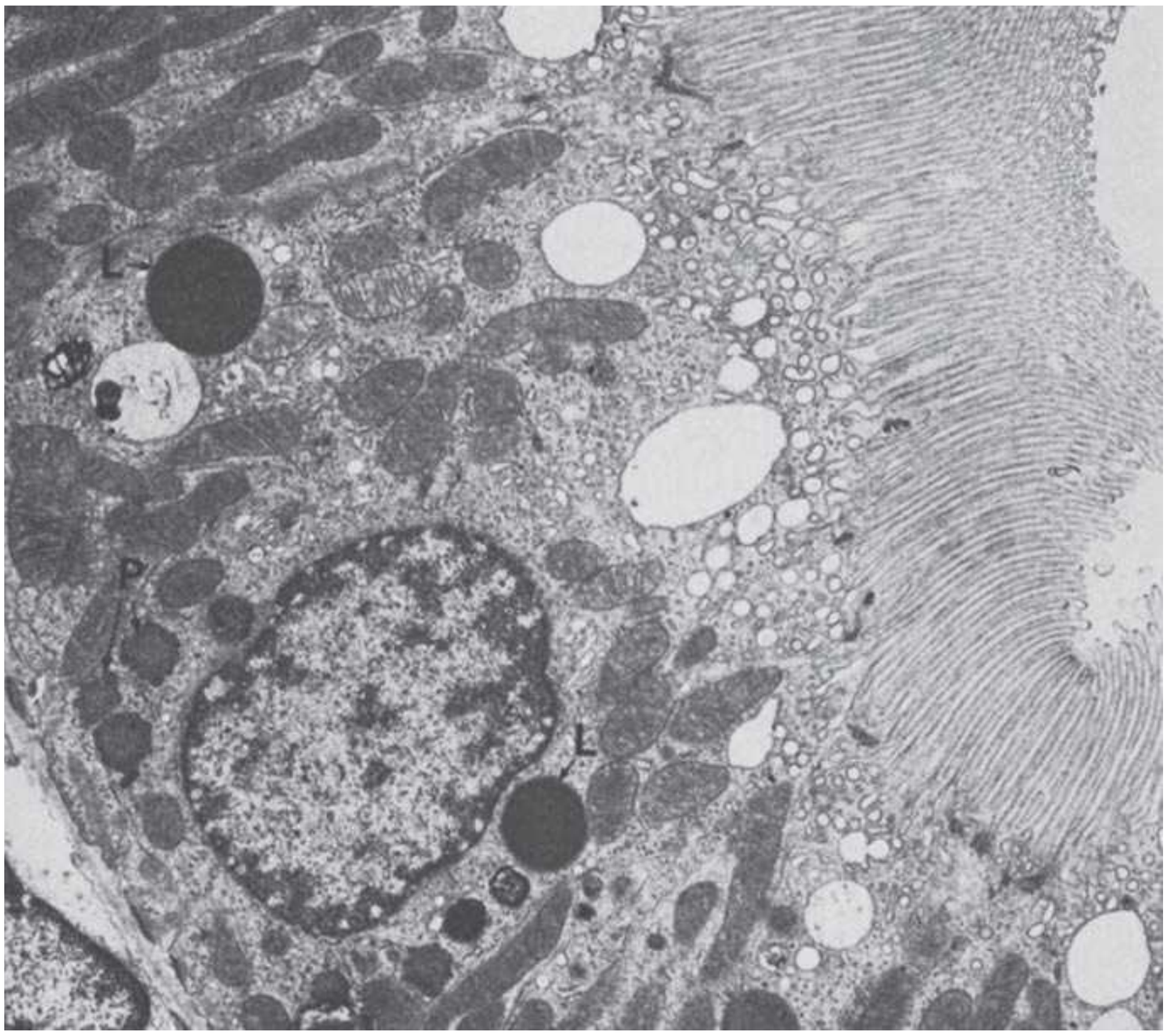

FIGURE 1.17 Transmission electron micrograph of a P2 segment from a rat kidney. Note the large dense lysosomes (*L*) and peroxisomes (*P*). (Magnification ×10,000.)

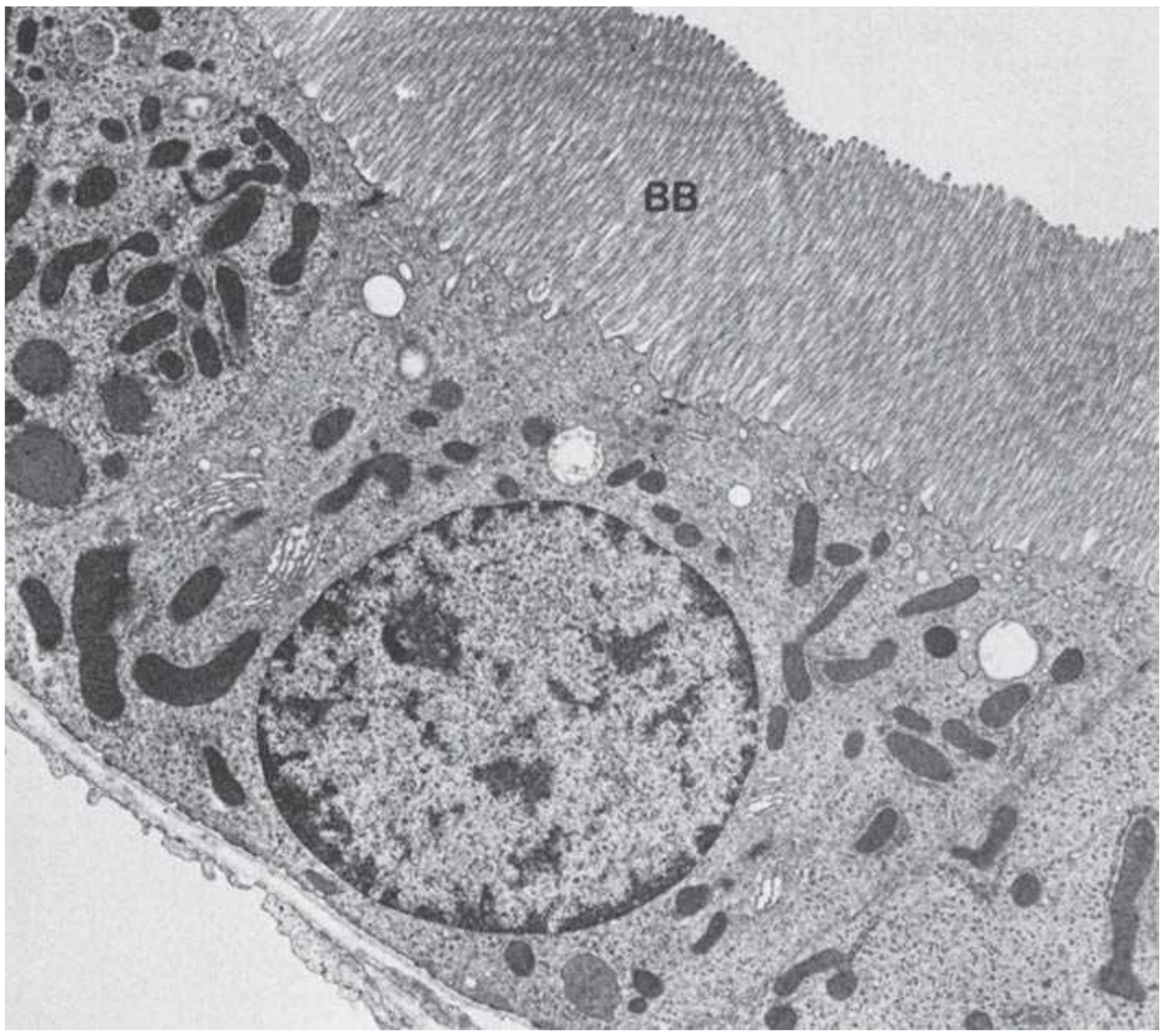

FIGURE 1.18 Transmission electron micrograph of a P3 segment from a rat kidney showing the extensive microvillus border (*BB*) and more simple cell shape of this segment. (Magnification ×8,000.)

Proximal Convoluted Tubule (P_1 and Part of P_2)

The proximal convoluted tubule is the longest and largest segment of the mammalian nephron. The tubule is lined by cells that have an elaborate cell shape based on extensive basolateral interdigitations (Figs. 1.19 to 1.21), a well-developed microvillus border, a prominent intracellular digestive tract (endocytic apparatus and lysosomes (Fig. 1.15), and numerous large peroxisomes (microbodies). The single ovoid nucleus lies in the middle to basal region of the cytoplasm.

Cell Shape and Mitochondria

The cells are characterized by an extensive system of lateral cell processes that interdigitate with lateral processes from adjacent cells (Figs. 1.19 to 1.21). These lateral processes can extend the entire height of the epithelium, especially in the P_1 segment, but become more elaborate toward the basal regions of the lateral surface (Fig. 1.16). The complex shape of these cells serves to increase the lateral cell surface area manyfold, which provides a greater area for transporters, above all of the Na^+-K^+-ATPase. These lateral extensions usually contain one or two layers of mitochondria (Fig. 1.20). The mitochondria are long, narrow rods that branch and double back on themselves. They are oriented perpendicular to the basement membrane and lie adjacent to the cell membrane, to which they presumably supply energy for transport processes.

The lateral extensions and their mitochondria cause the pattern of basal striations that are typical for numerous transporting cells. The lateral processes of proximal convoluted tubule cells in humans are not as elaborate as those seen in rats (compare Figs. 1.15 and 1.16). In rabbits, the lateral cell surface is increased 20 times over that of the basal cell surface.[163] The lateral extensions also establish a complex and extensive surface labyrinth of lateral intercellular spaces ("basal labyrinth").

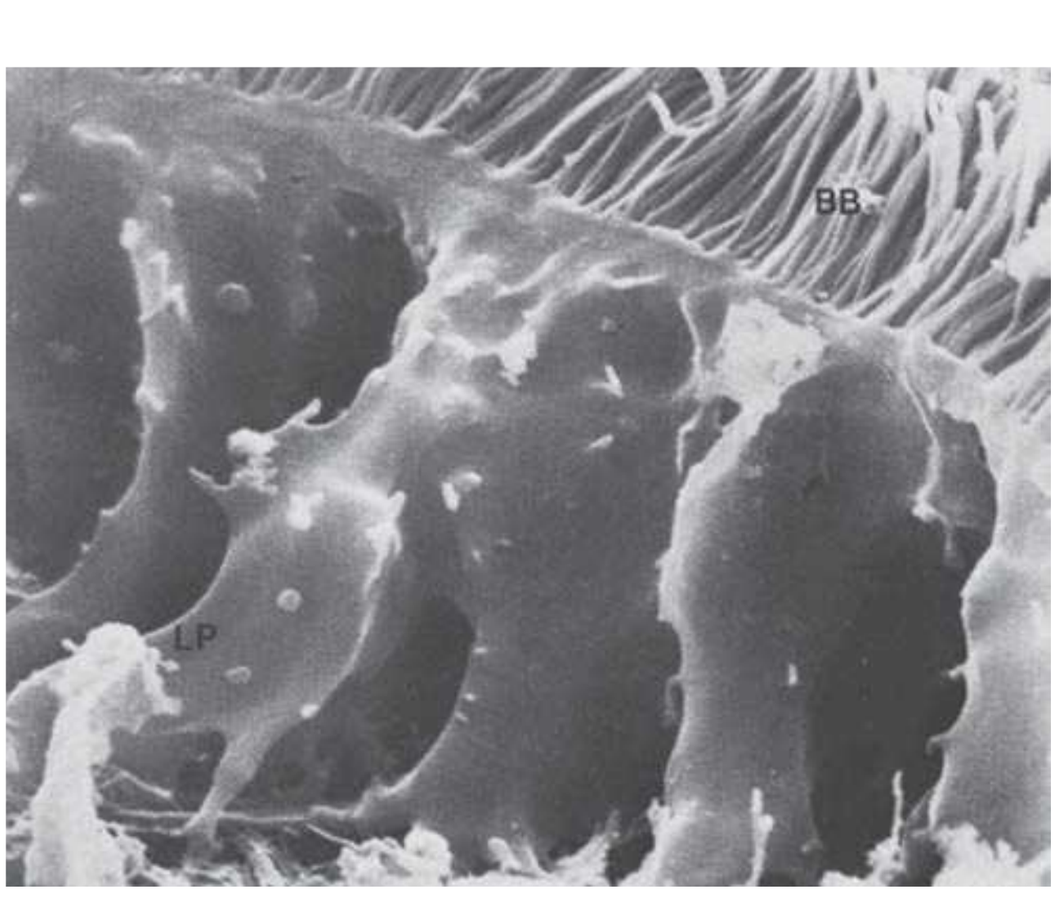

FIGURE 1.19 Scanning electron micrograph of a rat proximal tubule epithelial cell showing the apical brush border (*BB*) and the lateral processes (*LP*). (Magnification ×14,700.)

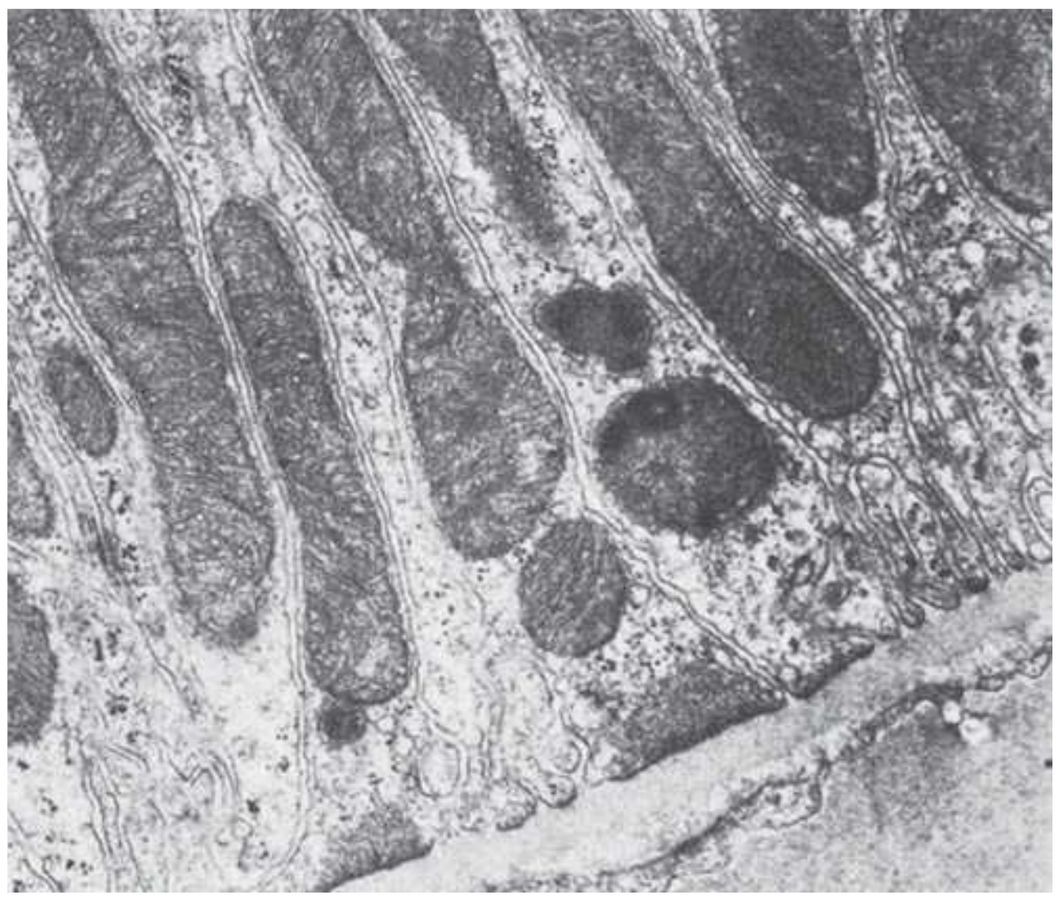

FIGURE 1.20 Transmission electron micrograph of the basal cytoplasm from a rat proximal tubular cell. (Magnification ×20,600.)

Cell Junctions

The proximal convoluted tubular cells have an apical junctional complex that consists of a shallow, beltlike, tight junction next to the tubular lumen; a deeper, beltlike intermediate junction (the zonula adherens); and only small and infrequently seen desmosomes. The proximal tubular tight junctions are shallow and consist of only one or two lines of fusion of the outer leaflet of the cell membrane (Fig. 1.22). Freeze-fracture studies of normal proximal tight junctions, however, reveal focal discontinuities. During volume expansion, striking increases in the length of discontinuities were found.[164] Transmission micrographs also show multiple areas of nonfusion of tight junctions associated with renal venous constriction and increased ureteral pressure.[165] These sites of nonfusion may explain the increased permeability seen in these situations. Proximal tubular cells are electrically coupled by gap junctions (Fig. 1.22).[166]

Microvilli

A layer of slender (approximately 80 to 90 μm), finger-shaped processes extends into the tubular lumen, forming the microvillus, or brush border. The length and number of processes vary with the segment and species. The luminal surface of the pars convoluta is increased 40 times in rats.[157] The luminal surface is increased 36 times in the pars convoluta and 15 times in the pars recta in rabbits.[163] Each microvillus has a core of microfilaments that extend into the apical cytoplasm connecting them to the cytoskeleton.

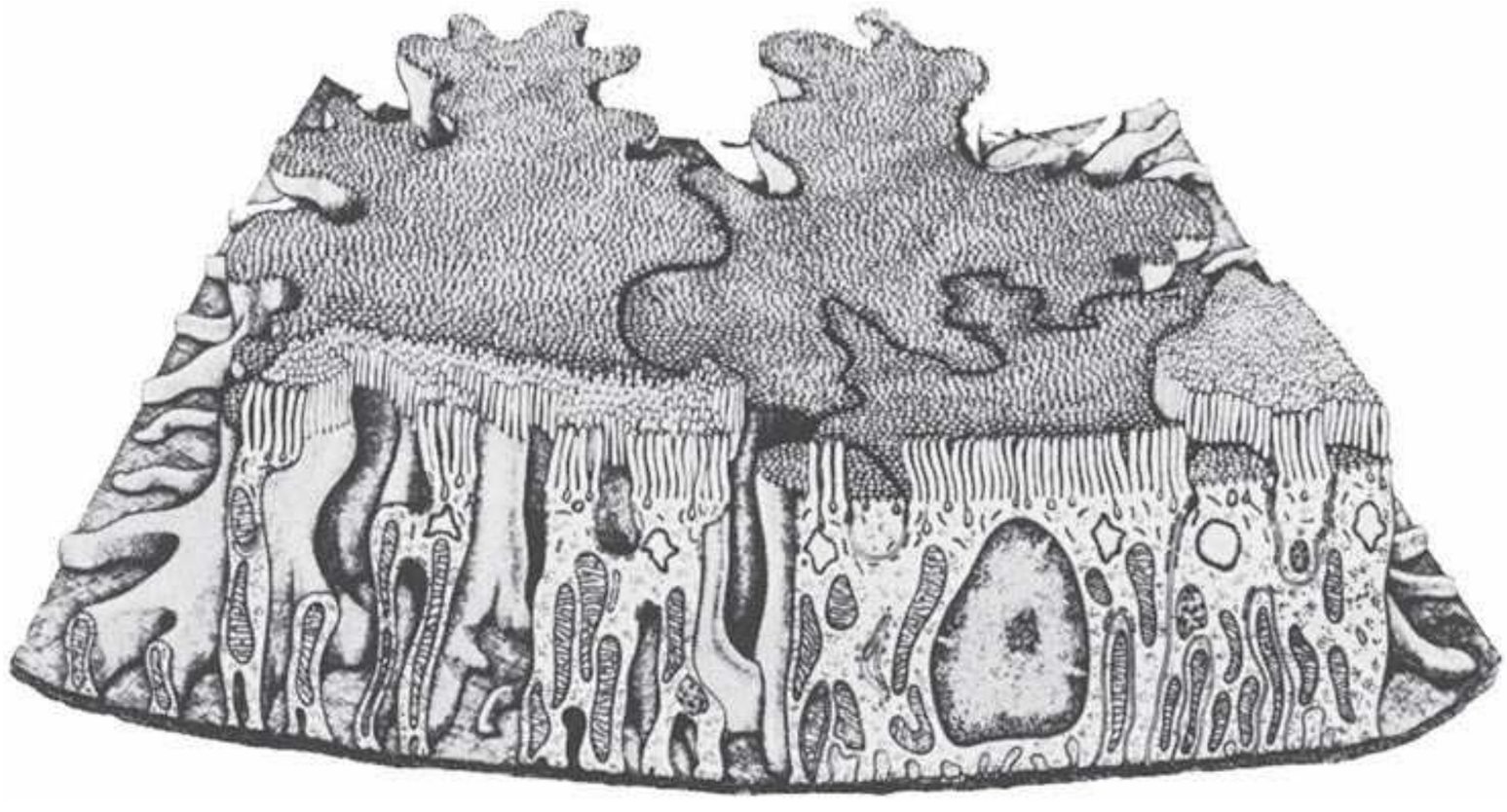

FIGURE 1.21 Diagram of a proximal convoluted tubular cell showing the elaborate shape of these cells. Some interdigitating processes extend the full height of the cells. The apical and basal cytoplasmic regions also have smaller, more elaborate interdigitating processes. (From Bulger RE. The shape of rat kidney tubular cells. *Am J Anal.* 1965;116:237, with permission.)

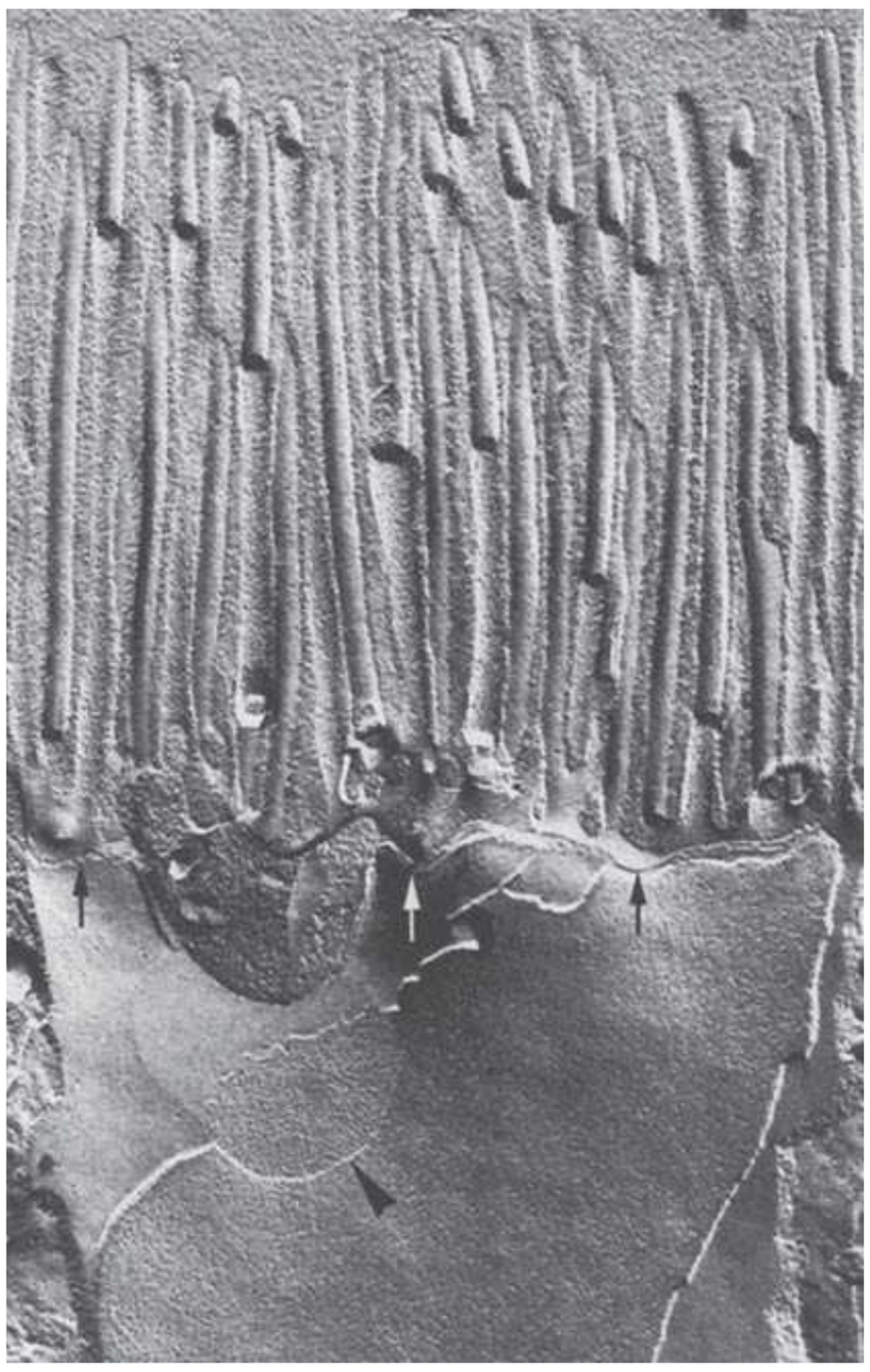

FIGURE 1.22 Freeze-fracture electron micrograph of the apical part of proximal tubule cells (rabbit) showing the shallow tight junction (*arrows*) and a gap junction (*arrowhead*). (Magnification ×37,000.) (From Kriz W, Kaissling B, Schiller A, et al. Morphologische merkmale transportie-render epithelien. *Klin Wochenschr.* 1979;57:967, with permission.)

Cytoplasm

The cells contain a very prominent vacuolar apparatus (see later text), a Golgi apparatus, free ribosomes, and cisternae of rough and smooth surface endoplasmic reticulum. The latter forms specialized cisternae, called the perimembranous cisternal system, near the lateral cell membranes.[80] In addition, the cells contain many peroxisomes that frequently have eyecatching shapes.[167] Peroxisomes are limited by a single membrane and contain a dense matrix, frequently exhibiting crystalloid nucleoids (Fig. 1.17); platelike inclusions at the peroxisomal edge, which are called marginal plates, are also frequently encountered. Peroxisomes are invariably wrapped by elements of the smooth-surfaced endoplasmic reticulum. In the kidney, large peroxisomes are exclusively found in the proximal tubule, most frequently in the P_3 segments[167]—all other nephron portions contain only microperoxisomes. Peroxisomes contain enzymes from a primitive respiratory chain in which oxidases produce hydrogen peroxide, which is, in turn, destroyed by the catalase, hence the name peroxisome.[168] Peroxisomes participate in the breakdown of very-long-chain fatty acids by lipid β-oxidation; in addition, they may play a protective role by destroying hydrogen peroxide produced by free radicals.

Straight Part of the Proximal Tubule (Last Part of P_2 and All of P_3)

The straight part of the proximal tubule (pars recta) begins in the medullary ray and penetrates into the outer stripe of the outer zone of the medulla (Fig. 1.18). The proximal pars recta converts into the thin limb near the junction of the inner and outer stripe. In rats, the pars recta includes the final region of both P_2 and P_3,[169] and the transition

between the two segments occurs at various levels in the medullary ray. This region is marked by a sudden increase in microvillar length, a decrease in endocytic apparatus, and a decrease in interdigitation between adjacent cells. The microvilli of the pars recta cells decrease in height and number in rabbits[158] and humans[162] but remain high in rats (Fig. 1.18).

In general, the P_3 pars recta cells have been described as lower in height with a less elaborate shape. In humans, the pars recta cells have a convex apical surface, and some lipid droplets are found in the basal cytoplasm. The mitochondria are fewer and no longer closely applied to the cell membrane. The lysosomes are smaller and the Golgi and endocytic apparatuses are less well developed. Peroxisomes are more numerous in the pars recta.[80,162] The tight junctions of P_3 can be more complex in shape, consisting of several junctional strands in rats, dogs, and cats.[170]

Structure–Function Correlations

The functional relevance of the proximal tubule is manifold and quantitatively enormous. It reabsorbs about 70% of filtered Na^+, Cl^-, and water; 95% of bicarbonate; 60% of Ca^{2+}; and sodium phosphate. Reabsorption of the filtered glucose is complete, whereas reabsorption of amino acids is almost complete. This occurs either by transcellular transport via specific channels and transporters in both membranes (water, sodium, phosphate, glucose, amino acids, and bicarbonate in a specific enzyme-mediated mode) or predominantly by paracellular transport through the leaky tight junctions (Ca^{2+}, Cl^-). Furthermore, filtered macromolecules undergo reuptake by a prominently developed endocytotic apparatus. In addition, the proximal tubule (predominantly S_3 segments) secretes organic cations and anions, which constitute an extraordinarily diverse array of compounds of physiologic, pharmacologic, and toxicologic importance. The transepithelial transport involves separate entry steps at the basolateral membrane and exit steps at the luminal membrane with specific transporters at both sites.[171–174] Other potentially toxic xenobiotic compounds are metabolized within the well-developed smooth endoplasmic reticulum of S_3 segments.[175]

Unique to the proximal tubule is the reabsorption and degradation of filtered protein and peptides (Figs. 1.15 and 1.16). As discussed previously, all proteins smaller than albumin leak through the glomerular filter; even albumin, in small amounts, is always contained in the filtrate. All these diverse macromolecules are taken up by proximal tubule cells via receptor-mediated endocytosis and degraded in lysosomes. In proteinuric states, this function is greatly enhanced. The uptake and digestion include the following steps.[176,177]

1. Binding of the filtered protein to two multiligand receptors, megalin and cubulin, which are densely accumulated within clathrin-coated pits in the intermicrovillar areas of the apical membrane.

   Megalin is a 600-kDa transmembrane protein belonging to the LDL-receptor family (see reviews).[176,177] The extracellular domain contains four clusters of cysteine-rich, complement-type repeats, constituting the ligand-binding regions. Cubulin is a 416-kDa peripheral membrane protein identical to the intrinsic factor vitamin B_{12} receptor, known from the small intestine. It contains 27 CUB domains, which are responsible for the ability to interact with a great variety of ligands.
2. Small apical vesicals pinch off from the tubular invagination at the intermicrovillar areas to ferry the protein to the next component.
3. Large apical vacuoles located in the apical cytoplasm are formed by fusion of small vesicles representing the early endocytotic compartment.
4. Condensing vacuoles form in which the protein is condensed. These vacuoles move basally in the cell and acquire hydrolytic enzymes by fusion either with primary or secondary lysosomes. The proteins sequestered within lysosomes appear to be broken down into amino acids that are reused by the cell.
5. Already sequestered in the early endosomal compartment, the receptors are concentrated in dense, apical tubules by which they are returned to the apical plasma membrane.

This process of megalin-mediated internalization appears to be of even much wider relevance. As mentioned previously, the proximal tubule reabsorbs phosphate, representing a key element in phosphate homeostasis. Depending on the amount of sodium phosphate cotransporters present in the brush border cell membrane, the reabsorption varies. Internalization of the phosphate transporter type II (e.g., PTH induced to downregulate reabsorption) occurs via megalin-mediated endocytosis.[178,179] The proximal tubule has also endocrine relevance. In response to stimulation by PTH, it produces, by adding a second hydroxyl group, the active vitamin D_3, calcitriol.

Thin Limbs of the Loop of Henle (Intermediate Tubule)

Thin limbs can be short, occurring only along the descending limb, or they can be long, reaching varying distances into the inner medulla. In the long-looped variety, thin limb segments compose part of both the descending and ascending limbs. Four types of thin limb segments are routinely identified: (1) descending thin limbs of short-looped nephrons (SDTL) (Figs. 1.23 to 1.25), (2) upper portions of descending thin limbs of long-looped nephrons (LDTL up), (3) lower portions of descending thin limbs of long-looped nephrons (LDTL lp), and (4) ascending thin limbs of long-looped nephrons (ATL) (Figs. 1.24 and 1.25). This pattern has been observed in rats,[180,181] mice,[182] syric hamsters,[183] the desert rodent Psammomys obesus,[184,185] and the rabbit.[158] Thin limbs have not been studied as carefully in humans as

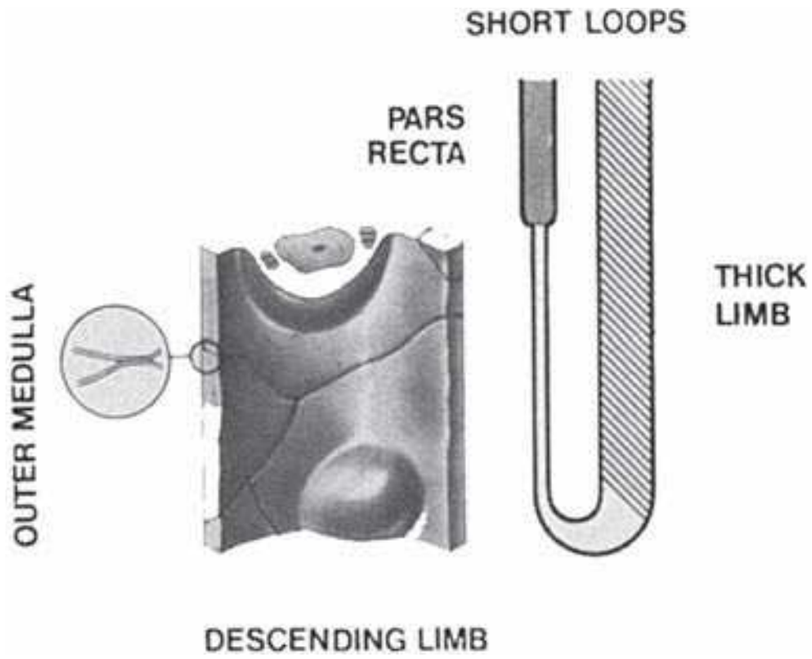

FIGURE 1.23 Diagrammatic representation of thin limb structure in short loops of Henle showing the shapes of constituent cells and the morphology of the occluding junctions (*inset*). (From Schwartz MM, Venkatachalam MA. Structural differences in thin limbs of Henle: physiologic implications. *Kidney Int*. 1974;6:193, with permission.)

in several other animal species.[13,186,187] An additional subsegment of thin limbs has been identified in chinchillas.[188]

Surprisingly, as seen by light microscopy, these simple looking epithelia are strikingly different from each other—not only the ascending from the descending limbs but, most remarkably, the descending limbs of short from those of long loops. Furthermore, within the descending segments, the proximal portion, although structurally not different from the distal portion, express a different pattern of transporters than the distal portion. Even islets or interposed limb pieces of functionally different cells are encountered within an otherwise homogenous thin limb segment.[189,190] Beyond all of these heterogeneities, there are prominent differences among species. This situation may explain the doggedly persistent discussion about the integrated function of thin limbs in the urine-concentrating process; a generally accepted concept of how the final concentration of the urine in the inner medulla occurs is lacking.

The type-1 epithelium lining (SDTL) is composed of flat, noninterdigitating cells, joined by tight junctions that consist of several anastomosing strands. Cell organelles are exceedingly sparse. Functionally, this segment contains aquaporin 1 (AQP1) and the urea transporter UT-A2 in its membranes.[191–194] Thus, it is water and urea permeable. However, these properties are unequally distributed; within the proximal part, the water permeability is high, whereas, within the distal part, the urea permeability is high.[191,193,195] In species with complex vascular bundles (rat, mouse, etc.), the SDTLs lie within vascular bundles[187]; in these surroundings, the thin limbs are in an ideal position to recycle urea from the ascending vasa recta into the short-loop nephrons.

The descending limbs of long loops (LDTL) are generally much larger in diameter and have a thicker epithelium than those of short loops (Fig. 1.25). Moreover, these thin limbs segments are heterogeneous; those of the longest long loops begin in the inner stripe as a much thicker tubule than those of shorter long loops. The character of the epithelium gradually changes as the limbs descend toward and into the inner medulla. The subdivision of the long descending thin limbs into an upper part (type-2 epithelium) and a lower part (type-3 epithelium) is an approximation and reflects the gradual change

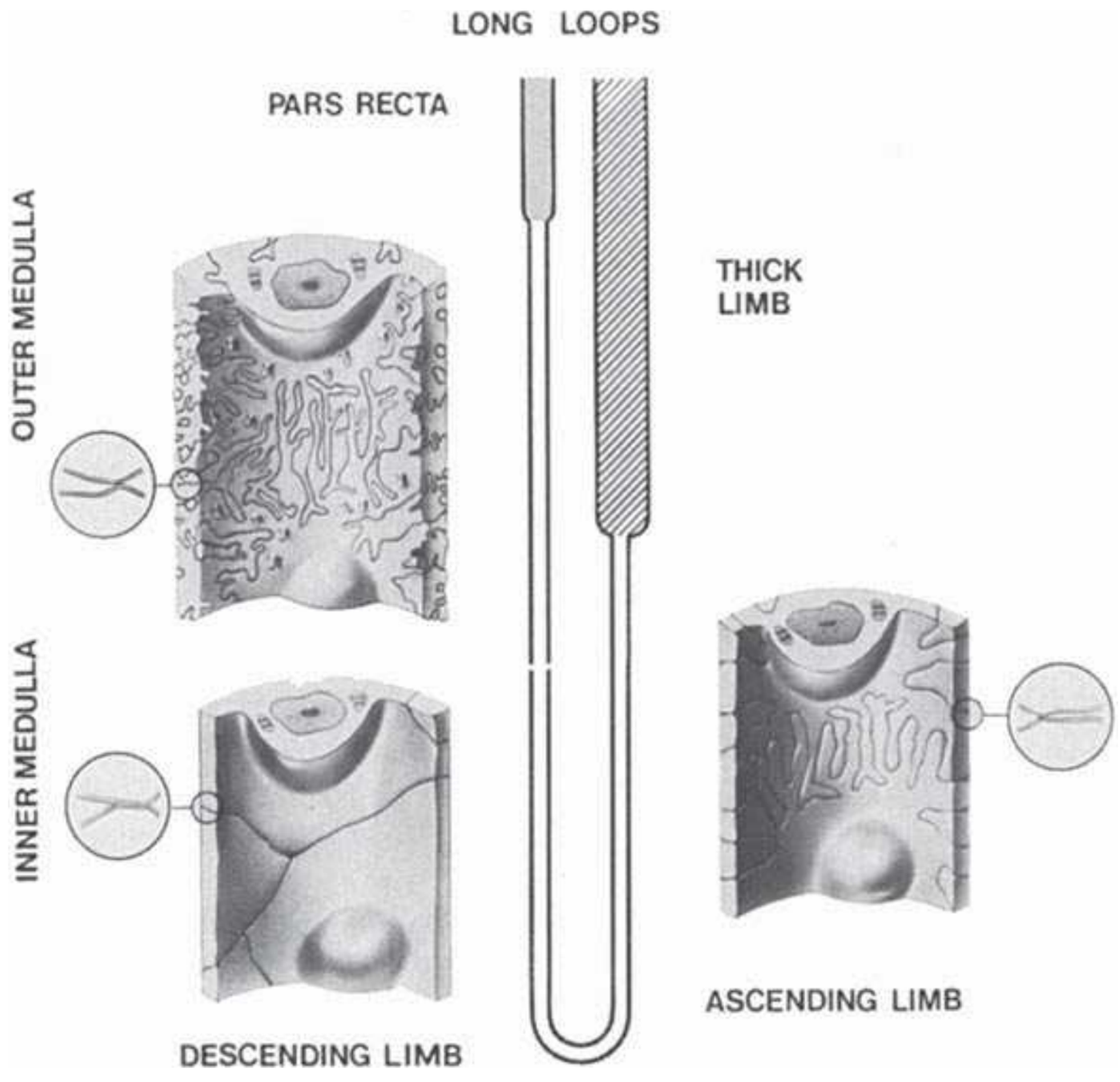

FIGURE 1.24 Diagrammatic representation of thin limb structure in long loops of Henle, showing the shapes of constituent cells and the morphology of the occluding junctions (*inset*). (From Schwartz MM, Venkatachalam MA. Structural differences in thin limbs of Henle: physiologic implications. *Kidney Int*. 1974;6:193, with permission.)

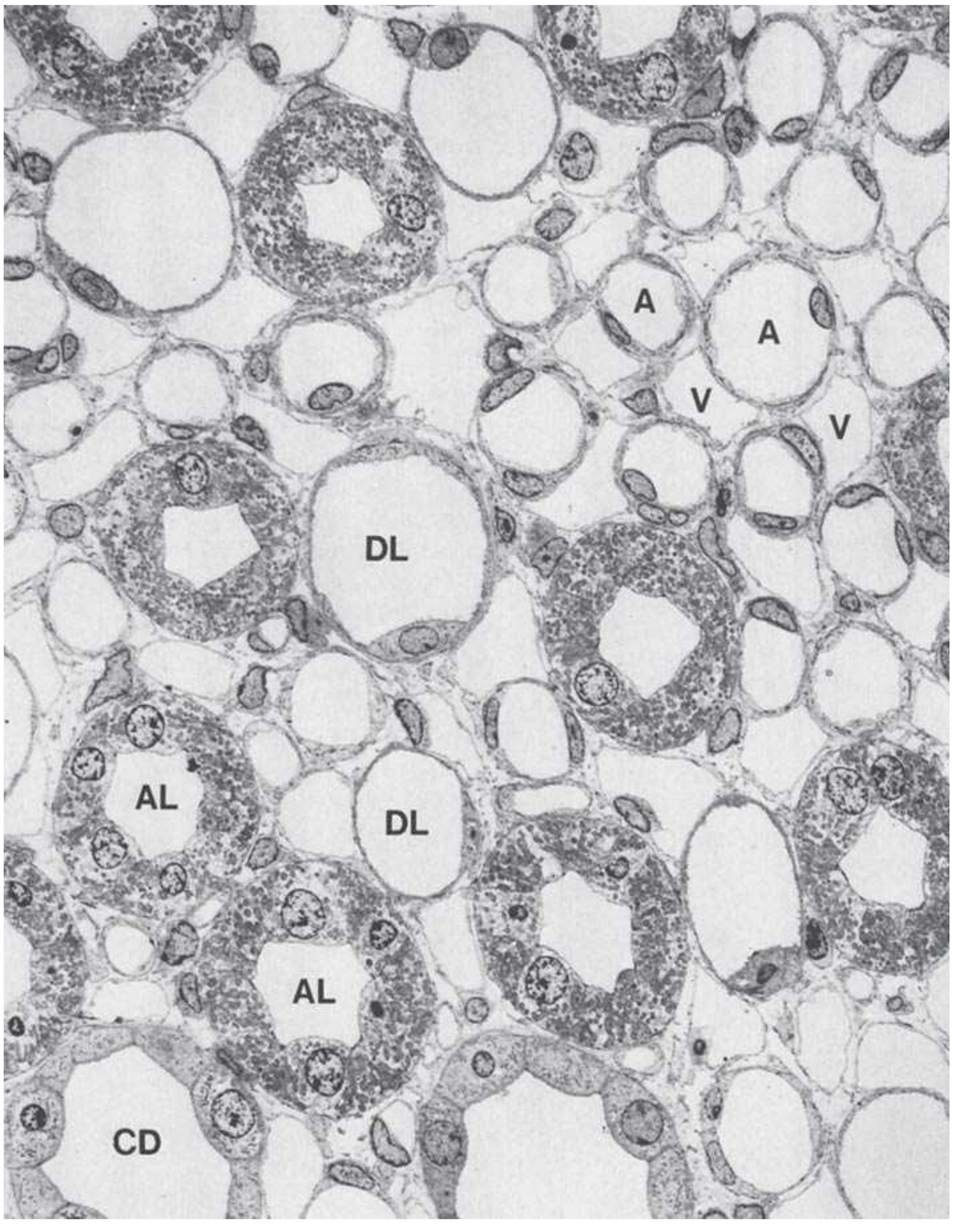

FIGURE 1.25 Low power electron micrograph of a cross-section through the inner stripe (rabbit). A vascular bundle with arterial (*A*) and venous (*V*) vasa recta is surrounded by descending thin limbs (*DL*; the small profiles belong to short loops and the large profiles to long loops), and thick ascending limbs (*AL*) and collecting ducts (*CD*); note the dense pattern of capillaries between the tubules. (Magnification ×900.)

between the two epithelia. Moreover, this process of epithelial transformation appears to be related to the length of each loop. It occurs earlier and more quickly in short long loops and is delayed in the longest long loops.[158,159,181,182,187,189,196]

Furthermore, considerable interspecies differences, particularly prominent in type 2 epithelia, complicate the situation. Two patterns of type-2 epithelium may be distinguished.[187,197] In one group of species (mouse, rat, Psamomys, etc.),[159,184,185,198,199] the type-2 epithelium is characterized by an extremely high degree of cellular interdigitation and a shallow tight junction consisting of only one junctional strand pointing to prominent paracellular transports. In addition, the epithelium has numerous apical microvilli, considerable numbers of mitochondria, and exhibits a high expression of Na^+-K^+-ATPase.[200,201] In a second group of species (rabbit, minipig, and, possibly, man),[202,203] the type-2 epithelium is much more simply organized. The prominent paracellular pathway is lacking; the cells do not interdigitate and are joined by deep tight junctions. In other respects, however, the epithelia are similar in the two groups: numerous luminal microvilli, many mitochondria, and a dense assembly of intramembrane particles in luminal and basolateral membranes are present in both groups. The high density of intramembrane particles may, at least, be partially due to the high density of AQP1 channels in both membranes—corresponding to the decrease of particle density along its descending course. The density of AQP1 channels also decreases and finally terminates completely.[195,204,205] Because structurally a clear cut border between the upper and the lower segment of the LDTL cannot be defined, it may be reasonable to discriminate both segments by the absence of AQP1 in the lower segments.[189,195,204]

Type-3 epithelium (found in LDTL lp) is comparably simple; interspecies differences are no longer prominent. The epithelium consists of flat, noninterdigitating cells, joined by tight junctions of intermediate apico-basal depth[181]; it lacks AQP1 and may, accordingly, have a very low water permeability. Regarding the permeability to urea and the distribution of the urea transporter, UT-A, conflicting data are published, especially when comparing data from different species.[190,191,204,206–208]

The ascending thin limb (ATL) is present only in long-loop nephrons and is uniformly organized among mammals. Generally the transition from the type-3 epithelium of the DTL to the type-4 epithelium of the ATL occurs in a short, but fairly constant, distance before the bend ("prebend segment").[180,185,189] Therefore, functionally, the entire bend should be regarded as part of the ATL. The type-4 epithelium is characterized by very flat but heavily interdigitating cells joined by shallow tight junctions, consisting of only one, but prominent, junctional strand. This leaky organization of the paracellular pathways correspond with functional studies,[209,210] which all demonstrate that the ATLs are highly permeable for ions.

The change from the type-3 epithelium to the type-4 epithelium coincides with the full disappearance of the urea transporter UT-A and the abrupt beginning of the expression of the chloride channel ClC-K1[189,204]; aquaporins are also lacking. Thus, the ATL is water and urea impermeable, but highly permeable for Cl^- and also Na^+.

In humans,[211,212] dogs,[161] and minipigs,[203] a gradual transition is seen from the thin limb to the ascending thick limb; however, an abrupt transition is seen in most other species.[158,213,214]

THE DISTAL TUBULE OVERVIEW

The distal tubule of mammalian kidneys has been defined in many and conflicting ways. For morphologists, the distal tubule is divided into several serial segments with differing locations in the kidney and of varying ultrastructural patterns[215] (Fig. 1.2). The first morphologic segment of the distal tubule for long-looped nephrons begins at the boundary between the inner zone of the medulla and the inner stripe of the outer zone of the medulla. At this boundary, the cells lining the ascending thin limbs of long-looped nephrons increase in height, forming the MTAL. The MTALs of short-looped nephrons are encompassed within the inner stripe of the outer zone in which the descending thin limb of short-looped nephrons converts into a descending thick limb, which then makes a hairpin turn and ascends as an MTAL. The MTAL traverses the inner stripe of the outer zone of the medulla and continues toward the cortex through the outer stripe of the outer zone of the medulla. The MTAL then enters the cortex, ascending within the medullary ray as the CTAL. These two segments, the MTAL and CTAL, are also called the straight part of the distal tubule. The CTAL then leaves the medullary ray and enters the pars convoluta of the cortex, running between the afferent and efferent arteriole of the renal corpuscle from which that tubule was derived. A plaque of taller, but narrower, cells is found in the wall of the CTAL in this region; this plaque of cells forms the macula densa (JGA). In humans, the cells of the MTAL are not as elaborately shaped as those described in the majority of laboratory animals that have been studied.[212]

After a short post macula densa region of the CTAL, the distal tubule becomes more convoluted and it is now lined by epithelial cells that increase in height from the CTAL, which forms the distal convoluted tubule (DCT) (see Fig. 1.27).[214,216] In rabbits, the DCT contains one type of cell known as the distal convoluted tubular cell.[158] In this species, the DCT is abruptly replaced by the connecting tubule (CNT). In other species, such as rats and mice,[217] humans,[218] or minipigs,[203] the transition is more gradual with intermixing of cells so that in the late DCT of these species connecting tubule cells and intercalated (IC) cells begin to dominate, although DCT cells and principal cells of the collecting duct also can be identified. This segment is then defined as the CNT. The CNT of superficial nephrons begin as unbranched segments, each emptying into a collecting duct (some investigators call the first part of the collecting duct the initial collecting duct). In midcortical and juxtamedullary nephrons, the change from the DCT to the CNT occurs a few cells before the fusion of the two tubules.[158] These CNT segments join to form branching connecting tubule segments called arcades, which arch upward in the cortex and then empty into a CCD.[7] The number of each type of CNT architecture varies with the species.

Medullary Thick Ascending Limb

The MTAL is lined by cells of one type that has extensive basal interdigitating processes filling the basal three-fourths of the cytoplasm (Fig. 1.26). The larger cell processes contain large mitochondria that are elongated on an axis perpendicular to the tubular basement membrane. In addition to their normal contents, the mitochondria contain prominent intramitochondrial granules and occasional filamentous bodies.[219] The epithelium lining the MTAL is approximately 7 μm in height.[213,220]

The apical surface of the MTAL cells does not have an elaborate shape in rabbits[158]; it is more elaborate in rats.[221] Tisher and associates,[213,216,220] using scanning electron microscopy, have described two surface configurations of the MTAL cells, with variations in apical cell outlines and in the number of apical microplications. Some cells have smooth apical surfaces with a few microprojections, whereas others have a rough surface with numerous microprojections. The MTAL cells have both extensive invaginations of the basolateral plasma membrane, as well as a large lateral interdigitating process of adjacent cells.[220] Because a main function of the TAL is the reabsorption of sodium and chloride from the tubular lumen to the interstitium, these basolateral processes have Na^+-K^+-ATPase activity.[222] In addition, they have an apical bumetanide-sensitive sodium-potassium-2 chloride cotransporter called NKCC2 located in the apical

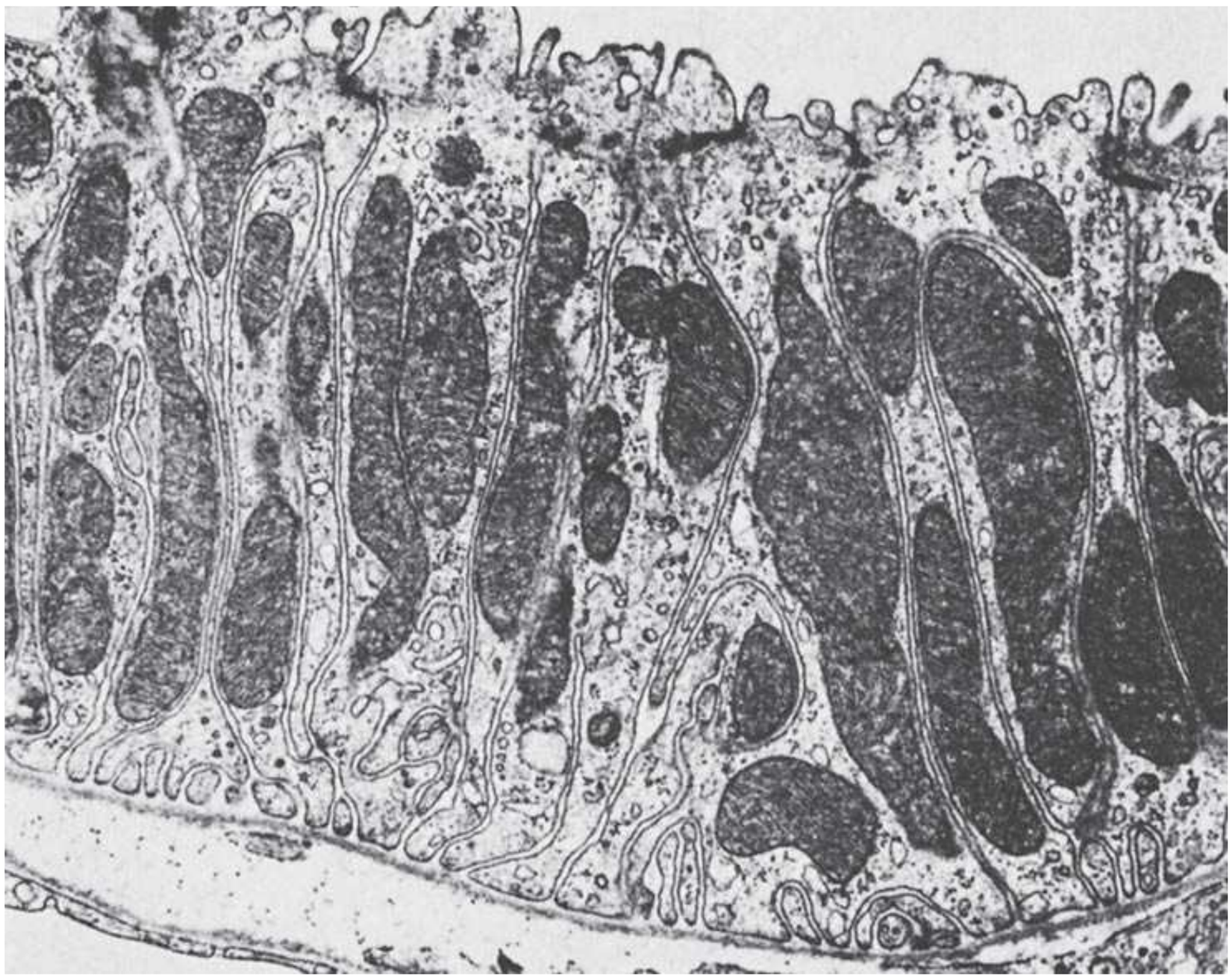

FIGURE 1.26 Transmission electron micrograph of the pars recta of the distal tubule from a rat showing the interdigitating cellular processes. (Magnification ×15,000.)

membrane (see the discussion of the membrane amplification principle later in this chapter). The MTAL demonstrates a low permeability for water so the active transport of the sodium ions out of the basolateral membranes of the cells in exchange for potassium ions participates in forming the hypertonicity of the medullary interstitium. The apical cytoplasm contains a variable number of vesicles and a prominent Golgi apparatus. Cisternae of rough-surfaced endoplasmic reticulum can be seen throughout the cytoplasm. The tight junction is of low to intermediate apical–basal depth, consisting of several parallel strands.[223] These tight junctions appear to be related to the relative impermeability to water (see discussion later in this chapter of tight junction structure and their role in transepithelial solute and water transport). As the MTAL traverses the outer stripe in rats, it decreases in cell height, but retains its prominent lateral interdigitations. In rabbits, the apical surface becomes more elaborate in this region.[158]

The administration of vasopressin (antidiuretic hormone) to rats that have hereditary diabetes insipidus causes hypertrophy of the MTAL in Brattleboro rats.[224] This effect can also be shown by water restriction in normal rats[225] and after high protein intake.[226,227]

Cortical Thick Ascending Limb

The cells of the CTAL are lower in height than those of the MTAL in the rat, measuring about 5 μm in height[221] and 2 μm in the rabbit.[2] The cells still have prominent basolateral interdigitating cell projections, which increase the basolateral cell membrane approximately tenfold over the apical or basal cell surface.[228] These interdigitating processes are more prominent in a circumferential direction.[228] Mitochondria are still prominent in the basolateral cell processes, but somewhat smaller than those of the MTAL. The apical cell border becomes more tortuous in this segment, having more prominent invaginations of the entire lateral cell margins, including the apical region of the cell,[158] and has more microvilli along its surface.[213] Tamm–Horsfall glycoprotein has been identified covering the plasma membrane in the TAL of rat.[229,230]

The MTAL and CTAL differ from each other physiologically, especially in hormone responsiveness.[231,232] The MTAL has a high density of Na^+-K^+-ATPase.[233] Hebert et al.[222] have shown in mice that antidiuretic hormone (ADH) increases the transepithelial voltage and net chloride reabsorption in the medullary, but not the cortical, region of the ascending thick segment. The ascending thick region functions in flow-dependent absorption of NaCl mediated by the furosemide (bumetanide)-sensitive cotransport NKCC2.[234,235] Nielsen et al.[236] and Obermuller et al.,[237] using immunohistochemistry, have demonstrated bumetanide-sensitive Na-K-2Cl labeling in the apical plasma membrane and the subapical intracellular vesicles of MTAL and CTAL in the rat and rabbit. The apical plasma membrane of the macula densa region also had distinct labeling consistent with a role in tubuloglomerular feedback.

The TAL in the inner stripe has a greater reabsorptive capacity for NaCl than the cortical segment,[238] but the cortical segment can maintain a higher concentration gradient[239] (see the discussion of Na^+-K^+-ATPase and the basolateral membrane area later in this chapter). The sodium chloride

reabsorbed by the TAL contributes to the hypertonicity of the medullary interstitium. As the CTAL ascends toward the renal corpuscle from which it was derived, there is an increase in apical plasma membrane surface area, both by an increase in apical microvilli and by an increase in lateral cell margins.[221]

The macula densa region is formed by a plaque of cells in the wall of the CTAL (see Fig. 1.35), where the ascending thick tubule runs between the afferent and efferent arterioles of the renal corpuscle from which the tubule is derived. A group of extraglomerular mesangial cells (lacis cells, Polkissen cells) fills the cone-shaped area formed by those three structures.[240] These four elements—the afferent and efferent arterioles, the extraglomerular mesangium, and the macula densa—constitute the juxtaglomerular apparatus, which will be discussed separately in more detail later in this chapter.

Distal Convoluted Tubule

The DCT (distal pars convoluta) is shorter than the proximal convolution, being about 1.2 mm in length in the rat.[217] Therefore, fewer profiles are seen in sections of the renal cortex. The DCT begins with a rather marked increase in the height of the lining cells from those of the TAL, although the cells are similar to those lining the TAL. In the rabbit, DCT cells are three to four times taller in the DCT than the cells lining the CTAL.[214] The DCT tubule has a variable diameter and contains one type of cell with more nuclear profiles than are seen in the proximal convoluted tubule (Fig. 1.27). The DCT extends from the CTAL to the CNT. The cells lining the DCT have short, bulbous luminal microvilli, but no regular brush border. The microvilli are more numerous than seen on the TAL cells, the CNT cells, or the principal cells of the CCD.[241] In humans, small lipid droplets are seen in the cytoplasm.[212] The endocytic apparatus is not well developed, but some vacuoles and numerous small vesicles are seen in the apical region. Dorup[241] describes four types of vesicles in these cells: intermediate vesicles (80 to 200 μm), which are generally uncoated; small vesicles with a mean diameter of 50 μm that are continuous with these intermediate vesicles; large vesicles (>200 μm); and tubular profiles (these being less frequent in DCT cells). Some rough-surfaced endoplasmic reticulum and lysosomes are also present in this segment. The cell nuclei occupy an apical position, because the basal two thirds of the cytoplasm is filled with extensive lateral interdigitating processes surrounded by basolateral cell membranes. These basolateral processes are filled with large elongated mitochondria that have their longitudinal axis perpendicular to the basement membrane. The presence of the large mitochondria lying adjacent to the basolateral cell membranes is consistent with the need for ATP for the continued active reabsorption of solute that occurs in this tubule (see Fig. 1.27). The volume of mitochondria in the DCT cells is larger than in the CNT cells or cortical collecting duct (CCT) cells.[241] An increased delivery of sodium to the DCT brings about an increase in the volume of the cell, in the mitochondrial volume, and in the proliferation of the basolateral membranes in the cells of the DCT, as well as in the CNT cells and the principal cells of the collecting ducts.[242–244]

The apical membrane of the DCT cells has numerous small microprojections. The tight junctions between the cells of the distal tubule are elaborate and are composed of multiple lines of membrane fusion,[245] a characteristic that correlates with the ability of the cells to maintain a large

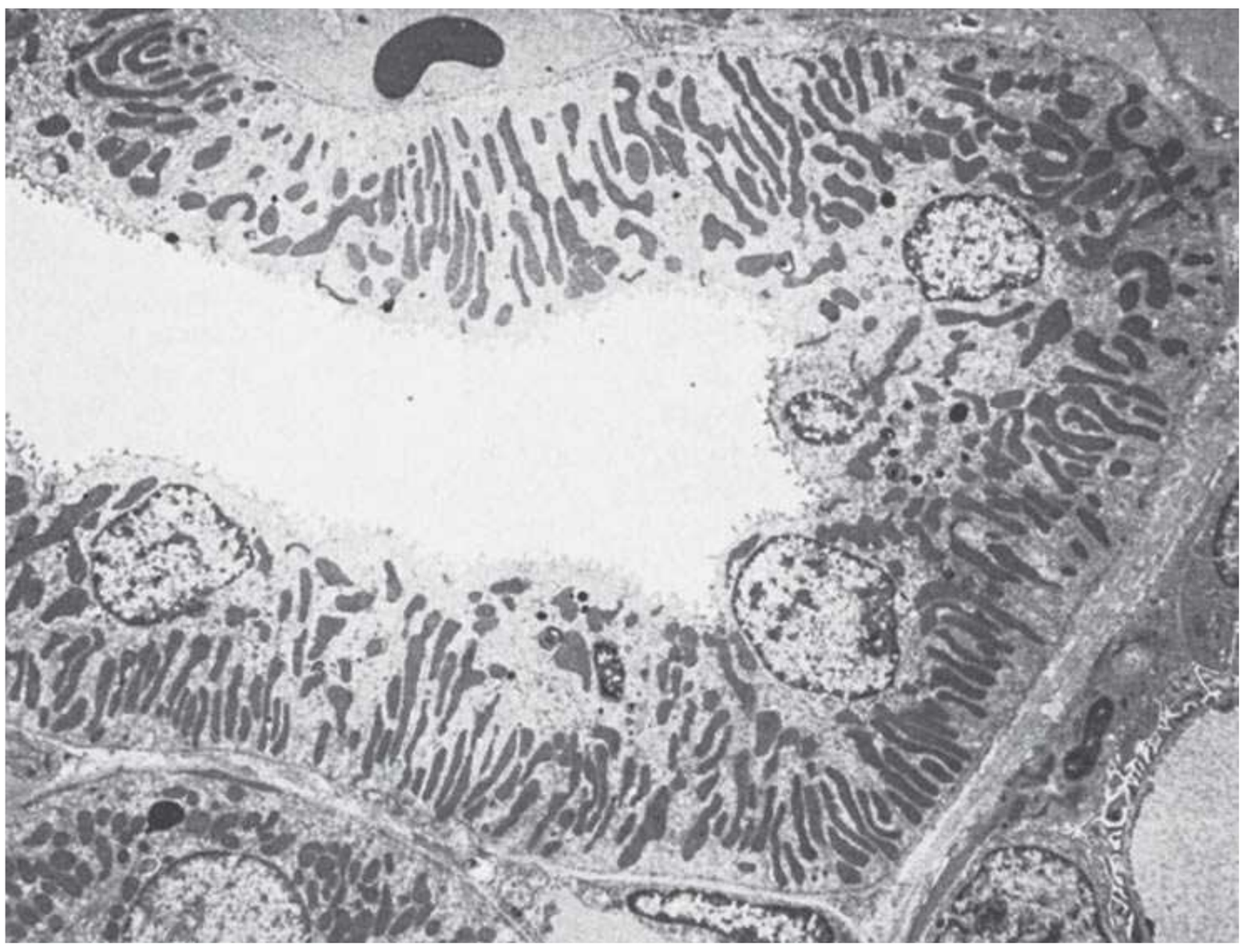

FIGURE 1.27 Transmission electron micrograph from a rat distal convoluted tubule showing the numerous mitochondria within interdigitating processes. (Magnification ×2,850.)

electrochemical gradient. The DCT reabsorbs NaCl against a steep chemical gradient and, as expected for such a sodium-absorbing epithelium, contains abundant Na^+-K^+-ATPase on its basal lateral cell membrane.[233,246,247] DCT proliferation and basolateral membrane amplification occur when active sodium reabsorption increases.[248,249] Kaissling et al.[250] increased the NaCl load to this segment by administering furosemide and demonstrated a marked adaptive increase in the basolateral membrane in the DCT.

In rabbits, an abrupt transition is seen from the distal tubule to the connecting piece of the nephrons.[158] The situation is less clear in other species, in which the transition does not appear to be either as abrupt or as completely studied. Recent studies by Biner et al.[251] used immunohistochemistry to localize the various transport systems along the human cortical distal nephron. The DCT demonstrates luminal thiazide-sensitive sodium-chloride cotransporter (NCC). The NCC overlaps with epithelial sodium chloride channels (ENaC) for a short region at the end of the DCT. IC cells were interspersed among the DCT cells near the end of the DCT. (For more detailed information, see recent reviews from the groups of Kaissling[251,252] and Bachmann.[253])

The Connecting Tubule

The CNT forms the next region of the distal nephron and lies between the DCT and the collecting duct system. At the present time, the CNT may be best classified as part of the DCT because it appears to be derived from the metanephric blastema.[4] Peter[7] believed that the arcades arise from the ureteric bud, whereas Oliver,[5] Potter,[254] and, more recently, Neiss,[4] all believe that the metanephric blastema is the correct source. However, Howie et al.,[255] using immunohistologic methods with substances related to the ABO blood groups, various cytokines, and Tamm–Horsfall protein, found that the ureteric bud and the connecting piece express the same antigens. The morphology of the CNT cells appears to have features of both the DCT cells, such as some degree of lateral interdigitations that contain mitochondria, but also has features of the CCD cells, such as the presence of more true basal infoldings (Fig. 1.28). Because of the intermixing of DCT cells, CNT cells, IC cells, and principal cells of the CCD in some species, such as rats and mice, there is a gradual transition from the DCT to the CNT in these species.[213,217] Neiss[4] demonstrated that IC cells (also called dark cells) in the CNT arose from the metanephric blastema, whereas the IC cells found in the collecting duct arose from the ureteric bud. Kim et al.,[256] using specific antibodies to carbonic anhydrase II, H^+-ATPase, and band-3 protein, demonstrated that IC appeared simultaneously in both the CNT and the medullary collecting duct. These IC cells differentiated from separate foci: one in the nephron (developing from the metanephric blastema) and one in the collecting duct (developing from the ureteric bud). When first identified, cells with distinct apical staining for H^+-ATPase (presumed to be type A intercalated cells), as well as cells with distinct basolateral H^+-ATPase labeling

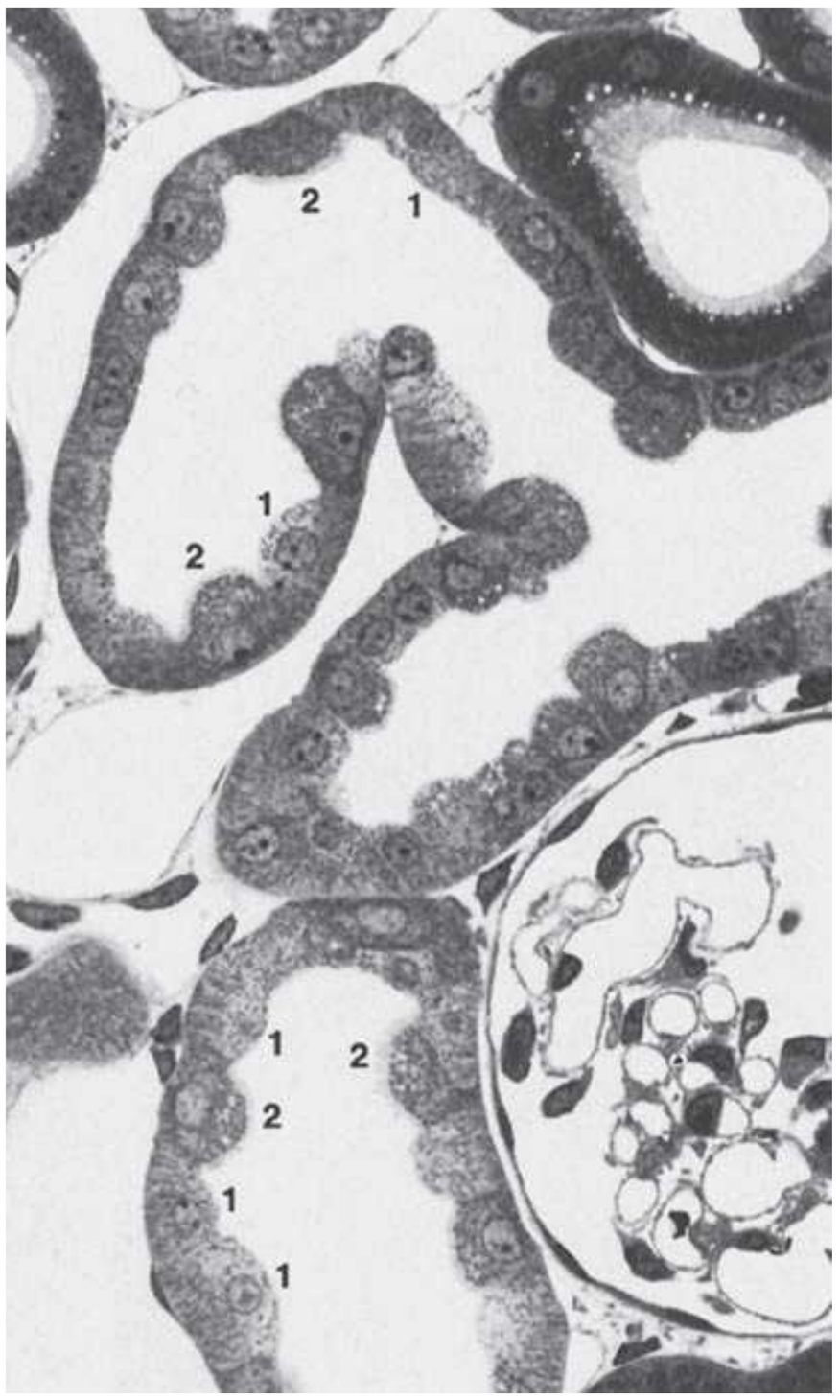

FIGURE 1.28 Light micrograph of the renal cortex (rabbit) showing a connecting tubule composed of connecting tubule cells (*1*) and intercalated cells (*2*). (Magnification ×900.) (From Kaissling B, Zurich, with permission.)

(presumed to be type B intercalated cells), were observed seemingly being developed from two embryologically distinct parts of the kidney. Some of these IC cells in certain locations subsequently disappeared.[256]

The CNT of superficial nephrons are short and drain individually into the collecting duct (some classify the point of junction as the initial collecting duct). CNTs of juxtamedullary and some midcortical nephrons generally form arched collecting ducts in many species. The arched duct starts deep within the cortex with the conversion and confluence of several DCT into the arcade and then ascends, while collecting parts of other nephrons, before the duct turns and enters a medullary ray. This arched duct results from an early embryonic type of nephron induction.[4,7] The number of nephrons that empty directly into the CCD, compared with the number that enter first into an arched tubule, varies with the species.[5] Both types occur in humans.

Two types of cells generally line the CNT, although intermixing of these two cell types with cells of other cell types, such as the DCT cells and the principal cells of the CD, are seen in some species. The two main types of cells

seen are CNT and IC cells (Fig. 1.28). The CNT cells appear to be characterized mainly by extensive true infoldings of the basal cell membrane, which can extend quite deeply into the cytoplasm. However, basolateral interdigitations have also been described, but are less pronounced than seen in DCT cells.[241] In rabbits, the plicated membranes can reach the apical cytoplasm.[158] Stanton et al.[244] demonstrated a striking increase in basolateral membranes in the rat CNT and the initial CCD of potassium-adapted animals, indicating that potassium is secreted by the CNT cells, as well as the principal cells of the (initial) collecting duct. In this study, no changes were seen in the IC cells. This suggests that potassium is secreted by the CNT cell and the principal cell of the initial collecting duct.[244,257]

The basolateral membranes of CNT cells are partially separated by mitochondria, which are smaller, more randomly distributed, and less numerous than those found in the DCT. The volume density of mitochondria in rat CNT cells was significantly lower than in the DCT cells.[241] This arrangement differs from principal cells of the collecting duct, in which the mitochondria are found mainly above the basal infoldings, not among the basolateral membranes. Microvilli on the apical surface tend to be slender and infrequent. Apical vesicles were about as frequent as seen in the DCT cells.[241] Mitochondria, the nucleus, and other cell organelles fill the apical cytoplasm. The CNT cells appear to exist in most species, including rats, mice,[212,217] and humans.[212]

Biner et al.[251] demonstrated an ENaC along the entire CNT in humans. The major part of the CNT also coexpresses aquaporin 2 with the ENaC. IC cells were identified interspersed among the CNT cells in the human. Loffing and Kaissling[258] reviewed the transport pathways along several mammalian distal nephrons and showed that ENaC was present along the CNT from the rabbit, rat, mouse, and human. Frindt et al.,[259] using patch clamp techniques in rat kidney tubule segments, demonstrated that the CNT could reabsorb sodium at a rate 10 times higher than that of the CCT. Using immunogold labeling and electron microscopy, aquaporin 2 (apical), 3, and 4 (basolateral) were all shown to be colocalized in CNT cells of rat.[260]

The CNT cell displays an amplification of basal cell membrane in rats[244] and rabbits[249] in situations in which there is a low Na^+ and high K^+ intake. This effect is axial along the tubule, being greatest at the early segment of the CNT and decreasing along its length.[249] The axial change in structure is paralleled by similar changes in Na^+-K^+-ATPase.[261]

The second cell type is the IC cells (or dark cells). Three types of IC cells have been described: type A involved with the secretion of protons into the lumen; type B involved with the secretion of bicarbonate into the tubular lumen; and non-A–non-B, which may be able to secrete both protons and bicarbonate into the tubular lumen. IC cells will be discussed under the collecting ducts, because these cells comprise such an important number of the cells lining the tubule in that region. Electrophysiologic studies in rabbits suggest that approximately 98% of the IC cells in the connecting tubule are the HCO_3^--secreting B type.[262]

THE COLLECTING DUCTS

The collecting ducts extend from the CNT through the medullary rays as CCDs. They then cross the outer and inner stripe of the outer medulla as well as the inner medulla, to empty their contents at the tip of the renal papillae. They include the CCDs (including the initial collecting ducts), the outer medullary collecting ducts (OMCDs), and the inner medullary collecting ducts (IMCDs).

The collecting ducts are the final regulators of fluid and electrolyte balance, playing roles in the handling of Na^+, Cl^-, K^+, and acid and base. Although there has been great emphasis on the role of the collecting ducts as the main controllers of urinary sodium and potassium excretion, Meneton et al.[263] stress the pivotal role played by both the late part of the DCT and the CNT, especially in situations that prevail in our current environment, in which the dietary sodium intake is high and the potassium intake is low. They propose that a large proportion of the aldosterone-regulated sodium reabsorption and potassium secretion occurs before the tubular fluid reaches the collecting duct. The difference between the function of the late DCT and the CNT compared to the collecting duct seems to be more quantitative than qualitative, with a large proportion of the aldosterone-regulated sodium reabsorption and potassium secretion being done in the late DCT and CNT. The collecting duct would function mainly when the requirement for sodium and water conservation is maximal and the upstream segments are overloaded by diet or some genetic defect.

The collecting ducts are lined by two types of cells: collecting duct principal (light) cells and intercalated (dark) cells (Figs. 1.29 and 1.30). About 30% of CCD cells are IC cells in rat.[264] Kaissling and Kriz[158] estimate that rabbits have 33% IC cells in the CCD and 50% in the outer medullary collecting duct. About one-third of the cells lining the outer medullary collecting duct in the rat are IC cells.[265] The number of IC cells decreases as the collecting duct descends into the medulla and are absent below the first portion of the IMCD. The principal cells of the collecting duct gradually change in morphology as they descend toward the papilla. They increase in cell height and have more complex tight junctions, whereas the amount of basal infoldings and the number of mitochondria decrease. Fusions of the collecting ducts occur in the inner renal medulla to form the large papillary collecting ducts (ducts of Bellini). These large collecting ducts exit at the papillary tip in an area known as the area cribrosa.

The principal cells of the collecting duct in the cortex are cuboidal in humans[218] and low cuboidal in rats (see Fig. 1.29). They form the most numerous cell types. They have a simple cell shape, with fairly straight lateral cell borders that have small interlocking projections. Their

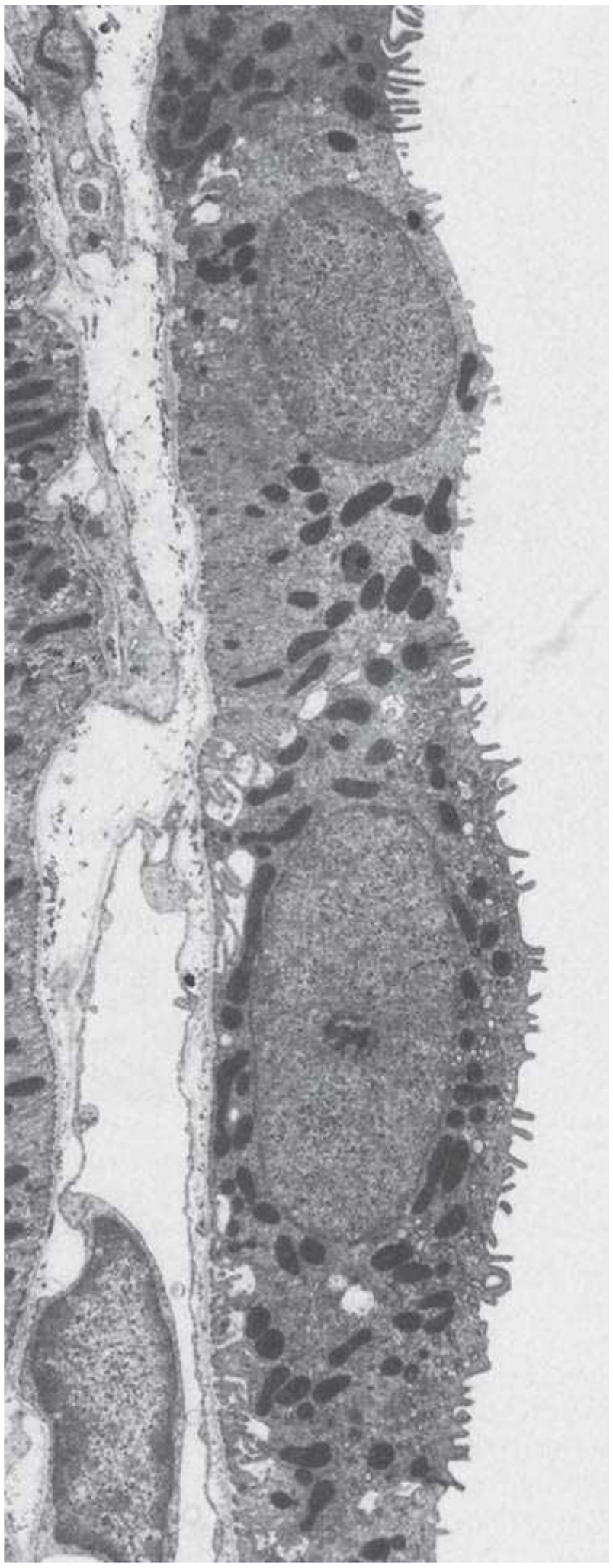

FIGURE 1.29 Transmission electron micrograph of the epithelium of a cortical collecting duct (rat) showing a collecting duct cell (principal cell) (*above*) and an intercalated cell (A-type) (*below*). Note the basal infoldings in the collecting duct cell and the apical vesicles in the intercalated cell. (Magnification ×5,000.)

pale-staining cytoplasm contains a few small, oval, randomly oriented mitochondria and other organelles, and the nucleus is situated in the middle to upper one-half of the cell in the cortex. The luminal surface is generally smooth with a few short microvilli and a single cilium. The basal surface is characterized by true basal infoldings, with few lateral interdigitations. The amplification factor of basolateral membranes was significantly lower than in the CNT cells.[241] Because these infoldings are short and closely spaced, they do not have mitochondria lying between them. The mitochondria are located mainly above the infoldings and in the apical cytoplasm, which contained few intermediate and small vesicles, tubular profiles, and large vesicles.[241] The tight junctions are deep,[223,266] and the apical surface has a prominent glycocalyx.[267]

Conditions that increase potassium secretion, such as potassium adaptation or high endogenous or exogenous mineralocorticoid levels, bring about dramatic increases in these basal cell membrane infoldings.[249,262,268,269] For example, striking increases in the basolateral membranes of the principal cells of the initial segment of the collecting duct have been demonstrated in potassium-adapted animals.[244] In addition, the principal cells in rats showed a 35% decrease in the basolateral membranes in adrenalectomized animals that was restored to control levels by the administration of physiologic amounts of aldosterone, but not of glucocorticoids.[270] In addition, increasing the dose of aldosterone over control levels caused an increase in the basolateral membranes by 111% compared with controls. They did not note changes in the luminal membranes of the principal cells.[270] These

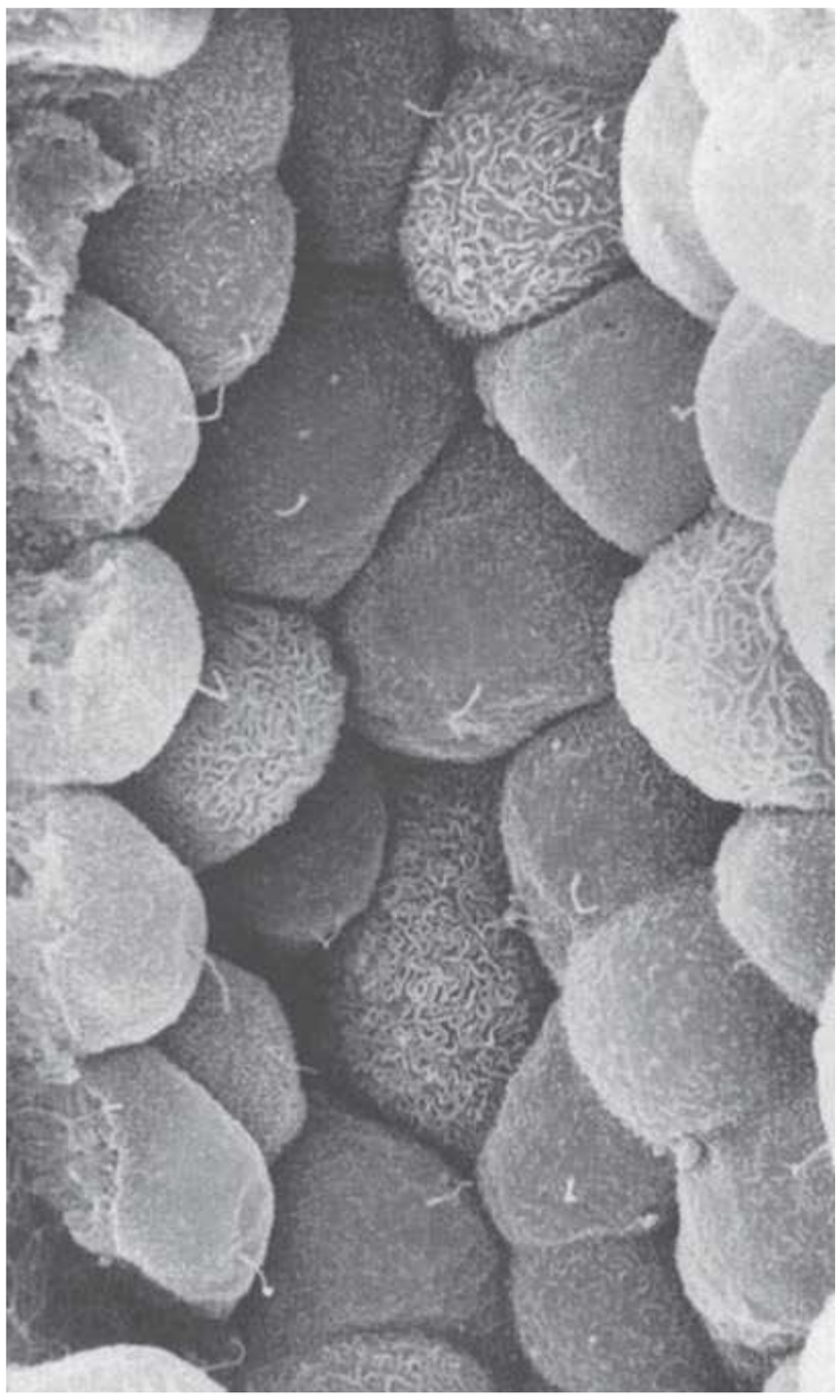

FIGURE 1.30 Scanning electron micrograph of a cortical collecting duct (rat) showing the apical aspect of collecting duct cells (with an apical cilium) and intercalated cells (with apical microfolds). (Magnification ×2,400.)

studies provide evidence that principal cells in the collecting duct are involved with potassium secretion.

The collecting duct responds to ADH by an increase in water permeability. The principal cells are vasopressin sensitive and show dramatic increases in water permeability of the apical membrane. Sun et al.[271] have demonstrated direct evidence that AQP2 on principal cells is located in clathrin-coated pits that recycle between the plasma membrane and intracellular vesicles in response to the availability of ADH. The mechanisms underlying these changes are discussed in detail later in this chapter.

Biner et al.,[251] using immunohistochemical localization techniques on human kidney, demonstrated the presence of an amiloride-sensitive ENaC and AQP2 activity on collecting duct principal cells. Loffing et al.[272] using immunohistochemistry in rabbit kidney cortex, demonstrated that ENaC is found in the CNT cells and the CCD cells. The ENaC shifted from the apical membrane in the upstream CNT cells to a cytoplasmic location downstream in the CNT and CCD cells. In the rabbit, the AQP2 was seen only on the CCD cells. The apical membranes of the collecting duct principal cells of humans contain ENaC and AQP2, whereas the basal membranes contain Na^+-K^+-ATPase and aquaporins 3 (AQP3) and 4 (AQP4); hence, the CCD plays a critical role in the concentration of urine. The CCD also responds to the mineralocorticoid aldosterone.[273]

The collecting duct cells undergo gradual, although considerable, changes from the cortex downstream to the upper one-third of the inner medulla.[158,218] The cells of the outer medulla include principal cells similar to those seen in the cortex; however, the cells become taller with decreasing concentrations of several cellular organelles and basal infoldings. IC cells similar to type A are found in the outer medulla. From the deeper cortical levels downward into the inner medullary region, the basal labyrinth of the principal cells continues to decrease gradually, with a steeper reduction within the outer stripe.[158,215,218] The number of mitochondria also continues to decrease, whereas lysosomal elements and apical-coated vesicles seem to increase. The density of the cytoskeletal network lying under the apical cell membrane becomes more prominent and the tight junctional belt becomes deeper.[158]

From the second one-third of the inner medulla, collecting duct cell size increases steeply. These tall IMCD cells are distinct from collecting duct cells upstream according to several criteria[213,220,274] (Fig. 1.31). Their luminal membrane is covered by numerous stubby microvilli and lacks the central cilium. The lateral intercellular spaces are more extensively developed and are prominent by their dense assembly of microvilli and microfolds projecting from the lateral cell membranes. A prominent feature of principal cells of the last one-third of IMCDs is the expression of the ADH-sensitive

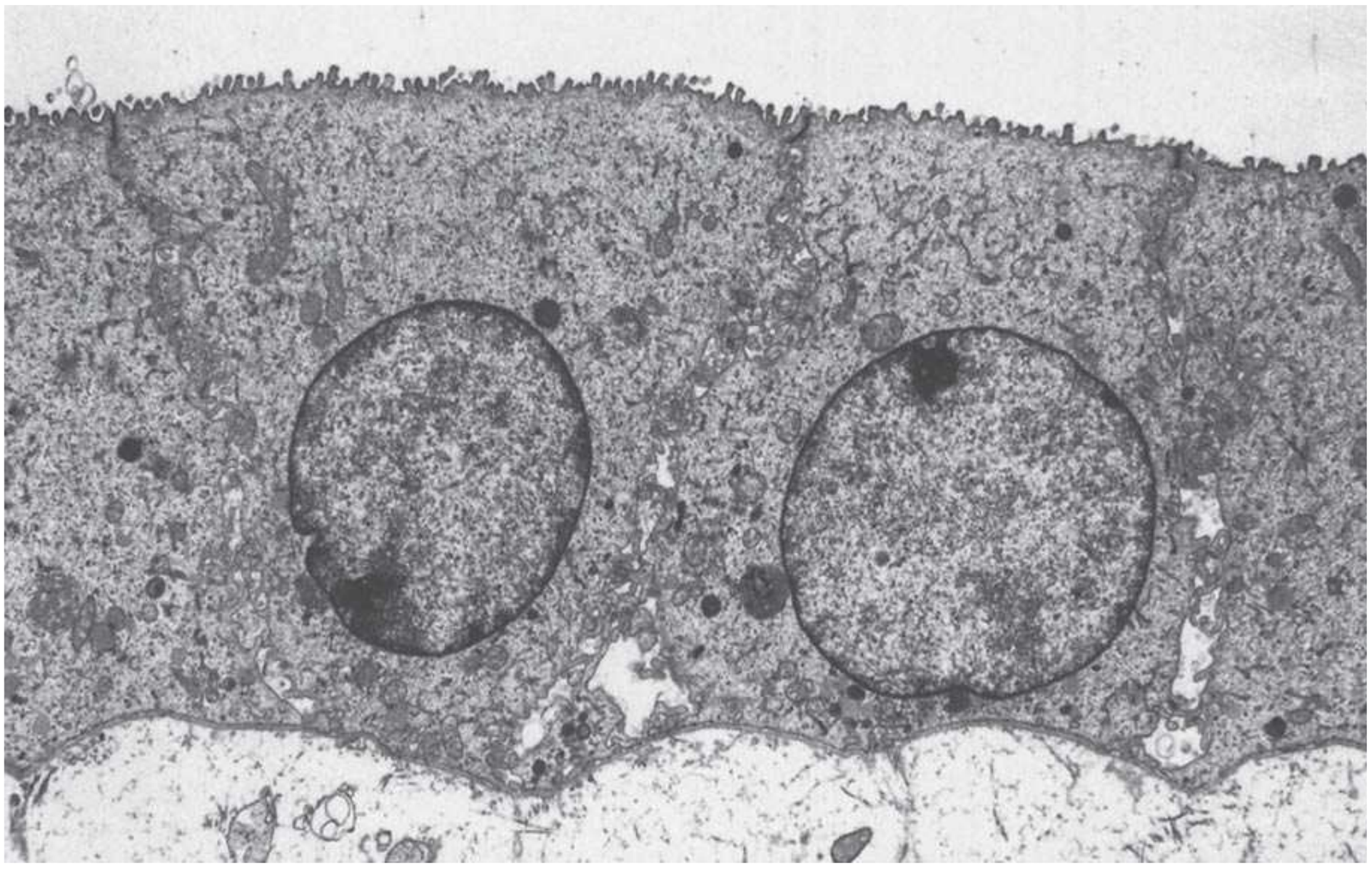

FIGURE 1.31 Transmission electron micrograph of the inner medullary collecting duct epithelium (rat) showing the high inner medullary collecting duct cells with many stubby microvilli of the luminal membrane and prominent lateral intercellular spaces filled with lateral microfolds. (Magnification ×15,500.)

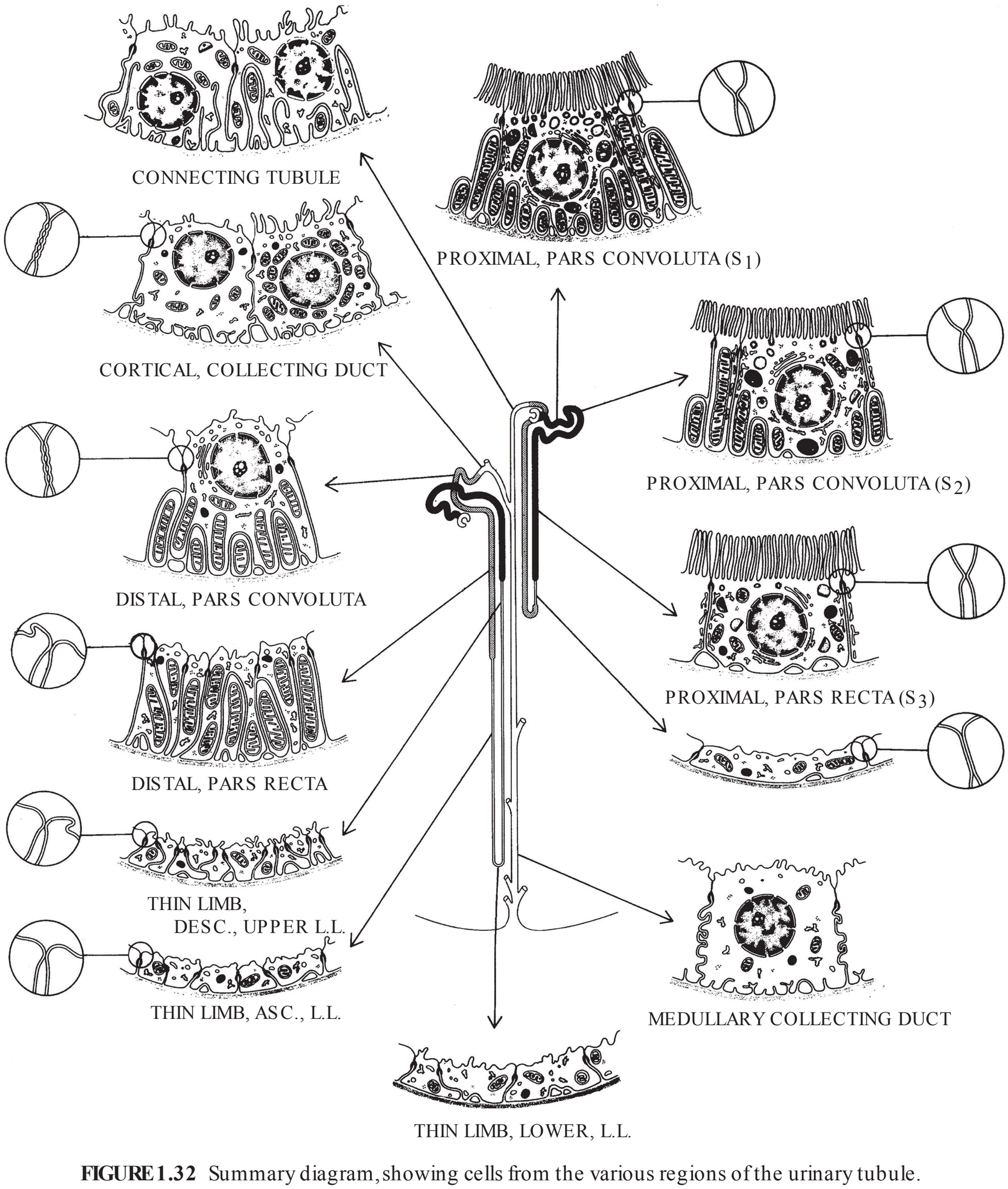

FIGURE 1.32 Summary diagram, showing cells from the various regions of the urinary tubule.

urea transporter UT-A1.[193,275] In most other respects, IMCD cells resemble the other collecting duct cells. The morphology of the various regions of the renal tubule is summarized in Figure 1.32.

Intercalated Cells

IC cells have long been identified in CCDs in a variety of species such as rats,[213,217,264,276–279] mice,[264,280] humans,[218,251] and rabbits[158,248,256,281–283] (Figs. 1.29 and 1.33). It has become obvious that IC cells are not only found in the CCD but, depending on the species, in the latter region of the DCT in humans[218,251,278] and rat,[217,241,265,278] in the connecting tubule in rabbits[158,248] and humans,[251] in the CCD (as listed previously), in the outer medullary collecting ducts in rats,[265] and in the upper part of the inner medullary cells in rats and rabbits.[158] IC cells constitute about 37% to 40% of the cells in CCD in rats and rabbits.[265,280,283] Kaissling and Kriz[158] estimate that rabbits have 33% IC cells in the CCD and 50% in the outer medullary collecting duct, whereas Hansen et al.[265] estimate that 36% to 40% of IC cells are present in the outer medullary collecting ducts in rat. IC cells show a slow decrease in the upper part of the IMCD in rats.[283]

IC cells (Fig. 1.33) are sometimes called dark cells because their cytoplasm stains more densely. They exhibit

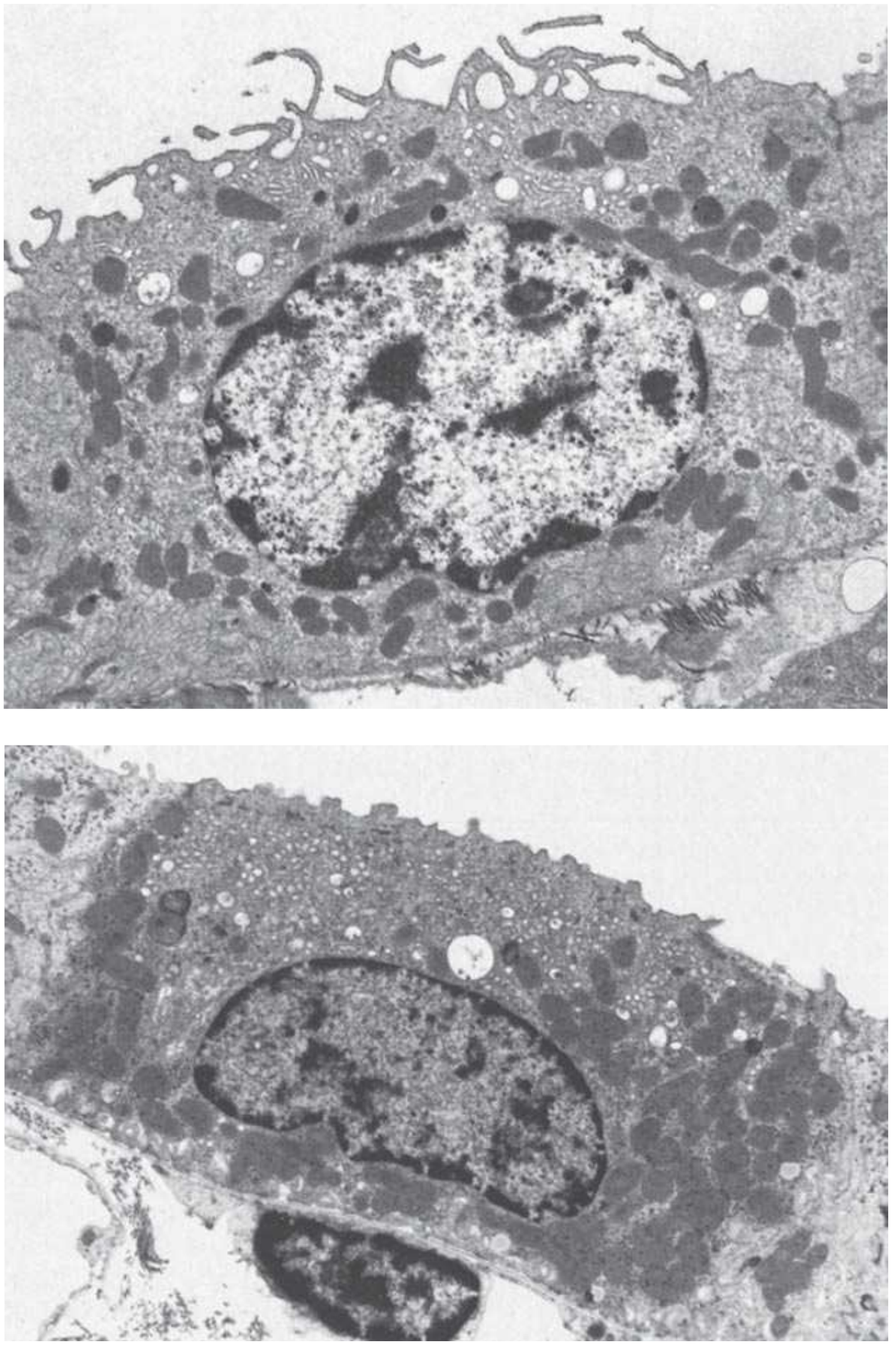

FIGURE 1.33 Transmission electron micrographs of intercalated cells (rat). **A:** Type A exhibiting apical microfolds and flat vesicles in the apical cytoplasm. (Magnification ×6,800.) **B:** Type B showing a rather smooth apical surface, many small round vesicles, and mitochondria located predominantly in the lateral and basal parts of the cell. (Magnification ×6,800.)

significant structural heterogeneity even within a single segment of the collecting duct. IC cells can also be distinguished from principal cells by differences in cell shape, cytochemical staining, and uptake of the pH-sensitive fluoroprobe, 2′,7′-bis(carboxyethyl)—5,6-carboxyfluorescein (BCECF). IC cells have a more circular, rather than hexagonal, profile that bulges into the tubule lumen when observed in isolated perfused tubules by means of interference-contrast optics. In rabbits, IC cells can be identified by positive staining with peanut lectin[284,285] and by luminal uptake of acetoxymethyl BCECF.[285] The apical surface of the IC cell is frequently adorned by luminal extensions, which include microvilli and microridges (called microplicae). Basal membrane infoldings resemble those of the collecting duct cell.

Three types of IC cells have been defined morphologically and by immunohistochemical staining, including type A, type B, and non-A–non-B.[264,280] However, there is a striking difference in the number and distribution of the various types of IC cells from animal to animal and among the nephron segments of a particular species.[264] Carbonic anhydrase II immunoreactivity was seen in all IC cells, but type A stained more intensely than type B. The immunostaining in type A cells was pronounced in the apical cytoplasm and apical microprojections. In type B cells, the staining was more diffuse throughout the cytoplasm. In the non-A–non-B cells, the staining was also diffuse.[286]

Type A IC cells tend to have a more circular apical cell profile,[278] a centrally placed nucleus, prominent apical microvilli and microplicae extending from the apical plasma membrane, and prominent apical cytoplasmic tubulovesicular

profiles (see Fig. 1.33A). Mitochondria are numerous and can be located above the nucleus, as well as between the nucleus and the basal membrane infoldings. Using freeze-fracture techniques, there are rod-shaped particles and studs present on the cytoplasmic face of the apical plasmalemma and on the tubulovesicular profiles in the IC cells of the CCD and the outer medullary collecting ducts.[280,287,288] H^+-ATPase is expressed on the apical plasma membrane and in the cytoplasmic tubulovesicular and vesicular profiles of type A IC cells. (See review of renal vacuolar H^+-ATPase.[289])

Verlander et al.[278] showed that IC cells in animals with respiratory acidosis show a striking increase in apical microprojections and tubulovesicular profiles as well as an increase in surface density of the apical plasma membrane. However, no changes were seen with the number of IC cells. When there was a stimulation of bicarbonate secretion in rats, Verlander and associates[288] documented a withdrawal of the marker for H^+-ATPase from the apical plasma membrane with its storage in apical cytoplasmic vesicles in IC cells in both the CCD and the OMCD. H^+-ATPase activity appeared to be inserted into the basal plasma membrane of type B IC cells.[288]

Luminal and/or tubulovesicular membranes exhibit two specific types of particles. Large club-shaped particles called "studs" have been observed on the cytoplasmic surface of the tubulovesicular structures on the cytoplasmic side of the apical plasma membrane; the rapid-freeze, deep-etch technique shows 10-μm spherical structures composed of multiple subunits and arranged in paracrystalline hexagonal arrays.[290] Brown et al.[291] have presented evidence that the studlike material coating the vesicles contains cytoplasmic domains of the proton-pumping H^+-ATPase. On the basis of both morphologic characteristics and immunocytochemistry, the structures appear to be (or related to) the vacuolar-type H^+-ATPase.[277,291] In addition, freeze-fracture studies have shown the presence of rod-shaped particles in vesicles and cell surface membranes,[292] which may form a component of this H^+-ATPase. Changes in membrane structure have been shown to be related to proton secretion.[248,261] When H^+ secretion is stimulated, cytoplasmic vesicles bearing rod-shaped intramembranous particles (IMPs) fuse with the apical plasma membrane, inserting IMPs into the membrane.

This supports the idea that type A IC cells demonstrate net excretion of protons into the tubular lumen that is accomplished by the vacuolar H^+-ATPase located in the apical plasma membrane and apical tubulovesicular profiles.[264,277,280,288,293,294] For this process, it has been suggested that the hydrogen ions are produced by cytosolic carbonic anhydrase in CNT cells and CCD cells of the mouse and rat[264,280,286,294,295] and human.[251,296,297] The bicarbonate that is generated is released by a band 3-like Cl^-/HCO_3^- exchanger AE1, located in the basolateral plasma membrane, into the interstitium at the base of the cell.

Medullary IC cells from rats fed a diet with a high K^+ content had a small luminal membrane area and a cell apex with numerous vesicles. The ingestion of a low K^+ diet led to an increased luminal membrane area with few apical vesicles.[268] It has, therefore, been postulated that IC cells function in potassium reabsorption.

A similar increase in the apical plasma membrane with a decrease in tubulovesicular profiles was seen in IC cells of the outer medulla in chronic metabolic acidosis[298] and acute respiratory acidosis in rats.[299] In respiratory acidosis, a marked increase in apical microprojections was seen as was an increase in the surface density of the apical membrane of type A cells. No changes were seen with type B cells in rat CCD.[278] Madsen and Tisher[213] postulated that hydrogen ion pumps located in the apical vesicles had been inserted into the apical cell membrane by vesicle fusion with the apical membrane.

Type B IC cells are present in the CCD and the CT of rats,[276,278,286,300] mice,[264,280] and rabbits.[230,256,281,301] The type B cell (Fig. 1.33B) has an angular outline[278] and a relatively smooth apical plasma membrane with short sparse microvilli (without rod-shaped studs in the apical membrane).[280] The apical membrane generally lacks studs, but the basolateral membrane exhibits studs.[278] The nucleus lies in an eccentric position and the numerous small mitochondria are densely packed and are concentrated at the basal part of the cytoplasm. The cytoplasm and the organelles stain more densely in light and electron microscopy. Cytoplasmic vesicles (mostly noncoated) are seen throughout the cell cytoplasm. In the type B cells, the H^+-ATPase is expressed in the basolateral plasma membrane and in the cytoplasmic vesicles throughout the cells.[277,280,291,300,302–305] Using freeze-fracture techniques, rod-shaped rectangular particles are found on the basal membranes in these cells and not on the apical plasma membrane.[277,300] The basal hydrogen ion secretion is thought to mediate HCO_3^- secretion into the luminal fluid by an apical Cl^-/HCO_3^- exchanger different from AE1.[256,264]

One candidate for this anion exchanger is pendrin, a Na^+-independent Cl^-/HCO_3^- exchanger. Quentin et al.[306] have shown that the Cl^-/HCO_3^- exchanger pendrin in rat kidney is specifically regulated in response to chloride balance independent of sodium and acid/base balance. Using a mouse model, Wall et al.[307] demonstrated that pendrin protein was localized in the apical cytoplasmic vesicles in both type B and non-A–non-B IC cells from a subset of cells in the DCT, the type B cells in the CNT, and the CCD. Pendrin mRNA was expressed mainly in the cortex. Pendrin immunoreactivity was highest in the apical cytoplasmic vesicles, although there was little immunogold staining along the apical plasma membrane of type B IC cells, but non-A–non-B IC cells had intense pendrin immunoreactivity along the apical plasma membrane. Kim et al.,[308] using immunoelectron microscopy, demonstrated pendrin in both the apical plasma membrane and intracellular vesicles throughout the cell. Kim et al.[286] found the carbonic anhydrase activity more diffuse in the cytoplasm of type B than type A cells.

The third type of IC cell is non-A–non-B cells that have been identified in the CT and the CCD of rats[264,276,286,309] and mice.[264,276,280] Non-A–non-B cells have vacuolar

type H^+-ATPase in both apical plasma membranes and apical vesicles, but do not have the basolateral band 3-like immunoreactivity of AE1.[264] In rabbits and mice, most non-A–non-B cells in the collecting duct have an electroneutral Na-independent Cl^-/HCO_3^- exchanger in the apical membrane.[264] Pendrin immunoreactivity is intense along the apical membrane, as well as being present in apical vesicles in some cells in the DCT, in the CNT, and CT.[307] Because both pendrin immunoreactivity and pendrin-mediated HCO_3^- secretion are present in the apical plasma membrane and apical intracellular vesicles in type B and non-A–non-B IC cells, Kim et al.[308] suggest that HCO_3^- secretion could be regulated by trafficking of pendrin between the two membraneous compartments. In addition, since non-A–non B cells seem capable of both apical HCO_3^- and H^+ secretion, the simultaneous secretion of both HCO_3^- in exchange for Cl^- and proton secretion mediated by electrogenic H^+-ATPase, would cause chloride reabsorption with no change in acid/base status.[308]

THE JUXTAGLOMERULAR APPARATUS

At the vascular pole of the renal corpuscle, the macula densa region of the CTAL comes into close proximity to the efferent and afferent arterioles and a group of cells called the extraglomerular mesangium.[310,311] The juxtaglomerular apparatus consists of four parts (Figs. 1.5 and 1.34): (1) a plaque of cells in the wall of the CTAL of the distal nephron in the region of the vascular pole of a renal corpuscle, called the "macula densa"; (2) the termination of the afferent arteriole as it enters this renal corpuscle; (3) the initiation of the efferent arteriole as it exits from the same renal corpuscle; and (4) a cone-shaped region of extraglomerular mesangial cells (also called the lacis, Polkissen, or Goomaghtigh cells) lying in the space between the macula densa and the two arterioles. This area receives a rich supply of sympathetic nerve endings.

In the human kidney, 40% of the basal lamina region of the macula densa lies adjacent to the base of the cone-shaped extraglomerular mesangium, 10% of the macula densa basal lamina is in contact with the afferent arteriole, and 5% is in contact with the efferent arteriole.[308]

The MD consists of the cells in the wall of the CTAL of the distal tubule, which lies adjacent to the glomerular vascular pole. The MD appears as a dense spot upon hematoxylin and eosin staining because the cells are narrow and the nuclei are close together. MD cells (Fig. 1.35) are not interdigitated with each other by large lateral cell processes, as in other regions of the distal tubule. In contrast, the lateral intercellular spaces between MD cells extend very straight in an apical–basal direction—their width appears to vary according to function.[312] The mitochondria are shorter and more randomly arranged. The Golgi apparatus lies on the basal side of the nucleus. The basal aspect of the MD touches

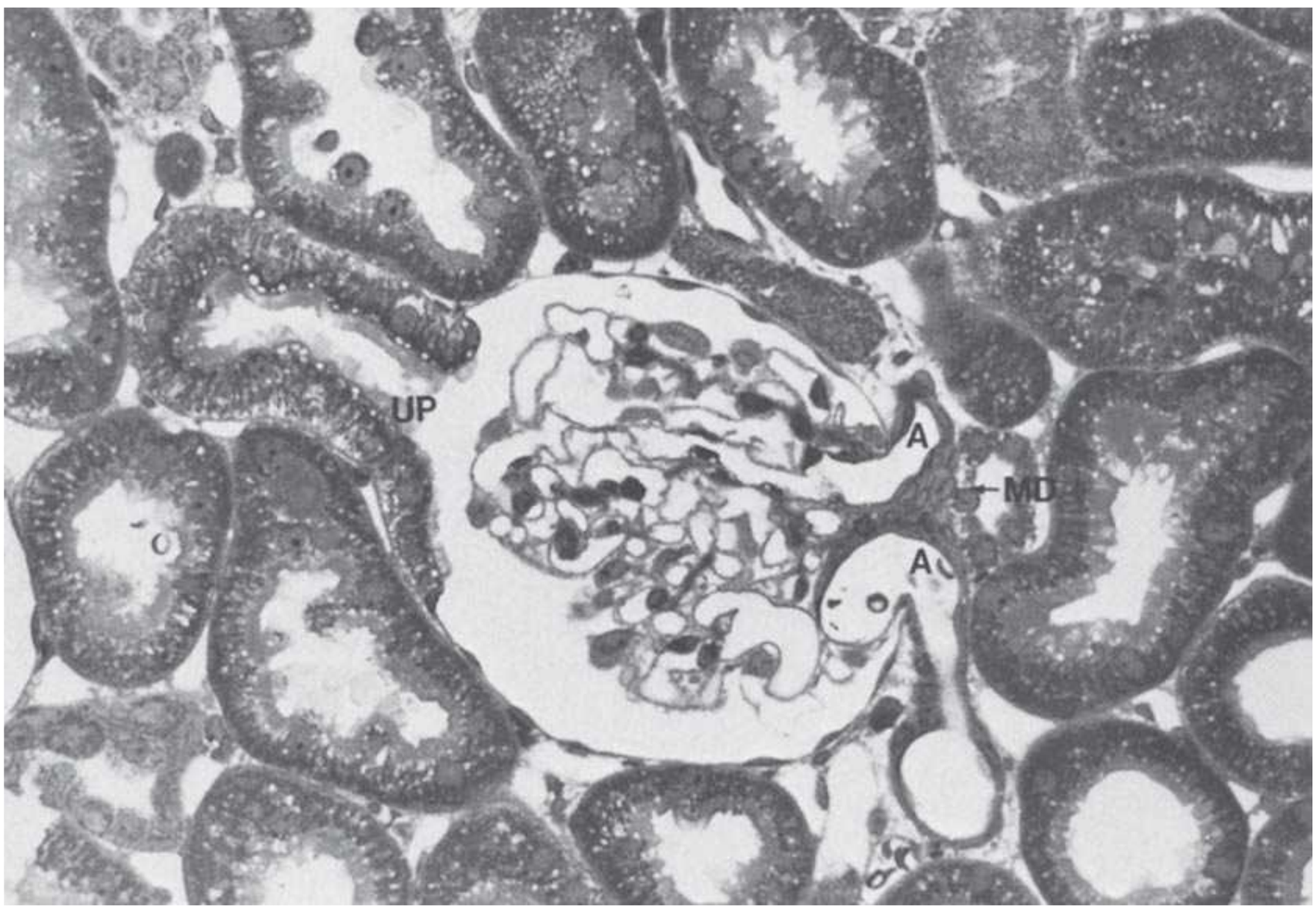

FIGURE 1.34 Light micrograph of a renal corpuscle with both urinary and vascular poles in the section. The juxtaglomerular apparatus contains the macula densa (*MD*), the two arterioles (*A*), and the extraglomerular mesangium (between the *A*s). The urinary pole (*UP*) is also apparent. (Magnification ×13,000.) (From Dobyan D, with permission.)

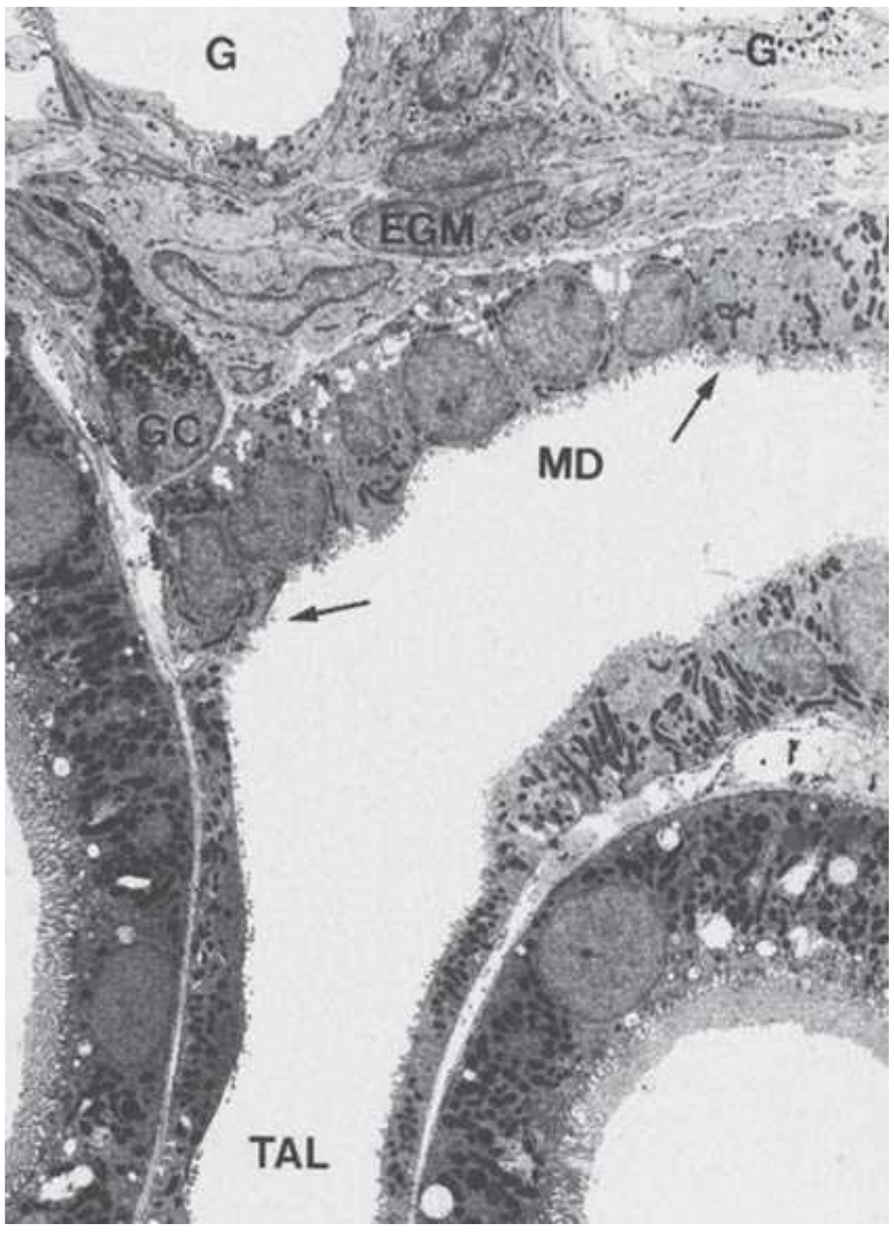

FIGURE 1.35 Transmission electron micrograph of the juxtaglomerular apparatus (rat). The transition of the thick ascending limb (*TAL*) into the macula densa (*MD*) is seen; the basal aspect of the macula densa abuts the extraglomerular mesangium (*EGM*) and also a granular cell (*GC*). *G*, glomerulus. (Magnification ×1,900.)

the extraglomerular mesangium. Additional, but variable, contacts are found with the efferent as well as the afferent arterioles.[13] The most conspicuous difference of MD cells to any other cells of the nephron is the occurrence of nitric oxide synthase I (see Fig. 1.37C).[313,314] A prominent feature of the MD is also the expression of cyclooxygenase-2.[315]

Modified smooth muscle cells in the wall of the afferent arterioles, called granular cells (formerly also called juxtaglomerular cells), contain specific membrane-bound granules (Fig. 1.36). In situ hybridization[316] and immunocytochemistry [317] have shown that these cells synthesize renin (Fig. 1.37A), which is then stored in granular form (Figs. 1.36B and 1.37B). The granules stain with the Bowie method and have a positive periodic acid-Schiff reaction. Like other smooth muscle cells, the juxtaglomerular cells also contain intracellular filaments and dense bodies, but they have more cisternae of rough-surfaced endoplasmic reticulum, a large Golgi apparatus, and mature and immature secretory granules in their cytoplasm, consistent with the ability of these cells to synthesize small peptides. The immature granules appear to have a paracrystalline structure.[80,318] The secretory product is released by exocytosis into the extracellular space within or surrounding the wall of the arteriole.[319,320] Processes of the juxtaglomerular cells contact the surrounding cells as well as the endothelial cells by means of gap junctions.[321]

The extraglomerular mesangium[310] (Goormaghtigh cells, polar cushion, Polkissen cells, and lacis cells) fills the area between the afferent and efferent arterioles and the MD (see Figs. 1.5 and 1.35). It is composed of nongranulated cells that are continuous with granular cells and smooth muscle cells of the arteriolar walls and with the intraglomerular mesangial cells.[310] The extraglomerular mesangial cells are "flatly pressed" cylinders with both ends splitting into a group of parallel processes. These extraglomerular mesangial cells are surrounded by abundant extracellular matrix. Numerous gap junctions occur between the processes of the same cell, with adjacent smooth muscle cells, with granular cells, and at the renal hilus with intraglomerular mesangial cells.[240,322,323]

The initmate and systematic juxtaposition of tubular and vascular cells within the JGA has given rise to early

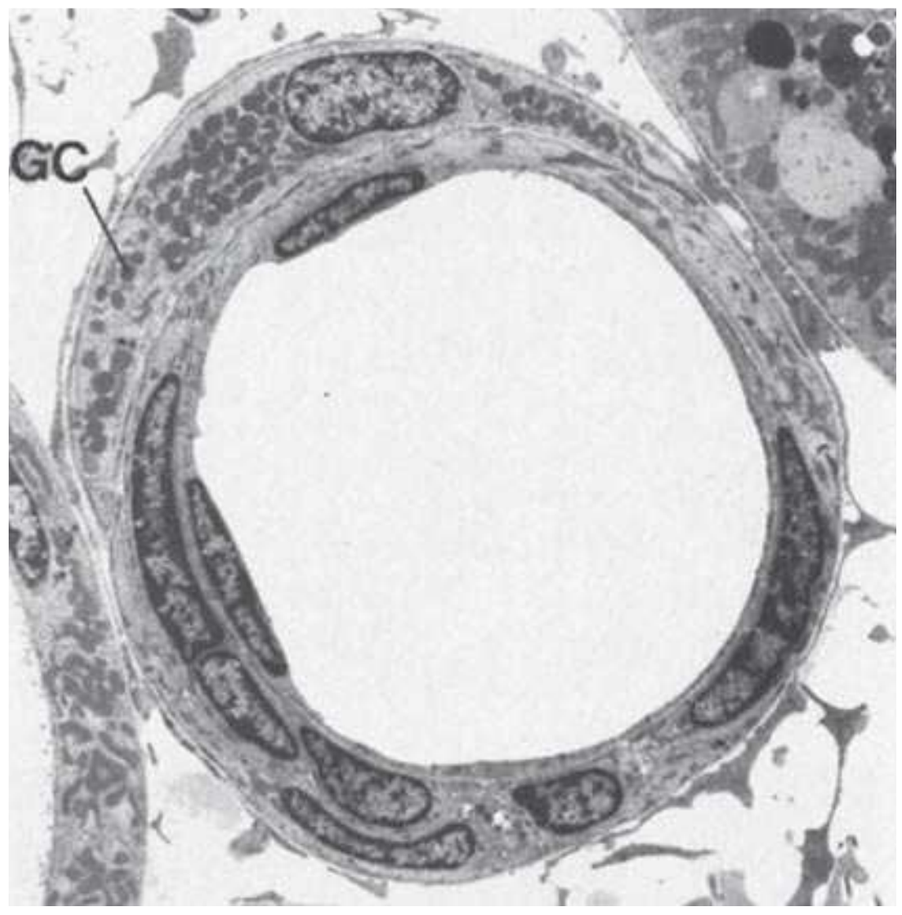

A

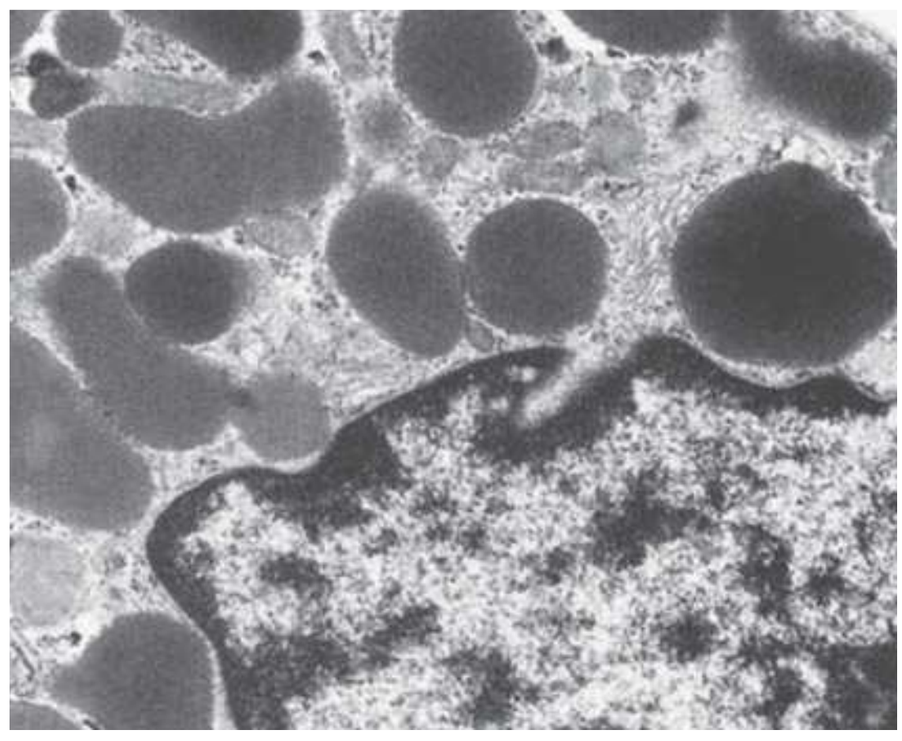

B

FIGURE 1.36 Transmission electron micrograph (rat). **A:** An afferent arteriole containing in its wall a granular cell (*GC*). (Magnification ×2,100.) **B:** Part of a granular cell containing in its cytoplasm specific membrane-bound granules. (Magnification ×14,500.)

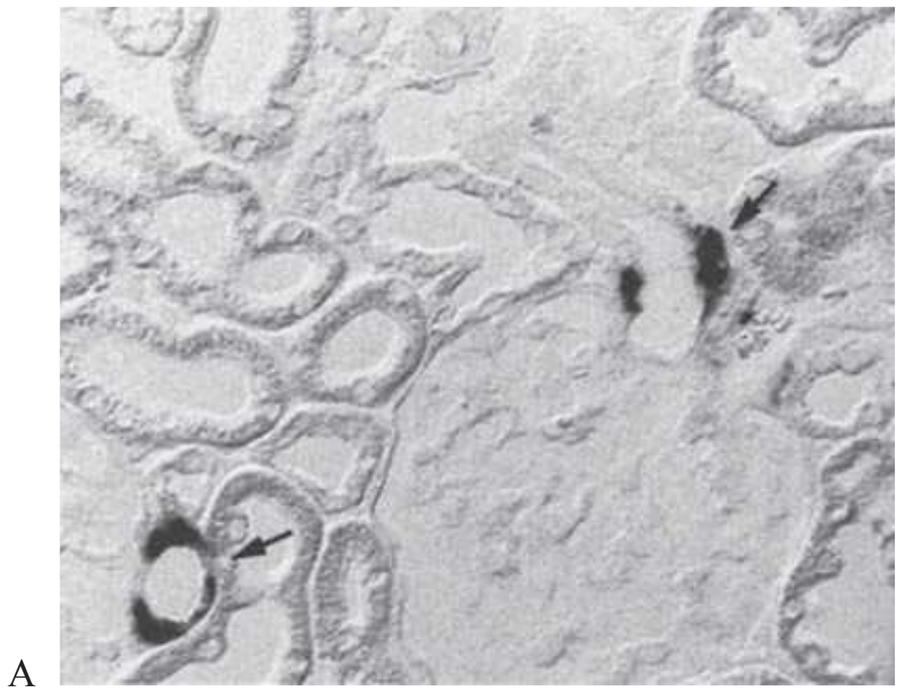

A

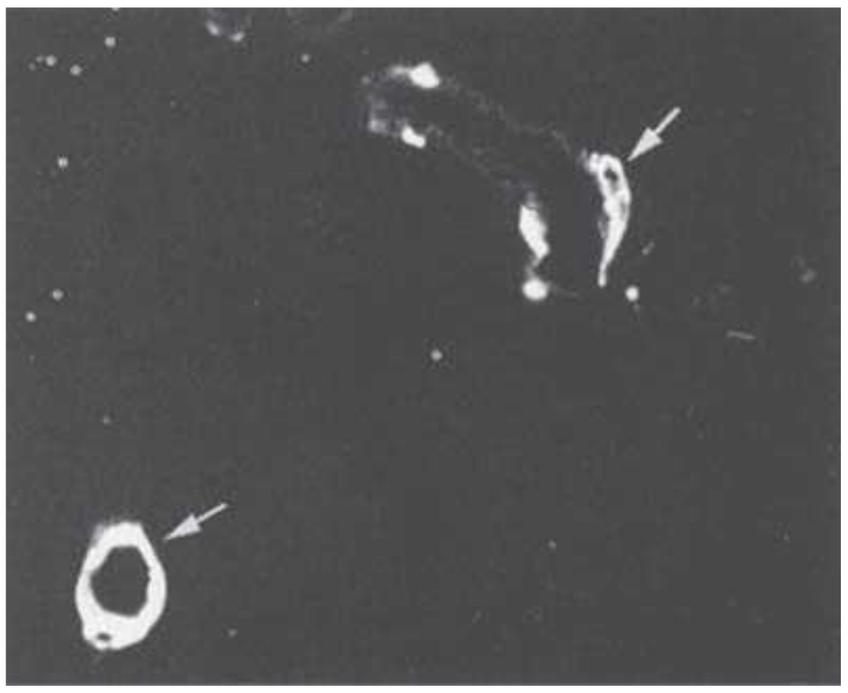

B

C

FIGURE 1.37 Rat kidney containing granular cells in afferent arterioles (*arrows*) of two glomeruli. The two pictures show that renin is synthesized **(A)** and stored **(B)** in the same cells (same section). **A:** In situ hybridization using a 330-bp rat renin riboprobe (*cRNA*) labeled with digoxygenin (detection system: alkaline phosphatase). **B:** Immunocytochemistry using a rabbit polyclonal antirat renin antibody (detection system: Texas red coupled second antibody). (From Bachmann S, Heidelberg, with permission.) **C:** NADPH diaphorese reaction showing positivity of exclusively macula densa cells reflecting activity of nitric oxide synthase. (From Bosse H-M, Heidelberg, with permission.)

speculations about a functional connection in which a signal related to the composition of the tubular fluid at the MD affects glomerular vascular tone and the glomerular filtration rate.[324] It has now become clear that the JGA serves two different functions: it regulates the flow resistance of afferent arterioles in the so-called tubuloglomerular feedback mechanism and it participates in the control of renin synthesis and release from granular cells in the afferent arteriole.[325] Researchers originally assumed that the two responses might be related to each other in that renin released from the granular cells not only has systematic relevance, but locally triggers the formation of angiotensin II and thus is responsible for the afferent vasoconstriction as well; however, it now appears that the final activation of smooth muscle and granular effector cells occurs through largely independent pathways. Renin release from granular cells is the major source of systemic angiotensin II and thus plays an essential role in controlling extracellular volume and blood pressure, whereas the vasoconstriction of the afferent arteriole locally serves to modulate the filtration of this nephron.

For both mechanisms, it is well established that changes in the chloride concentration of the tubular fluid at the MD cause graded releases of mediators that reach their target by diffusion, thus acting in a paracrine fashion.[326] Note that the extraglomerular mesangium that mediates the contact between the MD and the effector cells is not vascularized, so that the buildup of any paracrine agent would not be perturbed by blood flow.

With respect to renin release, the most likely paracrine mediators of this process are prostaglandin E_2 and nitric oxide.[314,327,328] With respect to the vasoconstrictor response purinergic mediators,, either ATP or adenosine, as first suggested by Oswald and colleagues in 1980,[329] appear to play the major role.[325,330,331] For an up-to-date discussion of the function of the JGA, see the reviews by Schnermann and Levine,[325] Persson and colleagues,[332] and Komlosi et al.[333]

RENAL BLOOD VESSELS

The renal arteries arise from the lateral region of the abdominal aorta at the level of the first and second lumbar vertebrae. Each artery divides into an anterior and posterior division before traversing the renal hilus. These divisions usually form a total of five segmental branches. The anterior division gives rise to the upper, middle, and lower segmental arteries, whereas the posterior division becomes the posterior segmental artery. The apical segmental artery can arise from either division. The segmental arteries give rise to interlobar arteries within the renal sinus. The interlobar arteries enter the renal columns adjacent to the renal pyramids.

The intrarenal microvaculature has been extensively studied by several groups[10,11,158,334]; a basic pattern is established throughout the mammalian kidneys that may be described as follows. At the corticomedullary junction, the interlobar artery branches into several arcuate arteries that

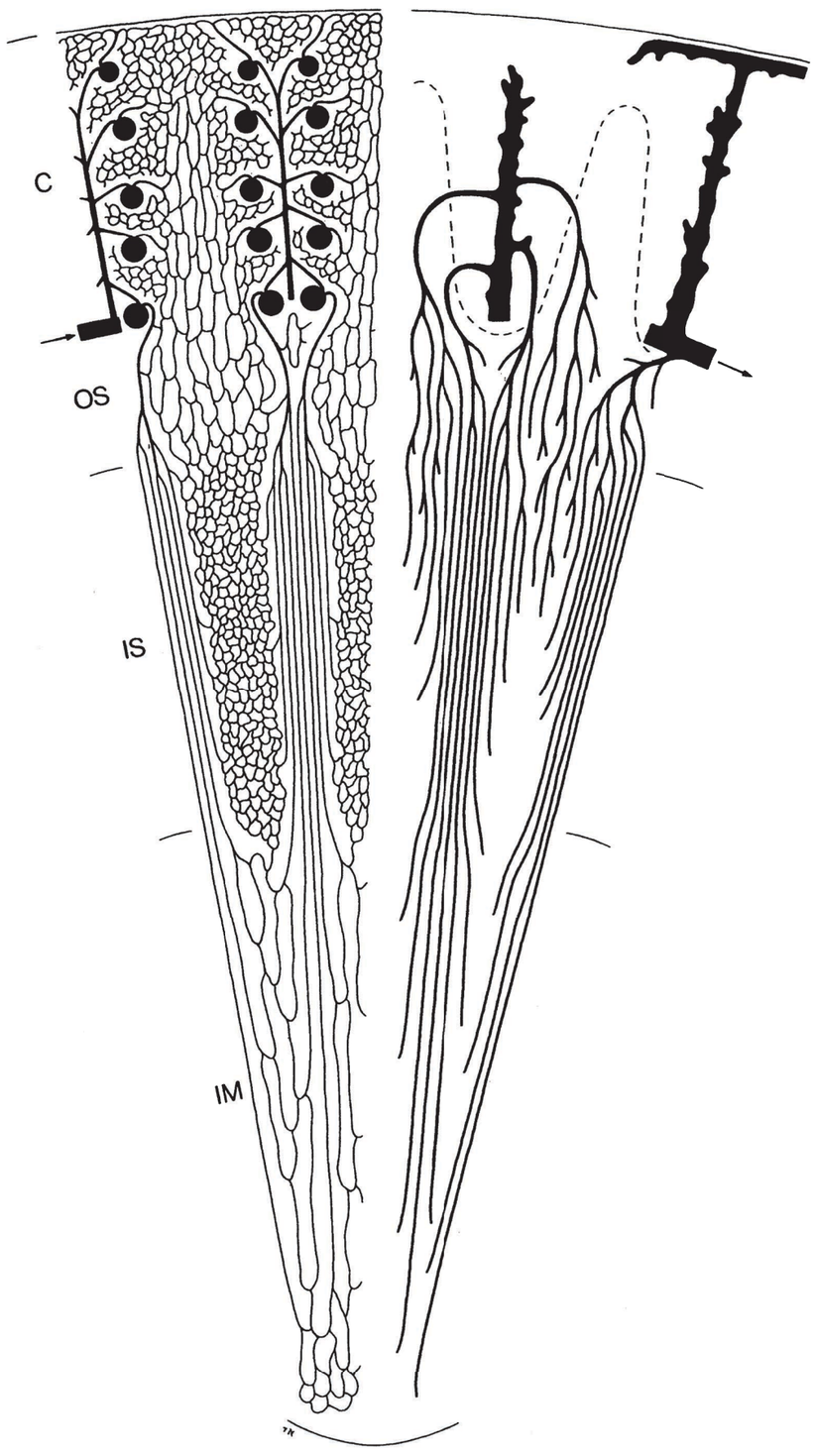

FIGURE 1.38 A basic pattern of renal microvasculature. *C*, cortex; *OS*, outer stripe; *IS*, inner stripe; *IM*, inner medulla. The *left panel* shows the arterial vessels and capillaries. An arcuate artery (*arrow*) gives rise to cortical radial arteries from which the glomerular afferent arterioles originate. Efferent arterioles of juxtamedullary glomeruli descend into the medulla and divide into the descending vasa recta, which, together with ascending vasa recta, form the vascular bundles. At intervals, descending vasa recta leave the bundles to feed the adjacent capillaries. The *right panel* shows the venous vessels. The cortical radial veins start within the superficial cortex; in the human kidney, some of them start as stellate veins on the surface of the kidney (shown on the right side). They all drain into arcuate veins. The venous drainage of the medulla is carried out by venous vasa recta; those from the inner medulla all traverse the inner stripe within the vascular bundles, whereas most of the venous vasa recta from the inner stripe ascend outside the bundles. After traversing the outer stripe as wide tortuous channels, the ascending vasa recta drain into arcuate or cortical radial veins. (From Rollhäuser H, Kriz W. Das Gefäss-system der Rattenniere. *Z Zellforsch*. 1964;64:381, with permission.)

arch across the base of the renal pyramid (Fig. 1.38). The arcuate arteries give rise to interlobular arteries (cortical radial arteries) that course peripherally, between the medullary rays and, thus, within the cortical labyrinth. The interlobular arteries also branch, and the branches give rise to afferent arterioles that supply the renal corpuscles.

Glomerular capillaries are derived from the afferent arteriole, which—strictly at the entrance level—divides into several (two to five) primary capillary branches.[335–337]

Each of these branches gives rise to an anastomosing capillary network that runs toward the urinary pole and then turns back toward the vascular pole. Thereby, the glomerular tuft is subdivided into several lobules, each of which contains an afferent and efferent capillary portion. The lobules are not strictly separated from each other—some anastomoses between lobules occur. The capillaries converge to form the more centrally located efferent arteriole, which is already established inside the glomerular tuft. Thus, the efferent arteriole has a significant intraglomerular segment that runs through the glomerular stalk (Fig. 1.5).[337] At this site a mesangial layer surrounds the vessel. After leaving the glomerulus, the efferent arteriole is reestablished as a proper arteriole.

The efferent arterioles of superficial (or subcapsular) glomeruli perfuse convoluted tubules through long pathways extending to the kidney surface or through intermediate branches near the renal corpuscle. In the midcortex, the efferents either branch near the glomerulus and perfuse convoluted tubules in that region or extend directly to the long meshed network of the medullary ray. Efferent arterioles from juxtamedullary nephrons extend downward to form the descending vasa recta (Fig. 1.38), and occasional branches to regions between the bundles. The early divisions give rise to capillaries located in the outer stripe of the outer medulla. The descending vasa recta then descend within the vascular bundles to the inner stripe and inner medulla (Fig. 1.39).[10] The medulla is drained by venous (ascending)

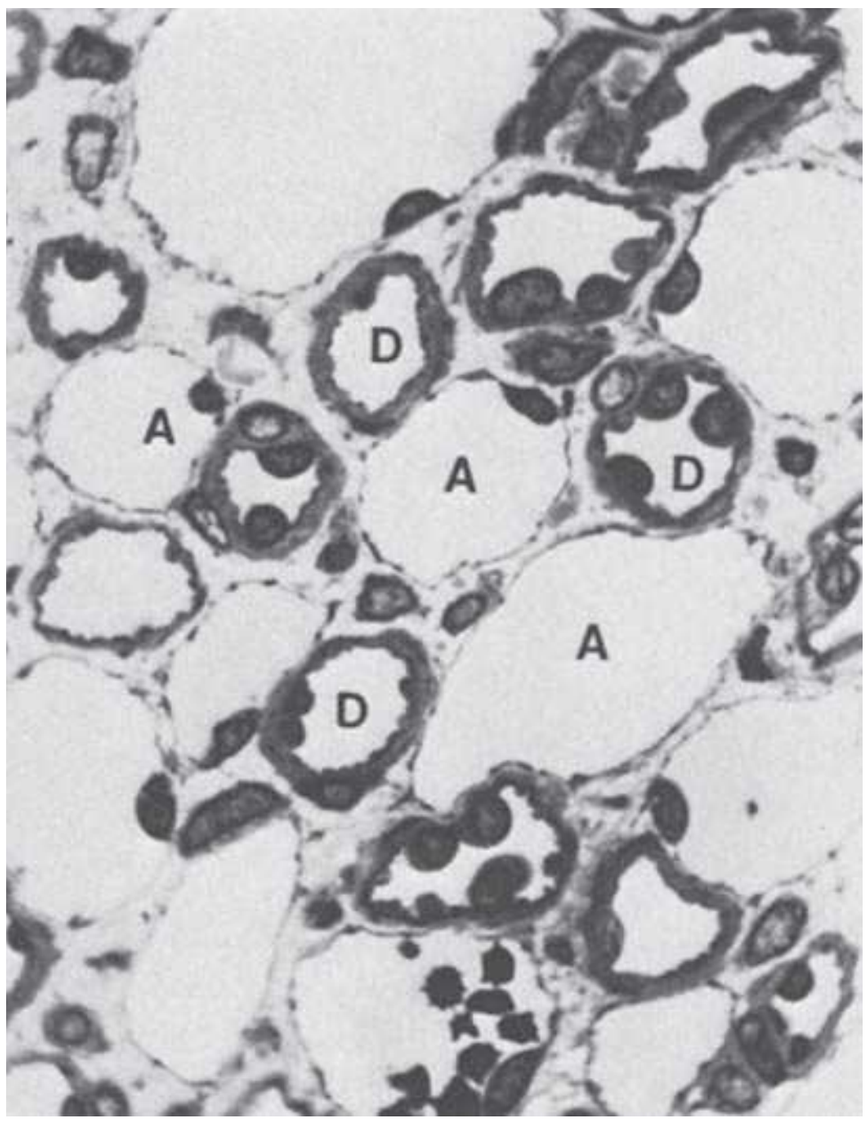

FIGURE 1.39 Light micrograph of a vasa recta bundle, showing descending (*D*) and ascending (*A*) vessels. (Magnification ×950.)

vasa recta, which lie adjacent to descending vasa recta, forming the vascular bundles that function as a countercurrent exchanger. Venous vasa recta that drain the inner medulla remain in the vascular bundles through the inner and outer stripe region. The venous vessels that drain the region of the upper and middle inner stripe ascend within the interbundle region to the outer stripe, there joining the vessels leaving the bundles to form together the major part of the blood supply to this region by a network of venous vessels. The density of capillaries that are derived directly from efferent arterioles is debated.[338] Finally, the ascending vasa recta empty into arcuate or interlobular veins (Fig. 1.38).

The cortical venous system is subject to some variation. In the human, the venous drainage starts on the renal surface beneath the capsule with small venules (stellate veins) that converge to form the interlobular veins (cortical radial veins); in most other species, the interlobular veins begin deeply beneath the cortical surface and stellate veins are lacking. Interlobular veins receive tributaries from the cortical peritubular capillary network (Fig. 1.38) and finally empty into arcuate veins that accompany the arcuate arteries. The arcuate veins receive blood from the venous vasa recta, as described in the preceding section. Interlobar veins form by confluence of arcuate veins and the latter finally form the renal vein. In contrast to the arcuate arteries, which are terminal arteries, the arcuate veins form true anastomosing arches at the corticomedullary border.

The morphology of the descending and ascending parts of the vasa recta differs markedly (Fig. 1.39).[187,339,340] The descending vasa recta are lined by a continuous nonfenestrated endothelium, with cells oriented longitudinally along the cell axis, forming 10 to 20 cell profiles in a single cross-section.[187,340] The endothelium contains the urea transporter UT-B1.[193] Pericytes are seen encircling the descending vasa recta, but they become less frequent as the vessels descend into the inner medulla, where these vessels finally convert into capillaries. As long as the descending vasa recta have pericytes nerve terminals are seen in their neighborhood.

The capillaries and the ascending vasa recta are lined by a thin fenestrated epithelium. The fenestrae are similar to those seen in peritubular capillaries, as well as in most regions of the body, being 40 to 70 μm in diameter[187] and bridged by a thin diaphragm. Uniquely, fenestrated endothelium can line quite large vessels in the kidney.

Lymphatic vessels are seen only in the cortex accompanying the arteries within the periarterial tissue sheaths (see below). The medulla has no lymphatic drainage.[341]

INTERSTITIUM

The interstitium of the kidney comprises the extravascular intertubular spaces of the renal parenchyma, with their attendant cellular elements and extracellular substances.[342,343] It is bounded on all sides by tubular and vascular basement membranes. The lymphatics are considered as part of the interstitium.

In functional studies, the interstitial volume of the kidney has been estimated to amount to 13% of the total kidney volume, whereas stereologically derived values for the cell-free interstitial space of the cortex and outer medulla of the rat range between 3% and 5%.[344–346] Thus, the functional interstitium includes more than just the peritubular spaces; the prominent periarterial connective tissue sheaths (see the following) may, in fact, account for one-half of the entire interstitial volume.[347]

The interstitium is differently developed within the various regions regions of the kidney.[342,343] In the cortex, the peritubular interstitium is distinguished from the periarterial connective tissue (Fig. 1.40). The peritubular interstitium consist of the narrow spaces between tubules and

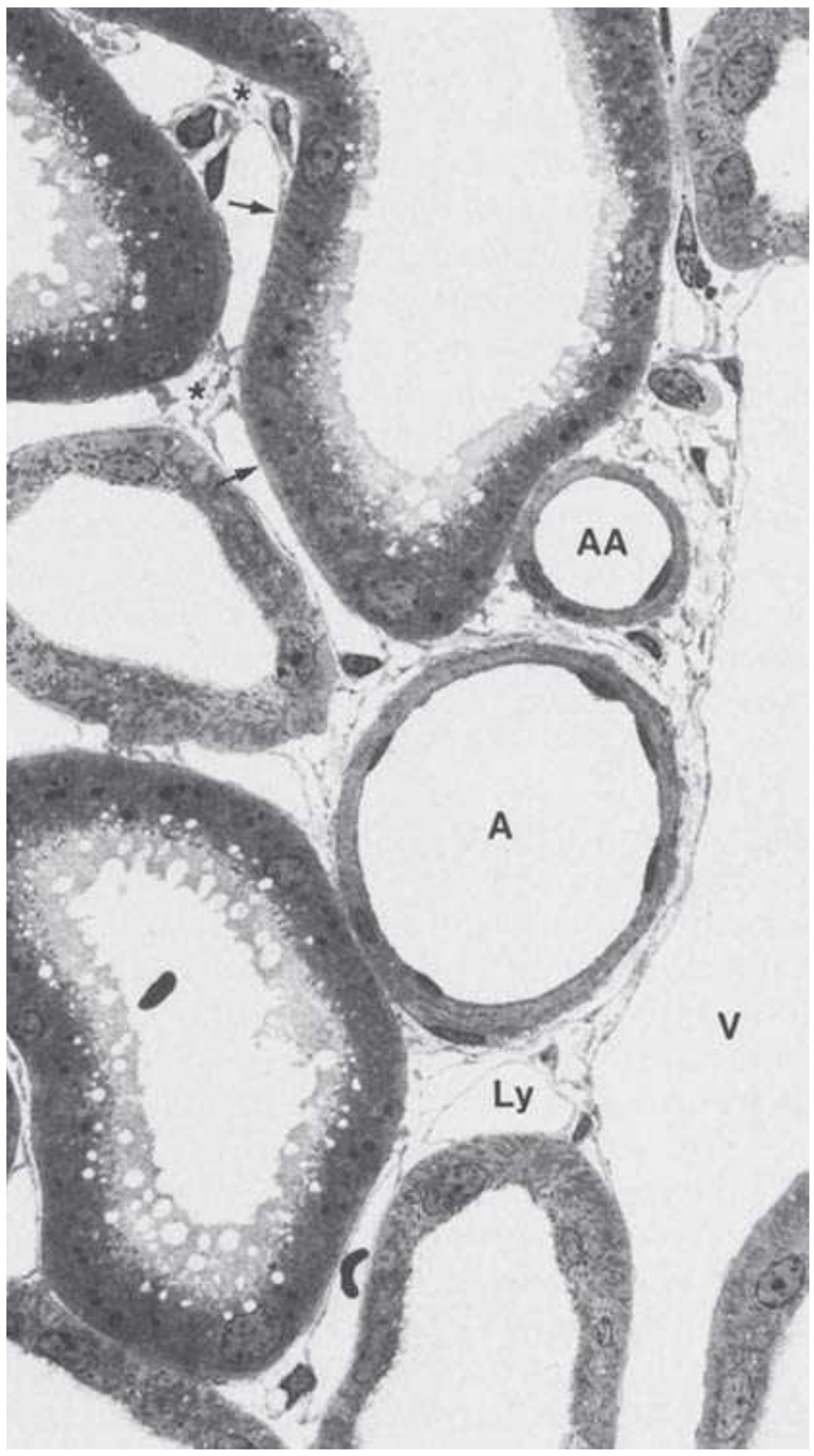

FIGURE 1.40 Low power electron micrograph of a cross-section through the renal cortex (rat). A cortical radial artery (*A*) and vein (*V*), an afferent arteriole (*AA*), and several tubular profiles are seen. The arteries are surrounded by the loose connective tissue sheath that contains the intrarenal lymphatics (*Ly*); the interstitial spaces of this sheath are continuous with the peritubular interstitium, which includes wide (*stars*) and narrow (*arrows*) portions. (Magnification ×1,000.)

around glomeruli. Sometimes, the peritubular capillaries are considered as part of the peritubular interstitium. Capillaries may abut directly to the the outer surface of tubules accounting for 54% to 67%[348] of the capillary surface, whereas only 26% of the tubular surface is directly adjacent to peritubular capillaries.[349] Thus, most of the exchanges among tubules and vessels have to pass through the interstitial compartment.

The periarterial connective tissue forms a fluid-rich loose connective tissue sheath that surrounds the intrarenal arteries and contains the lymphatic vessels of the kidney (Figs. 1.40 and 1.41).[341,347,350] The periarterial lymphatic sheath extends along the intrarenal arteries as far as the afferent arteriole, where it becomes quite attenuated. It is particularly well developed around the arcuate and cortical radial arteries. It contains the renal nerves.

The lymphatic capillaries begin within these sheaths; lymphatics do not, in general, penetrate the renal parenchyma proper and are not found in the medulla.[341,351] The lymphatic vessels converge along with the intrarenal arteries to emerge at the renal hilus. The peritubular interstitium of the cortex freely communicates with the periarterial tissue sheaths. Within the sheaths, fluid and solutes gradually may enter the lymphatic vessels as they converge toward the hilus (Fig. 1.41). In addition to lymphatic drainage, the periarterial connective tissue sheaths probably participate in the distribution of vasoactive substances alongside of the intrarenal arterioles and arteries.[350] It also serves for the intrarenal distribution of inflammatory cells.

In the medulla, the interstitium is differently developed within the three medullary regions[342]: outer and inner stripes and inner medulla. The relative interstitial volume exhibits a pronounced axial gradient from cortex to the inner medulla. The outer stripe has a very narrow, sparse interstitium, occupying 3% to 5% of outer stripe volume.[342,352] Also the vasa recta within the bundles of the inner stripe are very narrowly packed. The interstitial volume of the interbundle regions of the inner stripe is somewhat greater (10% in rats). The most elaborate and distinctive type of regional interstitium is that of the inner medulla. Here, the interstitium constitutes a much larger part of the total tissue volume (30% to 40%),[345,352] and shows a particular arrangement of its fibroblasts (see later).

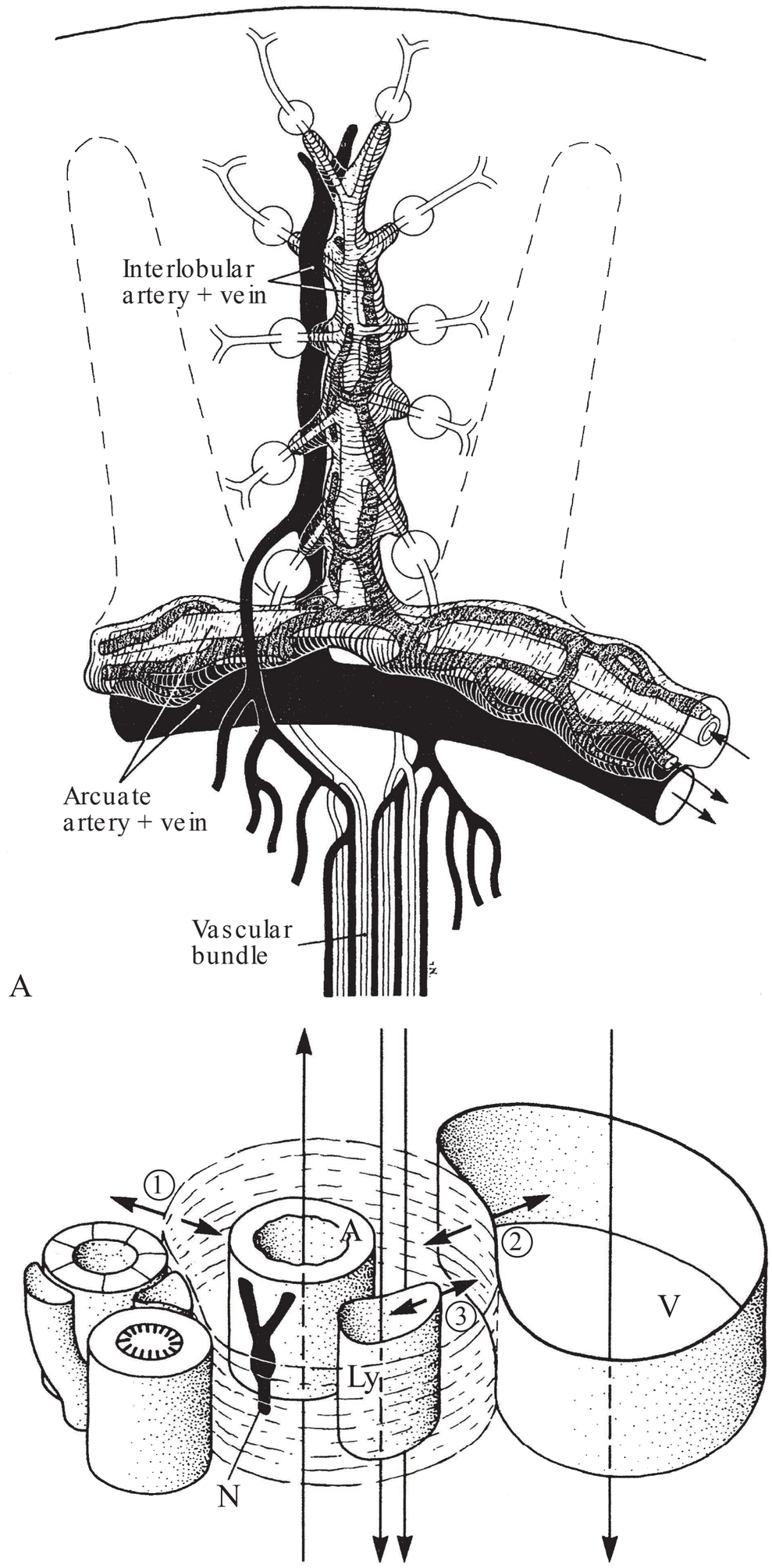

FIGURE 1.41 Schematics showing **(A)** the distribution and **(B)** the relationships of periarterial connective tissue sheath. The periarterial sheath is schematically indicated as a wide "stocking" drawn over the intrarenal arteries. In reality, there is no limiting membrane between the sheath and the surrounding interstitium. The lymphatics (*stippled area*) originate and travel within the periarterial sheath. The medullary rays are indicated by a broken line. The traverse section in **(B)** shows possible relationships between the sheath and the surrounding structures (*double-headed arrows*): (*1*) with the peritubular interstitium, (*2*) with the accompanying vein (*V*), and (*3*) with lymphatics (*Ly*). The *single-headed arrows* indicate the flow of the respective fluid. *N*, nerve. (From Kriz W. A periarterial pathway for intrarenal distribution of renin. *Kidney Int*. 987;31:551, with permission.)

The Cells of the Interstitium

The renal interstitium contains two types of cells: *fi*broblasts and dendritic cells. The fibroblasts are quite differently developed in the cortex and medulla.[342,353–356] Let us first consider the cortex. Within the peritubular interstitium roughly 50% of the cells normally present are fibroblasts and the other 50% dendritic cells, which cannot be separated from each other by simple light microscopy. The *fi*broblasts in this region are extensively branched, with long, often sheetlike processes (Fig. 1.42).[343,357,358] They contain abundant rough endoplasmic reticulum. Mitochondria,

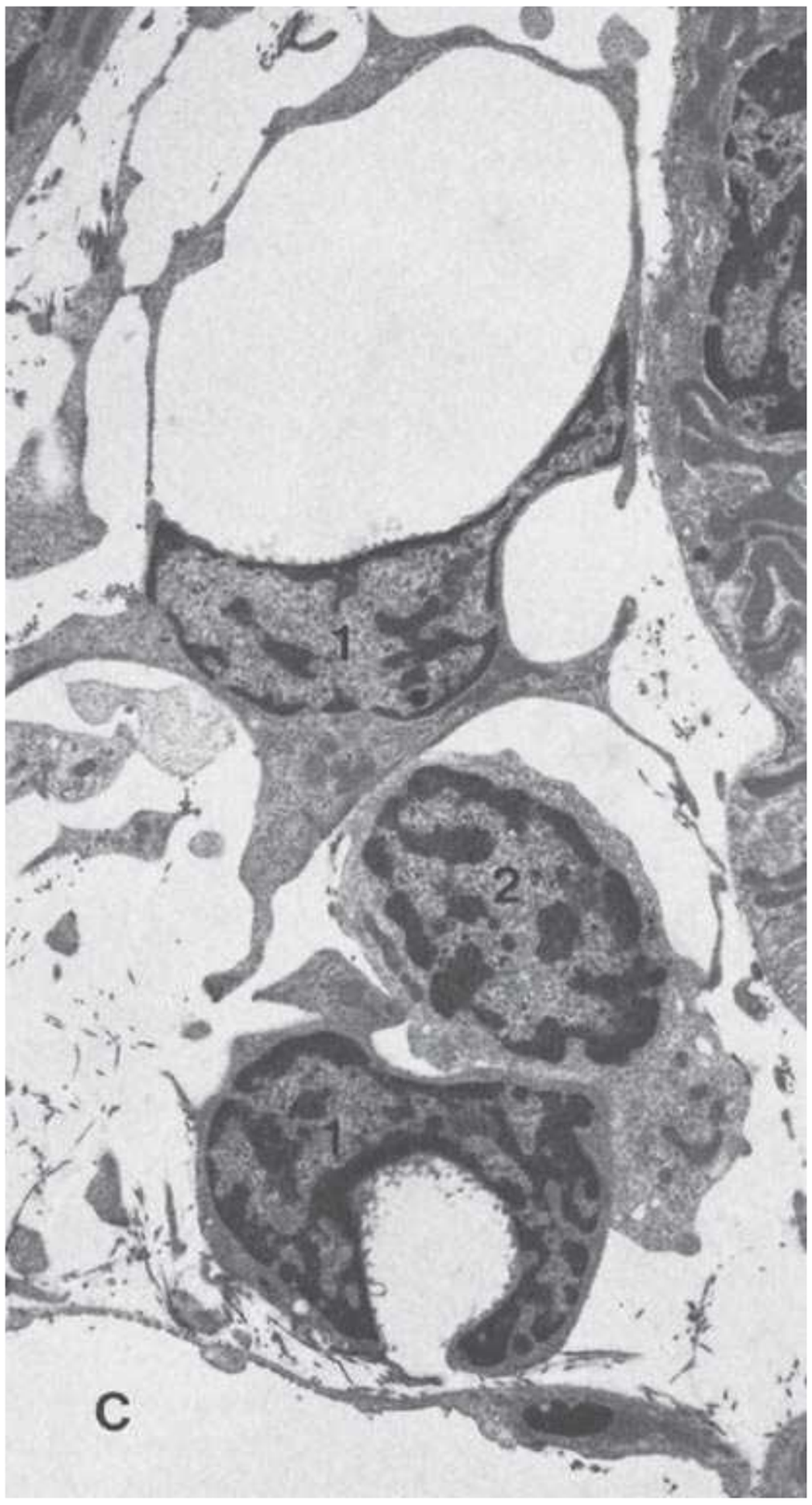

FIGURE 1.42 Transmission electron micrograph of interstitial cells in the cortical peritubular interstitium. Two types are seen: fibroblasts (*1*) with many processes and a dendritic cell (*2*). *C*, capillary. (Magnification ×5,800.)

Golgi complexes, lysosomes, and microfilament bundles are regularly encountered. Fibroblasts perform a scaffolding function interconnecting the nephrons and the peritubular capillaries. They perform this function by focal contacts of their cytoplasmic processes with neighboring fibroblasts as well as with capillaries and tubules.[343,356,357] In addition, they produce the fibrous matrix, which serves together with these cells as a common scaffold throughout the renal parenchyma. These fibroblasts can be unequivocally detected by electron microscopy and fluorescence microscopy by their strong expression of ecto-5′-nucleotidase (CD73),[343,356,357,359,360] as well as of the PDGF receptor beta (PDGFRβ).[361]

Fibroblasts of the renal cortex with their enzyme ecto-5′-nucleotidase[362,363] can generate adenosine within the cortical interstitium. In addition, a subfraction of cortical interstitial cells synthesize erythropoietin.[364–366]

In the inner medulla, the fibroblasts represent a particular variety. They contain numerous homogeneous osmiophilic lipid droplets. Hence, they are generally called lipid-laden interstitial cells (Fig. 1.43).[353,355,367] These star-shaped cells interconnect loops of Henle and vasa recta, spanning these axial structures like the rungs of a ladder.[342,358] They increase in number toward the tip of the papilla and have an abundant rough endoplasmic reticulum, with cisternae that are often dilated and filled with flocculent material. A cytoskeleton is especially well developed in their most peripheral cell processes. These cells possess receptors for angiotensin II and bradykinin.[368,369] They are responsible for

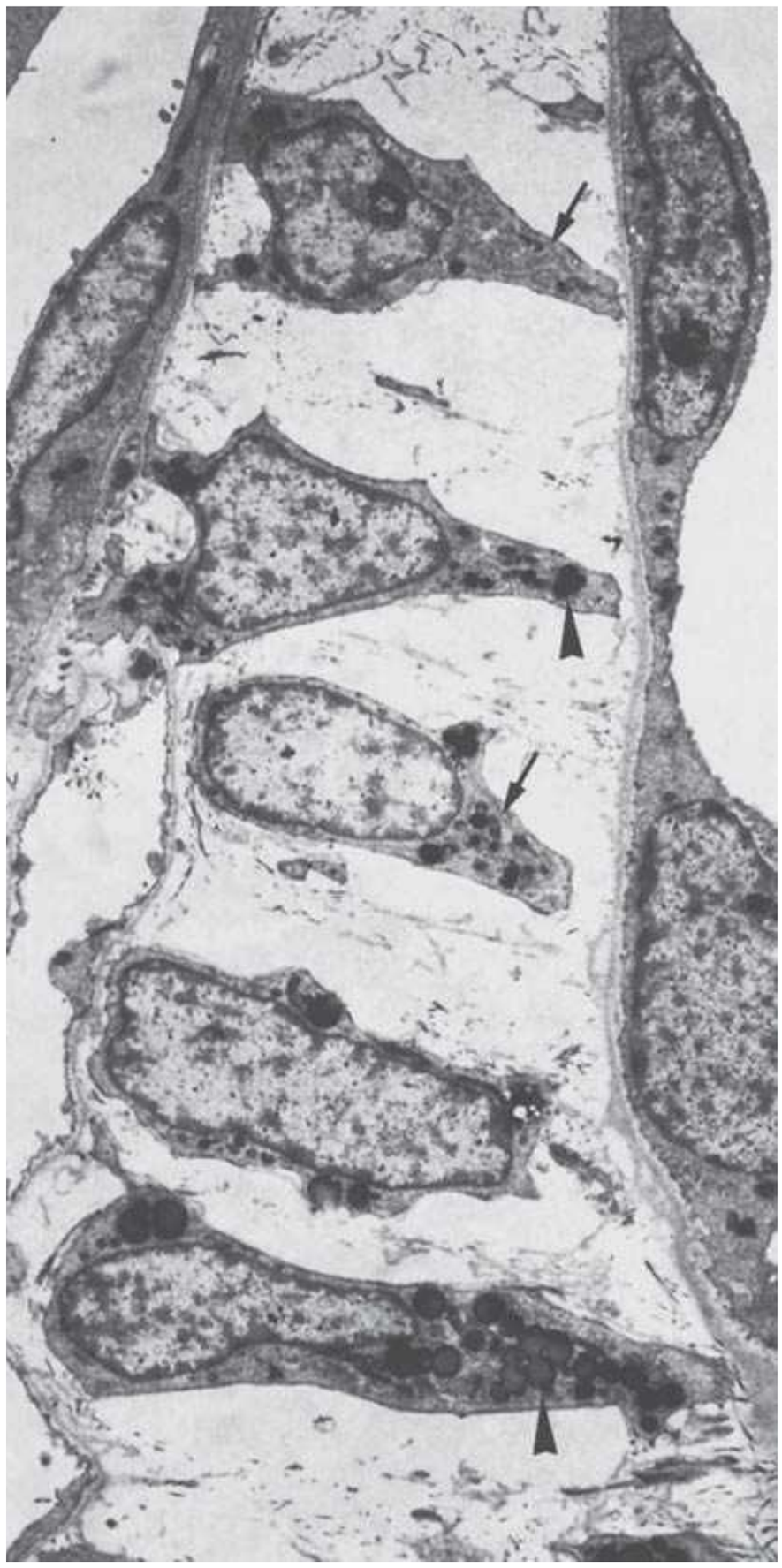

FIGURE 1.43 Transmission electron micrograph of a longitudinal section of the inner medulla (rat) showing lipid-laden interstitial cells arranged like the rungs of a ladder between parallel running tubes or vessels. Note the numerous lipid droplets (*arrowheads*) and the prominent endoplasmic reticulum (*arrows*). (Magnification ×3,300.)

the production of extracellular fibers and ground substance, including the abundant glycosaminoglycans and hyaluronic acid of the inner medulla.[370]

The lipid-laden interstitial cells participate in producing the medullary prostaglandins. The lipid droplets of these cells contain polyunsaturated fatty acids that appear to be precursors of prostaglandins and other lipid-derived hormones.[368,369] The cells produce vasodepressing lipids, in particular, prostaglandin E_2.[371,372]

The second abundant cell type in the renal interstitium is the dendritic cell (Fig. 1.42). They originate from the bone marrow and, as in other organs, are subject to a vivid turnover.[373] In the kidney, dendritic cells are found in the interstitium throughout the cortex and the outer medulla.[343,356,357] They enter the interstitium from the blood, reside for some days in interstitial spaces, and leave the interstitium with the lymph flow.

The extracellular components of the interstitium form a matrix that may be thought of as a hydrated gel of ground substance within a fibrillar reticulum.[342] Several fibers make up the interstitial reticulum. Collagen fibers (types I, III, and VI) are present in the matrix, both in isolation and in bundles. Type I collagen forms typical cross-banded fibers, generally more than 30 μm in diameter. Type III fibers (10 to 40 μm in diameter) and type VI fibers (6 to 10 μm in diameter) are often seen associated with type I fibers. In addition, unbanded microfibrils with a diameter of 15 to 30 μm and an electron-lucent core have been described.[342,354]

Myofibroblasts are absent from healthy kidneys. They differ from fibroblasts by their high production of extracellular matrix, expression of vimentin, and α-smooth muscle actin (αSMA).[343,374] The accumulation of myofibroblasts in a diseased kidney is generally suggested to occur by transformation of fibroblasts into myofibroblasts in response to stimuli from locally produced cytokines.[374,375] An alternative hypothesis postulates that myofibroblasts may develop by "epithelialmesenchymal transition" (EMT) from tubular cells[376]; however, the evidence for this origin is not conclusive.[377]

Macrophages (histiocytes) are also rarely found in the healthy kidney, except for the periarterial tissue sheaths[356] (Fig. 1.42). These round cells demonstrate primary and secondary lysosomes and characteristic surface folds. Along with interstitial affections, the number of macrophages may dramatically rise.

STRUCTURE–FUNCTION RELATIONSHIPS WITHIN THE RENAL MEDULLA

During phylogeny, the renal medulla has developed in response to the necessity to conserve water by excreting a concentrated urine.[378] Loops of Henle, collecting ducts, and a specific blood supply through vascular bundles have developed into a complex structural system that accounts for this function. Whereas the mechanisms to produce a concentrated urine up to a concentration of about 600 mOsmol/L in the outer medulla are fairly well known, the mechanisms underlying the final urine concentration in the inner medulla are still poorly understood.

Within the outer medulla the reabsorption of NaCl from the MTAL represents the driving force to produce a corticomedullary osmotic gradient that provokes the osmotic water withdrawal from the collecting duct passing through this region. ADH initiates the insertion of AQP2 channels into the apical plasma membrane of collecting duct principal cells. Together with the constitutive AQP3 and AQP4 channels in the basolateral membrane of these cells, this allows osmotic water withdrawal into the hypertonic interstitium of the outer medulla.[192] The reabsorbed water is brought back into the systemic circulation by venous vasa recta.[2]

The final step of the urine concentrating process in the inner medulla is basically identical insofar as water is reabsorbed by osmosis through ADH-stimulated water-permeable collecting ducts into a hypertonic interstitium. However, the mechanisms for creating the osmotic gradient in the inner medulla up to 1200 mOsmol/L in humans and much higher in many rodent species are much more complex than in the outer medulla and are insufficiently understood. A driving force like the sodium pump in MTALs in the outer medulla is lacking. This has led to several "passive" models,[379,380] which take into account the specific transport properties of thin limbs, collecting ducts, and vasa recta to elucidate, by mathematical modeling, how part of the osmotic energy produced by the function of MTALs in the outer medulla may be transferred into the inner medulla, leading there to an osmotic gradient toward the tip of the papilla. A review of these models is far beyond the scope of this chapter. From a structural point of view, two features appear most relevant.

1. **The shape of the inner medulla.** The inner medulla has a particular shape, tapering from a broad basis to a tiny papilla. The mass of the inner medulla is, therefore, unevenly distributed along the longitudal axis. A reconstruction study in the rat[2,381,382] has shown that the inner medulla is shaped like a mushroom, consisting of a broad head and a thin stalk. Calculations in the model have shown that the first one-half of the inner medulla comprises roughly 80% of the total inner medullary volume and, consequently, only 20% are left for the second, papillary, half. Thus, the decrease of the mass in the inner medulla along the longitudal axis is almost exponential. This shape perfectly reflects what happens with the structures within the inner medulla: loops of Henle, collecting ducts, and vasa recta all decrease rapidly in number from the base to the tip of the papilla.[381,382] It has been calculated that of an estimated 10,000 long loops entering the inner medulla at its base, only about 1,500 reach the papillary one-half

of the inner medulla.[2] Thus, the majority of thin limbs (the "short" long thin limbs) turn back shortly after entering the inner medulla; a smaller, but still substantial, number of thin limbs reach the middle part of the inner medulla; and only a small population of "long" long loops really reach the papilla.

This has led to the proposal[383] and, later, mathematical models[204,384] that this arrangement might account for a cascadelike transport of solutes toward the tip of the papilla. The large fraction of "short" long loops, by some way or another, manages the transport of solutes into the first one-third of the inner medulla, the intermediate fraction of long loops brings a proportion of these solutes further down into the middle part, and finally the small fraction of "long" long loops completes the transport of a still much smaller solute fraction down into the papilla.

2. **Structural arrangements in the renal medulla that allow the recycling of urea into the inner medulla via short loops of Henle.** The descending thin limbs of short loops in the outer medulla are arranged in a pattern that allows the shifting of urea from the venous blood coming up with the venous vasa recta from the inner medulla into tubular fluid of descending thin limbs of short loops. This possibility is perfectly developed in the complex vascular bundles in the outer medulla of rodents with high urine-concentrating abilities.[159,187,197,198] Within these vascular bundles, the SDTLs are arranged in a countercurrent fashion with ascending vasa recta coming up from the inner medulla. Thus urea, by countercurrent exchange, may directly enter the descending thin limbs through the urea transporter UT-A2[193,275] (the fenestrated endothelium of venous vasa recta may readily be expected to be highly permeable for urea). In a renal medulla with "simple" vascular bundles (as they are found in most species), countercurrent exchange of urea first occurs from ascending to descending vasa recta (which contain the urea transporter UT-B1), which, afterward, will deliver their blood to the capillary plexus of the interbundle region surrounding the thin limbs of short loops on their descending direction. Thus, even if probably less effectively, urea from the inner medulla has access to the SDTLs.[193,197,385,386]

Starting with the MTAL, thus abruptly at the end of the ATL, the uriniferous tubule is impermeable to urea until the terminal collecting duct in the inner medulla, which, starting abruptly, expresses the ADH-dependent urea transporter UT-A1.[193,275] Because of water reabsorption upstream from this segment, urea becomes concentrated within the tubular urine to levels always higher than the adjacent interstitium. In the terminal CD segment, a major part of this urea diffuses into the papillary interstitium and where it mixes with other solutes (NaCl), contributing to the osmotic driving force that reclaims water from the collecting duct. The locus of urea delivery in the papilla (i.e., at the "ultimate bend" of the complex countercurrent exchange system of the inner medulla) is optimal because (1) by countercurrent exchange in vasa recta and thin limbs, urea is largely trapped and distributed in a longitudinal gradient within the inner medulla and (2) the fraction of urea that escapes the inner medulla is subject to recycling via short loops back into the inner medulla. Thus, this latter fraction of urea is available another time within the papillary interstitium ready to withdraw and/or to balance water reabsorption from the collecting duct. Recycling is not simply trapping because this fraction of urea on its nephron way back into the inner medulla is concentrated a second time, essentially by the work of the sodium pump in the MTALs. In essence, urea recycling by short loops (not by long loops) represents an effective transport of osmotic energy from the outer into the inner medulla.

Whether these mechanisms are sufficient to build an osmotic gradient up to several osmoles in desert rodents, or whether there are additional sources complementing the solute gradients (e.g., continuous production of osmotic active substances), is presently unknown. Even if this question does not belong to the most urgent problems in medicine, it represents a highly challenging biologic enigma.

REFERENCES

1. Inke G. The Protolobar Structure of the Human Kidney. New York: Alan R. Liss, Inc.; 1988.
2. Jamison R, Kriz W Urinary Concentrating Mechanism. Structure and Function. New York: Oxford University Press; 1982.
3. Amann K, Plank C, Dotsch J. Low nephron number - a new cardiovascular risk factor in children? Pediatr Nephrol. 2004;19:1319–1323. http://www.ncbi.nlm.nih.gov/pubmed/15490250
4. Neiss W Morphogenesis and histogenesis of the connecting tubule in the rat kidney. Anat Embryol 1982;165:81. http://www.ncbi.nlm.nih.gov/pubmed/7149277
5. Oliver J. Nephrons and Kidneys. New York/Evanston/London: Harper & Row, Hoeber Medical; 1968.
6. Osathanondh V Potter E. Development of human kidney as shown by microdissection. III. Formation and interrelationship of collecting tubules and nephrons. Arch Pathol. 1963;76:290–302. http://www.ncbi.nlm.nih.gov/pubmed/14058156
7. Peter K. Untersuchungen über Bau und Entwicklung der Niere. Jena: Gustav Fischer; 1909.
8. Kriz W, Bankir L. A standard nomenclature for structure of the kidney. The Renal Commission of the International Union of Physiological Sciences (IUPS). Pfugers Arch. 1988;411:113–120. http://www.ncbi.nlm.nih.gov/pubmed/3353210
9. Beeuwkes R. Efferent vascular patterns and early vascular-tubular relations in the dog kidney. Am J Physiol. 1971;221:1361–1374. http://www.ncbi.nlm.nih.gov/pubmed/5124281
10. Beeuwkes R. The vascular organization of the kidney. Annu Rev Physiol. 1980;42:531–542. http://www.ncbi.nlm.nih.gov/pubmed/6996596
11. Rollhäuser H, Kriz W Heinke W Das Gefässsystem der Rattenniere. Z Zellforsch Mikrosk Anat. 1964;64:381–403. http://www.ncbi.nlm.nih.gov/pubmed/14320463
12. Sperber J. Studies of the mammalian kidney. Zool Bidrag. 1944;22:249–431.
13. Kriz W, Kaissling B. Structural organization of the mammalian kidney. In: Seldin D, Giebisch G, eds. The Kidney: Physiology and Pathophysiology. New York: Raven Press; 1992:707–777.
14. Pfeiffer E. Comparative anatomical observations of the mammalian renal pelvis and medulla. J Anat. 1968;102:321–331. http://www.ncbi.nlm.nih.gov/pubmed/5643845

15. Schmidt-Nielsen B, Pfeiffer E. Urea and urinary concentrating ability in the mountain beaver Aplodontia rufa. Am J Physiol. 1970;218:1370–1375.

16. van Liew J, Buentig W Stolte H, et al. Protein excretion: Micropuncture study of rat capsular and proximal tubule fluid. Am J Physiol. 1970;219:299–305. http://www.ncbi.nlm.nih.gov/pubmed/5448057

17. Pappenheimer J. Passage of molecules through capillary walls. Physiol Rev. 1953;33:387. http://www.ncbi.nlm.nih.gov/pubmed/13088295

18. Helmchen U. Die Zahl der Mesangiumzellen in einem normalen Glomerulum der Rattenniere: Eine dreidimensionale elektronenoptische Analyse. Tuebingen, Germany: Inaugural dissertation; 1980.

19. Zimmermann K. Ueber den Bau des Glomerulus der menschlichen Niere. Z Mikrosk Anat Forsch. 1929;18:520–552.

20. Arakawa M. A scanning electron microscopy of the glomerulus of normal and nephrotic rats. Lab Invest. 1970;23:489–496. http://www.ncbi.nlm.nih.gov/pubmed/5483882

21. Spinelli F. Structure and development of the renal glomerulus as revealed by scanning electron microscopy. Int Rev Cytol. 1974;39:345–381. http://www.ncbi.nlm.nih.gov/pubmed/4611944

22. Fries J, Sandstrom D, Meyer T, et al. Glomerular hypertrophy and epithelial cell injury modulate progressive glomerulosclerosis in the rat. Lab Invest. 1989;60:205–218. http://www.ncbi.nlm.nih.gov/pubmed/2915515

23. Sterzel R, Pabst R. The temporal relationship between glomerular cell proliferation and monocyte inf ltration in experimental glomerulonephritis. Virchows Arch B Cell Pathol Incl Mol Pathol. 1982;38:337–350. http://www.ncbi.nlm.nih.gov/pubmed/6121416

24. Kriz W Gretz N, Lemley K. Progression of glomerular diseases: Is the podocyte the culprit? Kidney Int. 1998;54:687–697. http://www.ncbi.nlm.nih.gov/pubmed/9734594

25. Kriz W, Le Hir M. Pathways to nephron loss starting from glomerular diseases - Insights from animal models. Kidney Int. 2005;67:404–419. http://www.ncbi.nlm.nih.gov/pubmed/15673288

26. Sagrinati C, Netti G, Mazzinghi B, et al. Isolation and characterization of multipotent progenitor cells from the Bowman's capsule of adult human kidneys.J Am Soc Nephrol. 2006;17:2443–2456. http://www.ncbi.nlm.nih.gov/pubmed/16885410

27. Ronconi E, Sagrinati C, Angelotti M, et al. Regeneration of glomerular podocytes by human renal progenitors. J Am Soc Nephrol. 2009;20:322–332. http://www.ncbi.nlm.nih.gov/pubmed/19092120

28. Appel D, Kershaw D, Smeets B, et al. Recruitment of podocytes from glomerular parietal epithelial cells. J Am Soc Nephrol. 2008;20:333–343. http://www.ncbi.nlm.nih.gov/pubmed/19092119

29. Smeets B, Uhlig S, Fuss A, et al. Tracing the origin of glomerular extracapillary lesions from parietal epithelial cells. J Am Soc Nephrol. 2009;20:2604–2615.

30. Rodewald R, Karnovsky M. Porous substructure of the glomerular slit diaphragm in the rat and mouse. J Cell Biol. 1974;60:423–433. http://www.ncbi.nlm.nih.gov/pubmed/4204974

31. Reiser J, Kriz W, Kretzler M, et al. The glomerular slit diaphragm is a modif ed adherens junction. J Am Soc Nephrol. 2000;11:1–8. http://www.ncbi.nlm.nih.gov/pubmed/10616834

32. Ruotsalainen V, Ljungberg P, Wartiovaara J, et al. Nephrin is specif cally located at the slit diaphragm of glomerular podocytes. Proc Natl Acad Sci USA. 1999;96(14):7962–7967. http://www.ncbi.nlm.nih.gov/pubmed/10393930

33. Donoviel D, Freed D, Vogel H, et al. Proteinuria and perinatal lethality in mice lacking NEPH1, a novel protein with homology to nephrin. Mol Cell Biol. 2001;21:4829–4836.

34. Inoue T, Yaoita E, Kurihara H, et al. Fat is a component of glomerular slit diaphragms. Kidney Int. 2001;59:1003–1012. http://www.ncbi.nlm.nih.gov/pubmed/11231355

35. Schnabel E, Anderson J, Farquhar M. The tight junction protein ZO-1 is concentrated along slit diaphragms of the glomerular epithelium. J Cell Biol. 1990;111:1255–1263. http://www.ncbi.nlm.nih.gov/pubmed/2202736

36. Boute N, Gribouval O, Roselli S, et al. NPHS2, encoding the glomerular protein podocin, is mutated in autosomal recessive steroid-resistant nephrotic syndrome. Nat Genet. 2000;24:349–354. http://www.ncbi.nlm.nih.gov/pubmed/10742096

37. Li C, Ruotsalainen V, Tryggvason K, et al. CD2AP is expressed with nephrin in developing podocytes and is found widely in mature kidney and elsewhere. Am J Physiol Renal Physiol. 2000;279(4):F785–F792.

38. Huber T, Kottgen M, Schilling B, et al. Interaction with podocin facilitates nephrin signaling. J Biol Chem. 2001;276:41543–41546. http://www.ncbi.nlm.nih.gov/pubmed/11562357

39. Schwarz K, Simons M, Reiser J, et al. Podocin, a raft-associated component of the glomerular slit diaphragm, interacts with CD2AP and nephrin. J Clin Invest. 2001;108:1621–1629.

40. Dunne J, Hanby A, Poulsom R, et al. Molecular cloning and tissue expression of FAT, the human homologue of the Drosophila fat gene that is located on chromosome 4q34-q35 and encodes a putative adhesion molecule. Genomics. 1995;30:207–223. http://www.ncbi.nlm.nih.gov/pubmed/8586420

41. Ciani L, Patel A, Allen N, et al. Mice lacking the giant protocadherin mFAT1 exhibit renal slit junction abnormalities and a partially penetrant cyclopia and anophthalmia phenotype. Mol Cell Biol. 2003;23:3575–3582. http://www.ncbi.nlm.nih.gov/pubmed/12724416

42. Miner J. Renal basement membrane components. Kidney Int. 1999;56: 2016–2024. http://www.ncbi.nlm.nih.gov/pubmed/10594777

43. Drenckhahn D, Franke R. Ultrastructural organization of contractile and cytoskeletal proteins in glomerular podocytes of chicken, rat, and man. Lab Invest. 1988;59:673–682. http://www.ncbi.nlm.nih.gov/pubmed/3141719

44. Sanden W, Elger M, Mundel P, et al. The architecture of podocyte cytoskeleton suggests a role in glomerular f ltration dynamics. Ann Anat. 1995;177:44–45.

45. Kaplan J, Kim S, North K, et al. Mutations in ACTN4, encoding a -actinin-4. cause familial focal segmental glomerulosclerosis. Nat Genet. 2000;24:251–256. http://www.ncbi.nlm.nih.gov/pubmed/10700177

46. Weins A, Kenlan P, Herbert S, et al. Mutational and biological analysis of alpha-actinin-4 in focal segmental glomerulosclerosis. J Am Soc Nephrol. 2005;16:3694–3701. http://www.ncbi.nlm.nih.gov/pubmed/16251236

47. Braun E, Schlondorff D, Becker D, et al. Mutations in the formin gene INF2 cause focal segmental glomeruloscerlosis. Nat Genet. 2010;42:72–76. http://www.ncbi.nlm.nih.gov/pubmed/20023659

48. Kreidberg J, Symons J. Integrins in kidney development, function, and disease. Am J Physiol Renal Physiol. 2000;279(2):F233–F242.

49. Adler S. Integrin receptors in the glomerulus: potential role in glomerular injury. Am J Physiol. 1992;262:F697–F704.

50. Raats C, van den Born J, Bakker M, et al. Expression of agrin, dystroglycan, and utrophin in normal renal tissue and in experimental glomerulopathies. Am J Pathol. 2000;156(5):1749–1765. http://www.ncbi.nlm.nih.gov/pubmed/10793086

51. Regele H, Fillipovic E, Langer B, et al. Glomerular expression of dystroglycans is reduced in minimal change nephrosis but not in focal segmental glomerulosclerosis. J Am Soc Nephrol. 2000;11(3):403–412.

52. Kerjaschki D, Sharkey D, Farquhar M. Identif cation and characterization of podocalyxin-the major sialoprotein of the renal glomerular epithelial cell. J Cell Biol. 1984;98:1591. http://www.ncbi.nlm.nih.gov/pubmed/6371025

53. Orlando R, Takeda T, Zak B, et al. The glomerular epithelial cell anti-adhesion podocalyxin associates with the actin cytoskeleton through interactions with ezrin. J Am Soc Nephrol. 2001;12:1589–1598. http://www.ncbi.nlm.nih.gov/pubmed/11461930

54. Michael A, Blau E, Vernier R. Glomerular polyanion. Alterations in aminonucleoside nephrosis. Lab Invest. 1970;23:649–657. http://www.ncbi.nlm.nih.gov/pubmed/4098608

55. Andrews P. Glomerular epithelial alterations resulting from sialic acid surface coat removal. Kidney Int. 1979;15:376–385. http://www.ncbi.nlm.nih.gov/pubmed/513496

56. Seiler M, Rennke H, Venkatachalam M, et al. Pathogenesis of polycation-induced alteration (fusion) of glomerular epithelium. Lab Invest. 1977;36:48–61. http://www.ncbi.nlm.nih.gov/pubmed/63647

57. Kerjaschki D, Vernillo A, Farquhar M. Reduced sialylation of podocalyxin-the major sialoprotein of the rat kidney glomerulusin aminonucleotide nephrons. Am J Pathol. 1985;118:343. http://www.ncbi.nlm.nih.gov/pubmed/3976840

58. Takeda T, McQuistan T, Orlando R, et al. Loss of glomerular foot processes is associated with uncoupling of podocalyxin from the actin cytoskeleton. J Clin Invest. 2001;108:289–301.

59. Pavenstadt H, Kriz W, Kretzler M. Cell biology of the glomerular podocyte. Physiol Rev. 2003;83:253–307. http://www.ncbi.nlm.nih.gov/pubmed/12506131

60. Reiser J, Polu K, Moller C, et al. TRPC6 is a glomerular slit diaphragm-associated channel required for normal renal function. Nat Genet. 2005;37: 739–774. http://www.ncbi.nlm.nih.gov/pubmed/15924139

61. Kazatchkine M, Fearon D, Appay M, et al. Immunohistochemical study of the human glomerular C3b receptor in normal kidney and in seventy-five cases of renal diseases. J Clin Invest. 1982;69:900–912.
http://www.ncbi.nlm.nih.gov/pubmed/7042757
62. Kerjaschki D, Farquhar M. Immunocytochemical localization of the Heymann antigen (gp 330) in glomerular epithelial cells of normal Lewis rats. J Exp Med. 1983;157:667–686.
http://www.ncbi.nlm.nih.gov/pubmed/6337231
63. Schiffer M, Schiffer L, Gupta A, et al. Inhibitory smads and TGF-b signalling in glomerular cells. J Am Soc Nephrol. 2002;13:2657–2666.
http://www.ncbi.nlm.nih.gov/pubmed/12397035
64. Wogensen L, Nielsen C, Hjorth P. Under control of the Ren-1c promoter, locally produced transforming growth factor-beta1 induced accumulation of glomerular extracellular matrix in transgenic mice. Diabetes. 1999;48:182–192.
http://www.ncbi.nlm.nih.gov/pubmed/9892241
65. Kriz W, Haehnel B, Rosener S, et al. Long-term treatment of rats with FGF-2 results in focal segmental glomerulosclerosis. Kidney Int. 1995;48:1435–1450.
http://www.ncbi.nlm.nih.gov/pubmed/8544400
66. Bulger R, Eknoyan G, Purcell D, et al. Endothelial characteristics of glomerular capillaries in normal, mercuric chloride-induced, and gentamicin-induced acute renal failure in the rat. J Clin Invest. 1983;72:128–141.
http://www.ncbi.nlm.nih.gov/pubmed/6223941
67. Elger M, Sakai T, Kriz W. The vascular pole of the renal glomerulus of rat. Adv Anat Embryol Cell Biol. 1998;139:1–98.
http://www.ncbi.nlm.nih.gov/pubmed/9386305
68. Dobyan D, Eknoyan G, Magill L, et al. A quantitative evaluation of the glomerular capillary endothelium in rat and human kidneys: Utilization of vascular perfusion, freeze-cracking of tissue, and scanning electron microscopy. J Electron Microsc Tech. 1984;1:185.
69. Savage C. The biology of the glomerulus: Endothelial cells. Kidney Int. 1994;45:314–319.
http://www.ncbi.nlm.nih.gov/pubmed/8164414
70. Kanwar Y, Linker A, Farquhar M. Increased permeability of the glomerular basement membrane to ferritin after removal of glycosaminoglycans (heparan sulfate) by enzyme digestion. J Cell Biol. 1980;86:688–693.
http://www.ncbi.nlm.nih.gov/pubmed/6447156
71. Latta H, Johnston W Stanley T. Sialoglycoproteins and filtration barriers in the glomerular capillary wall. J Ultrastruct Res. 1975;51:354–376.
http://www.ncbi.nlm.nih.gov/pubmed/48557
72. Mohos S, Skoza L. Histochemical demonstration and localization of sialoproteins in the glomerulus. Exp Mol Pathol. 1970;12:316–323.
73. Rostgaard J, Qvortrup K. Sieve plugs in fenestrae of glomerular capillaries - site of the filtration barrier? Cells Tissues Organs. 2002;170:132–138.
74. Hjalmarsson C, Johansson B, Haraldsson B. Electron microscopic evaluation of the endothelial surface layer of glomerular capillaries. Microvasc Res. 2004;67:9–17.
75. Ballermann B, Marsden P. Endothelium-derived vasoactive mediators and renal glomerular function. J Clin Invest. 1991;14:508–517.
http://www.ncbi.nlm.nih.gov/pubmed/1794204
76. Eremina V, Quaggin S. The role of VEGF-A in glomerular development and function. Curr Opin Nephrol Hypertens. 2004;13:9–15.
http://www.ncbi.nlm.nih.gov/pubmed/15090854
77. Satchell S, Anderson K, Mathieson P. Angiopoietin 1 and vascular endothelial growth factor modulate human glomerular cell barrier properties. Am Soc Nephrol. 2004;15:566–574.
http://www.ncbi.nlm.nih.gov/pubmed/14978158
78. Grandaliano G, Choudhury G, Poptic E, et al. Thrombin regulates PDGF expression in bovine glomerular endothelilal cells. J Am Soc Nephrol. 1998;9:583–589.
http://www.ncbi.nlm.nih.gov/pubmed/9555660
79. Jorgensen F, Bentzon M. The ultrastructure of the normal human glomerulus: Thickness of glomerular basement membrane. Lab Invest. 1968;18:42–48.
http://www.ncbi.nlm.nih.gov/pubmed/5643970
80. Trump B, Bulger R. Morphology of the kidney. In: Becker E, ed. Structural Basis of Renal Disease. New York: Harper&Row; 1968:1–92.
http://www.ncbi.nlm.nih.gov/pubmed/5702212
81. Abrahamson D. Structure and development of the glomerular capillary wall and basement membrane. Am J Physiol. 1987;253:F783–F794.
82. Miner J. Developmental biology of glomerular basement membrane components. Curr Opin Nephrol Hypertens. 1998;7:13–19.
http://www.ncbi.nlm.nih.gov/pubmed/9442357
83. Sariola H, Timpl R, von der Mark K, et al. Dual origin of glomerular basement membrane. Dev Biol. 1984;101:86–96.
http://www.ncbi.nlm.nih.gov/pubmed/6420214
84. St John P, Abrahamson D. Glomerular endothelial cells and podocytes jointly synthesize laminin-1 and -11 chains. Kidney Int. 2001;60:1037–1046.
85. Abrahamson D. Origin of the glomerular basement membrane visualized after in vivo labeling of laminin in newborn rat kidneys. J Cell Biol. 1985;100:1988–2000.
86. Daha M, Blok A, de Graeff J, et al. Synthesis and degradation of glomerular basement membrane in rats with nephrotoxic nephritis. Nephron. 1978;22:522–528.
http://www.ncbi.nlm.nih.gov/pubmed/740113
87. Cohen M, Surma M, Wu V. In vivo biosynthesis and turnover of glomerular basement membrane in diabetic rats. Am J Physiol. 1982;242:F385–F389.
88. Reddi A. Metabolism of glomerular basement membrane in normal, hypophysectomized, and growth-hormone-treated diabetic rats. Exp Mol Pathol. 1985;43:196–208.
89. Bernstein J, Cheng F, Roszka B. Glomerular differentiation in metanephric culture. Lab Invest. 1981;45:183–190.
http://www.ncbi.nlm.nih.gov/pubmed/7265915
90. Bonadio J, Sage H, Cheng F, et al. Localization of collagen types IV and V, laminin, and heparan sulfate proteoglycan to the basal lamina of kidney epithelial cells in transf lter metanephric culture. Am J Pathol. 1984;116:289–296.
http://www.ncbi.nlm.nih.gov/pubmed/6235751
91. Lee L, Pollock A, Lovett D. Asymmetric origin of the mature glomerular basement membrane. J Cell Physiol. 1993;157:169–177.
http://www.ncbi.nlm.nih.gov/pubmed/8408235
92. Davies M, Thomas G, Shrewing L, et al. Mesangial cell proteoglycans: synthesis and metabolism. J Am Soc Nephrol. 1992;2(10 Suppl):S88–94.
93. Martin J, Steadman R, Knowlden J, et al. Differential regulation of matrix melalloproteinases asn their inhibitors in human glomerular epithelial cells in vitro. J Am Soc Nephrol. 1998;9:1629–1637.
94. Martin J, Eynstone L, Davies M, et al. Induction of metalloproteinases by glomerular mesangial cells stimulated by proteins of the extracellular matrix. J Am Soc Nephrol. 2001;12:88–96.
http://www.ncbi.nlm.nih.gov/pubmed/12374147
95. Timpl R, Brown J. Supramolecular assembly of basement membranes. BioEssays. 1996;18 (2):123–132.
http://www.ncbi.nlm.nih.gov/pubmed/8851045
96. Groffen A, Ruegg M, Dijkman H, et al. Agrin is a major heparan sulfate proteoglycan in the human glomerular basement membrane. J Histochem Cytochem. 1998;46:19–27.
http://www.ncbi.nlm.nih.gov/pubmed/9405491
97. Hudson B, Reeders S, Tryggvason K. Type IV collagen: structure, gene organization and role in human diseases. J Biol Chem. 1993;268:26033–26036.
http://www.ncbi.nlm.nih.gov/pubmed/8253711
98. Inoue S. Ultrastructural architecture of basement membranes. Contrib Nephrol. 1994;107:21–28.
http://www.ncbi.nlm.nih.gov/pubmed/8004970
99. Madri J, Roll F, Furthmayr H, et al. Ultrastructural localization of fibronectin and laminin in the basement membranes of the murine kidney. J Cell Biol. 1980;86:G82–G87.
100. Timpl R, Dziadek M. Structure, development, and molecular pathology of basement membranes. Int Rev Exp Pathol. 1986;29:1–112.
http://www.ncbi.nlm.nih.gov/pubmed/3536789
101. Yurchenco P, Schittny J. Molecular architecture of basement membranes. FASEB J. 1990;4:1577–1590.
http://www.ncbi.nlm.nih.gov/pubmed/2180767
102. Colognato H, Yurchenco P. Form and function: the laminin family of heterotrimers. Dev Dyn. 2000;218:213–234.
http://www.ncbi.nlm.nih.gov/pubmed/10842354
103. Miner J, Yurchenco P. Laminin functions in tissue morphogenesis. Annu Rev Cell Dev Biol. 2004;20:255–284.
104. Kanwar Y, Farquhar M. Anionic sites in the glomerular basement membrane: In vivo and in vitro localization to laminae rarae by cationic probes. J Cell Biol. 1979;81:137–153.
http://www.ncbi.nlm.nih.gov/pubmed/90048
105. Sakai T, Kriz W. The structural relationship between mesangial cells and basement membrane of the renal glomerulus. Anat Embryol. 1987;176:373–386.
http://www.ncbi.nlm.nih.gov/pubmed/3631536
106. Drenckhahn D, Schnittler H, Nobiling R, et al. Ultrastructural organization of contractile proteins in rat glomerular mesangial cells. Am J Pathol. 1990;137:1343–1351.
http://www.ncbi.nlm.nih.gov/pubmed/2260624
107. Becker C. Demonstration of actomyosin in mesangial cells of the renal glomerulus. Am J Pathol. 1972;66:97–110.
http://www.ncbi.nlm.nih.gov/pubmed/4621555

108. Kriz W, Elger M, Lemley K, et al. Structure of the glomerular mesangium: A biomechanical interpretation. Kidney Int. 1990;38:S2–S9.
109. Courtoy P, Timpl R, Farquhar M. Comparative distribution of laminin, type IV collagen, and fbronectin in the rat glomerulus. J Histochem Cytochem. 1982;30:874.
http://www.ncbi.nlm.nih.gov/pubmed/7130672
110. Martinez-Hernandez A, Chung A. The ultrastructural localization of two basement membrane components entactin and laminin - in rat tissue. J Histochem Cytochem. 1984;32:289.
http://www.ncbi.nlm.nih.gov/pubmed/6198358
111. Schwartz E, Goldfscher S, Coltoff-Schiller B, et al. Extracellular matrix microfbrils are composed of core proteins coated with fbronectin. J Histochem Cytochem. 1985;33:268–274.
http://www.ncbi.nlm.nih.gov/pubmed/3980980
112. Gibson M, Kumaratilake J, Cleary E. The protein components of the 12-nanometer microfbrils of elastic and nonelastic tissues. J Biol Chem. 1989;264:4590–4598.
http://www.ncbi.nlm.nih.gov/pubmed/2647740
113. Sterzel R, Hartner A, Schlotzer-Schrehard U, et al. Elastic fber proteins in the glomerular mesangium in vivo and in cell culture. Kidney Int. 2000;58: 1588–1602.
http://www.ncbi.nlm.nih.gov/pubmed/11012893
114. Farquhar M, Palade G. Functional evidence for the existence of a third cell type in the renal glomerulus. Phagocytosis of fltration residues by a distinctive "third" cell. J Cell Biol. 1962;13:55–87.
http://www.ncbi.nlm.nih.gov/pubmed/19866600
115. Mundel P, Elger M, Sakai T, et al. Microfbrils are a major component of the mesangial matrix in the glomerulus of the rat kidney. Cell Tissue Res. 1988;254:183–187.
http://www.ncbi.nlm.nih.gov/pubmed/2461802
116. Inoue S, Leblond C. The microfbrils of connective tissue: I. Ultrastructure. Am J Anat. 1986;176:121–138.
http://www.ncbi.nlm.nih.gov/pubmed/2943153
117. Latta H, Maunsbach A, Madden S. The centrolobular region of the renal glomerulus studied by electron microscopy. J Ultrastruct Res. 1960;4:455–472.
http://www.ncbi.nlm.nih.gov/pubmed/13759385
118. Schlondorff D. The glomerular mesangial cell: an expanding role for a specialized pericyte. FASEB J. 1987;1:272–281.
http://www.ncbi.nlm.nih.gov/pubmed/3308611
119. Mauer S, Fish A, Blau E, et al. The glomerular mesangium. I. Kinetic studies of macromolecular uptake in normal and nephrotic rats. J Clin Invest. 1972;51:1092–1101.
120. Schreiner G, Unanue E. Origin of the rat mesangial phagocyte and its expression of the leukocyte common antigen. Lab Invest. 1984;51:515–523.
http://www.ncbi.nlm.nih.gov/pubmed/6238206
121. Kriz W, Elger M, Mundel P, et al. Structure-stabilizing forces in the glomerular tuft. J Am Soc Nephrol. 1995;5:1731–1739.
http://www.ncbi.nlm.nih.gov/pubmed/7787139
122. Kriz W, Haehnel B, Hosser H, et al. Pathways to recovery and loss of nephrons in anti-Thy-1 nephritis. J Am Soc Nephrol. 2003;14:1904–1926.
http://www.ncbi.nlm.nih.gov/pubmed/12819253
123. Welling L, Zupka M, Welling D. Mechanical properties of basement membrane. News Physiol Sci. 1995;10 (1):30–35.
124. Kriz W, Mundel P, Elger M. The contractile apparatus of podocytes is arranged to counteract GBM expansion. Contrib Nephrol. 1994;107:1–9.
125. Drumond M, Deen W. Structural determinants of glomerular hydraulic permeability. Am J Physiol. 1994;266:F1–F12.
126. Kiberd B. The functional and structural changes of the glomerulus throughout the course of murine lupus nephritis. J Am Soc Nephrol. 1992;3:930–939.
http://www.ncbi.nlm.nih.gov/pubmed/1450369
127. Guasch A, Myers B. Determinants of glomerular hypofltration in nephrotic patients with minimal change nephropathy. J Am Soc Nephrol. 1994;4: 1571–1581.
128. Drumond M, Kristal B, Myers B, et al. Structural basis for reduced glomerular fltration capacity in nephrotic humans. J Clin Invest. 1994;94:1187–1195.
http://www.ncbi.nlm.nih.gov/pubmed/8083359
129. Barnes J, Reznicek M, Radnik R, et al. Anionization of an antigen promotes glomerular binding and immune complex formation. Kidney Int. 1988;34: 156–163.
http://www.ncbi.nlm.nih.gov/pubmed/2460660
130. Simonson M, Dunn M. Leukotriene C4 and D4 contract rat glomerular mesangial cells. Kidney Int. 1986;30:524–531.
http://www.ncbi.nlm.nih.gov/pubmed/3465969
131. Savin V. In vitro effects of angiotensin II on glomerular function. Am J Physiol. 1986;251:F627–F634.
132. Scharschmidt L, Douglas J, Dunn M. Angiotensin II and eicosanoids in the control of glomerular size in the rat and human. Am J Physiol. 1986;250: F348–F356.
133. Blantz R, Konnen K, Tucker B. Angiotensin II effects upon the glomerular microcirculation and ultrafltration coeffcient of the rat. J Clin Invest. 1976;57:419–434.
http://www.ncbi.nlm.nih.gov/pubmed/1254727
134. Dworkin L, Ichikawa I, Brenner B. Hormonal modulation of glomerular function. Am J Physiol. 1983;244:F95–F104.
135. Haley D, Sarrafan M, Bulger R, et al. Structural and functional correlates of effects of angiotensin-induced changes in rat glomerulus. Am J Physiol. 1987;253:F111–F119.
136. Olivetti G, Giacomelli F, Wiener J. Morphometry of superfcial glomeruli in acute hypertension in the rat. Kidney Int. 1985;27:31–38.
http://www.ncbi.nlm.nih.gov/pubmed/3981871
137. Steinhausen M, Endlich K, Wiegman D. Glomerular blood flow. Kidney Int. 1990;38:769–784.
http://www.ncbi.nlm.nih.gov/pubmed/2266660
138. Farquhar M. The glomerular basement membrane: a selective macromolecular flter. In: Hay E, ed. Cell Biology of Extracellular Matrix. New York: Plenum Press; 1991:365–418.
139. Daniels B. The role of the glomerular epithelial cell in the maintenance of the glomerular fltration barrier. Am J Nephrol. 1993;13:318–323.
http://www.ncbi.nlm.nih.gov/pubmed/8116684
140. Daniels B, Deen W, Mayer G, et al. Glomerular permeability barrier in the rat. J Clin Invest. 1993;92:929–936.
http://www.ncbi.nlm.nih.gov/pubmed/7688767
141. Farquhar M, Wissig S, Palade G. Glomerular permeability: I.Ferritim transfer across the normal glomerular capillary wall. J Exp Med. 1961;113:47–66.
http://www.ncbi.nlm.nih.gov/pubmed/13698249
142. Chang R, Deen W, Robertson C, et al. Permselectivity of the glomerular capillary wall: III. Restricted transport of polyanions. Kidney Int. 1975;8:212–218.
http://www.ncbi.nlm.nih.gov/pubmed/1202253
143. Rennke H, Cotran R, Venkatachalam M. Role of molecular charge in glomerular permeability. Tracer studies with cationized ferritins. J Cell Biol. 1975;67:638–646.
http://www.ncbi.nlm.nih.gov/pubmed/1202017
144. Deen W, Bohrer M, Brenner B. Macromolecule transport across glomerular capillaries: Application of pore theory. Kidney Int. 1979;16:353–365.
http://www.ncbi.nlm.nih.gov/pubmed/529682
145. Burne M, Osicka T, Comper W. Fractional clearance of high molecular weight proteins in conscious rats using a continuous infusion method. Kidney Int. 1999;55:261–270.
http://www.ncbi.nlm.nih.gov/pubmed/9893135
146. Greive K, Nikolic-Paterson D, Guimaraes M, et al. Glomerular permselectivity factors are not responsible for the increase in fractional clearance of albumin in rat glomerulonephritis. Am J Pathol. 2001;159:1159–1170.
147. Smithies O. Why the kidney glomerulus does not clog: a gel permeation/diffusion hypothesis of renal function. Proc Natl Acad Sci USA. 2003;100: 4108–4113.
http://www.ncbi.nlm.nih.gov/pubmed/12655073
148. Hausmann R, Kuppe C, Egger H, et al. Electrical forces determine glomerular permeability. J Am Soc Nephrol. 2010;21:2053–2058.
http://www.ncbi.nlm.nih.gov/pubmed/20947631
149. Tryggvason K, Pettersson E. Causes and consequences of proteinuria: the kidney fltration barrier and progressive renal failure. J Intern Med. 2003; 254:216–224.
http://www.ncbi.nlm.nih.gov/pubmed/12930230
150. Bolton G, Deen W, Daniels B. Assessment of the charge selectivity of glomerular basement membrane using Ficoll sulfate. Am J Physiol. 1998;274: F889–F896.
151. Sorensson J, Ohlson M, Haraldsson B. A quantitative analysis of the glomerular charge barrier in the rat. Am J Physiol Renal Physiol. 2001;280: F646–F656.
http://www.ncbi.nlm.nih.gov/pubmed/11249856
152. Ciarimboli G, Hjalmarsson C, Bokenkamp A, et al. Dynamic alterations of glomerular charge density in fxed rat kidneys suggest involvement of endothelial coat. Am J Physiol Renal Physiol. 2003;285:F722–F730.
153. Ryan G, Karnovsky M. Distribution of endogenous albumin in the rat glomerulus. Role of hemodynamic factors in glomerular barrier function. Kidney Int. 1976;9:36–45.
http://www.ncbi.nlm.nih.gov/pubmed/940256
154. Schonheyder H, Maunsbach A. Ultrastructure of a specialized neck region in the rabbit nephron. Kidney Int. 1975;7:145–153.
http://www.ncbi.nlm.nih.gov/pubmed/1123890
155. Jacobsen N, Jorgensen F. Further enzyme histochemical observations on the segmentation of the proximal tubules in the kidney of the male rat. Histochemie. 1973;34:11–32.

156. Maunsbach A. Observations on the segmentation of the proximal tubule in the rat kidney. J Ultrastruct Res. 1966;16:239–258.
http://www.ncbi.nlm.nih.gov/pubmed/5333381
157. Maunsbach A. Ultrastructure of the proximal tubule. In: Orloff J, Berliner R, eds. Handbook of Physiology, vol.8. Washington: American Physiological Society; 1973:31–79.
158. Kaissling B, Kriz W. Structural analysis of the rabbit kidney. Adv Anat Embryol Cell Biol. 1979;56:1–123.
http://www.ncbi.nlm.nih.gov/pubmed/443090
159. Kriz W, Koepsell H. The structural organization of the mouse kidney. Z Anat Entwicklungsgesch. 1974;144:137–163.
http://www.ncbi.nlm.nih.gov/pubmed/4472393
160. Tisher C. Relationship between renal structure and concentrating ability in the rhesus monkey. Am J Physiol. 1971;220:1100–1106.
161. Bulger R, Cronin R, Dobyan D. Survey of the morphology of the dog kidney. Anat Rec. 1979;194:41–66.
http://www.ncbi.nlm.nih.gov/pubmed/443563
162. Tisher C, Bulger R, Trump B. Human renal ultrastructure. I. Proximal tubule of healthy individuals. Lab Invest. 1966;15:1357–1394.
http://www.ncbi.nlm.nih.gov/pubmed/5920363
163. Welling L, Welling D. Surface areas of brush border and lateral cell walls in the rabbit proximal nephron. Kidney Int. 1975;8:343–348.
http://www.ncbi.nlm.nih.gov/pubmed/1206850
164. Harmanci M, Wade J, DiScala V. Altered structure of tight junctions in rat proximal tubules with volume expansion. Kidney Int. 1975;8:478.
165. Bulger R, Lorentz W Jr, Colindres R, et al. Morphological changes in rat renal proximal tubules and their tight junctions with increased intraluminal pressure. Lab Invest. 1974;30:136–144.
http://www.ncbi.nlm.nih.gov/pubmed/4591678
166. Silverblatt F, Bulger R. Gap junctions occur in vertebrate renal proximal tubule cells. J Cell Biol. 1970;47:513.
http://www.ncbi.nlm.nih.gov/pubmed/19866748
167. Barrett J, Heidger P. Microbodies of the rat renal proximal tubule: Ultrastructural and cytochemical investigations. Cell Tissue Res. 1975;157: 283–305.
http://www.ncbi.nlm.nih.gov/pubmed/1122543
168. DeDuve C, Baudhuin P. Peroxisome (microbodies and related particles). Physiol Rev. 1966;46:323–357.
http://www.ncbi.nlm.nih.gov/pubmed/5325972
169. Jacobsen N, Jorgensen F. Ultrastructural observations on the pars decendens of the proximal tubule in the kidney of the male rat. Z Zellforsch Mikrosk Anat. 1973;136:479–499.
http://www.ncbi.nlm.nih.gov/pubmed/4346669
170. Roesinger B, Schiller A, Taugner R. A freeze-fracture study of tight junctions in the pars convoluta and pars recta of the renal proximal tubule. Cell Tissue Res. 1978;186:121–133.
http://www.ncbi.nlm.nih.gov/pubmed/627008
171. Koepsell H, Schmitt B, Gorboulev V. Organic cation transporters. Rev Physiol Biochem Pharmacol. 2003;150:36–90.
http://www.ncbi.nlm.nih.gov/pubmed/12827517
172. Burckhardt B, Burckhardt G. Transport of organic anions across the basolateral membrane of proximal tubule cells. Rev Physiol Biochem Pharmacol. 2003;146:95–158.
http://www.ncbi.nlm.nih.gov/pubmed/12605306
173. Lee W, Kim R. Transporters and renal drug elimination. Annu Rev Pharmacol Toxicol. 2004;44:137–166.
174. Wright S, Dantzler W. Molecular and cellular physiology of renal organic cation and anion transport. Physiol Rev. 2004;84:987–1049.
http://www.ncbi.nlm.nih.gov/pubmed/15269342
175. Lock E, Reed C. Xenobiotic metabolizing enzymes of the kidney. Toxicol Pathol. 1998;26:18–25.
http://www.ncbi.nlm.nih.gov/pubmed/9502382
176. Christensen E, Gburek J. Protein reabsorption in renal proximal tubule - function and dysfunction in kidney pathophysiology. Pediatr Nephrol. 2004;19:714–721.
http://www.ncbi.nlm.nih.gov/pubmed/15146321
177. Verroust P, Christensen E. Megalin and cubilin - the story of two multipurpose receptors unfolds. Nephrol Dial Transplant. 2002;17:1867–1871.
http://www.ncbi.nlm.nih.gov/pubmed/12401836
178. Bacic D, Wagner C, Hernando N, et al. Novel aspects in regulated expression of the renal type IIa Na/Pi-contransporter. Kidney Int. 2004;91:S5–S12.
179. Bachmann S, Schlichting U, Geist B, et al. Kidney-specif c inactivation of the megalin gene impairs traff cking of renal inorganic sodium phosphate cotransporter (NaPi-IIa). J Am Soc Nephrol . 2004;15:892–900.
http://www.ncbi.nlm.nih.gov/pubmed/15034091
180. Kriz W, Schnermann J, Dieterich H. Differences in the morphology of descending limbs of short and long loops of Henle in the rat kidney. In: Wirz H, Spinelli F, eds. Recent Advances in Renal Physiology. Basel: Karger; 1972: 140–144.
181. Schwartz M, Venkatachalam M. Structural differences in thin limbs of Henle: Physiological implications. Kidney Int. 1974;6:193–208.
http://www.ncbi.nlm.nih.gov/pubmed/4427417
182. Dieterich H, Barrett J, Kriz W, et al. The ultrastructure of the thin loop limbs of the mouse kidney. Anat Embryol. 1975;147:1–18.
http://www.ncbi.nlm.nih.gov/pubmed/1200392
183. Bachmann S, Kriz W. Histotopography an ultrastructure of the thin limbs of the loop of Henle in the hamster. Cell Tissue Res. 1982;225:111–127.
http://www.ncbi.nlm.nih.gov/pubmed/6889464
184. Barrett J, Kriz W, Kaissling B, et al. The ultrastructure of the nephrons of the desert rodent (Psammomys obesus) kidney. I. thin limbs of Henle of short looped nephrons. Am J Anat. 1978;151:487–498.
http://www.ncbi.nlm.nih.gov/pubmed/645614
185. Barrett J, Kriz W, Kaissling B, et al. The ultrastructure of the nephrons of the desert rodent (Psammomys obesus) kidney. II. Thin limbs of Henle of long-looped nephrons. Am J Anat. 1978;151:499–514.
http://www.ncbi.nlm.nih.gov/pubmed/645615
186. Dobyan D, Jamison R. Structure and function of the renal papilla. Semin Nephrol. 1984;4:5.
187. Kriz W. Structural organization of the renal medulla: Comparative and functional aspects. Am J Physiol. 1981;241:R3–R16.
188. Chou C, Nielsen S, Knepper M. Structural-functional correlation in chinchilla long loop of Henle thin limbs: a novel papillary subsegment. Am J Physiol. 1993;265:F863–F874.
189. Pannabecker T, Abbott D, Dantzler W. Three-dimensional functional reconstruction of inner medullary thin limbs of Henle's loop. Am J Physiol Renal Physiol. 2004;286:F38–F45.
190. Pannabecker T, Dahmann A, Brokl O, et al. Mixed descending- and ascending-type thin limbs of Henle's loop in mammalian renal inner medulla. Am J Physiol Renal Physiol. 2000;278:F202–F208.
191. Kim Y, Kim D, Han K, et al. Expression of urea transporters in the developing rat kidney. Am J Physiol Renal Physiol. 2002;282:F530–F540.
192. Nielsen S. Renal aquaporins: an overview. BJU International. 2002;90:1–6.
http://www.ncbi.nlm.nih.gov/pubmed/12445090
193. Bankir L, Trinh-Trang-Tan M. Renal urea transporters. Direct and indirect regulation by vasopressin. Exp Physiol. 2000;85:243S-252S.
http://www.ncbi.nlm.nih.gov/pubmed/10795928
194. Nielsen S, Kwon T, Christensen B, et al. Physiology and pathophysiology of renal aquaporins. J Am Soc Nephrol. 1999;10:647–663.
http://www.ncbi.nlm.nih.gov/pubmed/10073616
195. Nielsen S, Pallone T, Smith B, et al. Aquaporin-1 water channels in short and long loop descending thin limbs and in descending vasa recta in rat kidney. Am J Physiol Renal Physiol. 1995;268:1023–1037.
196. Kriz W, Schiller A, Taugner R. Freeze-fracture studies on the thin limbs of Henle's loop in Psammomys obesus. Am J Anat. 1981;162:23–34.
http://www.ncbi.nlm.nih.gov/pubmed/7030046
197. Kriz W Structural organization of the renal medullary counterflow system. Fed Proc. 1983;42:2379–2385.
198. Kaissling B, de Rouff gnac C, Barrett J, et al. The structural organization of the kidney of the desert rodent Psammomys obesus. Anat Embryol. 1975;148:121–143.
http://www.ncbi.nlm.nih.gov/pubmed/1211658
199. Schwartz M, Karnovsky M, Venkatachalam M. Regional membrane specialization in the thin limbs of Henle's loops as seen by freeze-fracture electron microscopy. Kidney Int. 1979;16:577–589.
http://www.ncbi.nlm.nih.gov/pubmed/548602
200. Majack R, Paull W, Barrett J. The ultrastructural localization of membrane ATPase in rat thin limbs of the loop of Henle. Histochemie. 1979;63:23–33.
http://www.ncbi.nlm.nih.gov/pubmed/159881
201. Ernst S, Schreiber J. Ultrastructural localization of Na + , K + -ATPase in rat and rabbit kidney medulla. J Cell Biol. 1981;91:803–813.
http://www.ncbi.nlm.nih.gov/pubmed/6276410
202. Schiller A, Taugner R, Kriz W. The thin limbs of Henle's loop in the rabbit: A freeze-fracture study. Cell Tissue Res. 1980;207:249–265.
http://www.ncbi.nlm.nih.gov/pubmed/7388918
203. Dobyan D, Bulger R. Morphology of the minipig kidney. J Electron Microsc Tech. 1988;9:213–234.
http://www.ncbi.nlm.nih.gov/pubmed/3199239
204. Layton A, Pannabecker T, Dantzler W, et al. Two modes for concentrating urine in rat inner medulla. Am J Physiol Renal Physiol. 2004;287:F816–F839.

205. Verbavatz J, Brown D, Sabolic I, et al. Tetrameric assembly of CHIP28 water channels in liposomes and cell membranes: a freeze-fracture study. J Cell Biol. 1993;123:605–618.
http://www.ncbi.nlm.nih.gov/pubmed/7693713
206. Hediger M, Knepper M. Introduction: recent insights into the urinary concentrating mechanism: from cDNA cloning to dodelin renal function. Am J Physiol. 1998;275:F317.
207. Trinh-Trang-Tan M, Bankir L. Integrated function of urea transporters in the mammalian kidney. Exp Nephrol. 1998;6:471–479.
http://www.ncbi.nlm.nih.gov/pubmed/9807016
208. Shayakul C, Knepper M, Smith C, et al. Segmental localization of urea transporter mRNAa in rat kidney. Am J Physiol. 1997;272:F654–F660.
209. Imai M. Function of the thin ascending limb of Henle of rats and hamsters perfused in vitro. Am J Physiol. 1977;232:F201–F209.
210. Jamison R. Micropuncture study of segments of thin loops of Henle in the rat. Am J Physiol. 1968;215:236–242.
http://www.ncbi.nlm.nih.gov/pubmed/5659337
211. Bulger R, Tisher C, Myers C, et al. Human renal ultrastructure. II. The thin limb of Henle's loop and the interstitium in healthy individuals. Lab Invest. 1967;16:124–141.
http://www.ncbi.nlm.nih.gov/pubmed/4164459
212. Tisher C, Bulger R, Trump B. Human renal ultrastructure. III. The distal tubule in healthy individuals. Lab Invest. 1968;18:655–668.
http://www.ncbi.nlm.nih.gov/pubmed/5667863
213. Madsen K, Tisher C. Structural-functional relationships along the distal nephron. Am J Physiol. 1986;250:F1–F15.
214. Kaissling B, Peter S, Kriz W. The transition of the thick ascending limb of Henle's loop into the distal convoluted tubule in the nephron of thr rat kidney. Cell Tissue Res. 1977;182:111–118.
http://www.ncbi.nlm.nih.gov/pubmed/884723
215. Kaissling B, Kriz W. Morphology of the loop of Henle, distal tubule and collecting duct. In: Windhager E, ed. Handbook of Physiology: Section on Renal Physiology. New York, NY: Oxford University Press; 1992:109–167.
216. Allen F, Tisher C. Morphology of the ascending thick limb of Henle. Kidney Int. 1976;9:8–22.
http://www.ncbi.nlm.nih.gov/pubmed/181632
217. Crayen M, Thoenes W. Architecture and cell structures in the distal nephron of the rat kidney. Cytobiol. 1978;17:197–211.
http://www.ncbi.nlm.nih.gov/pubmed/689251
218. Myers C, Bulger R, Tisher C, et al. Human renal ultrastructure. IV. Collecting duct of healthy individuals. Lab Invest. 1966;15:1921–1950.
http://www.ncbi.nlm.nih.gov/pubmed/5335544
219. Suzuki T, Mostof F. Intramitochondrial flamentous bodies in the thick limb of Henle of the rat kidney. J Cell Biol. 1967;33:605–623.
http://www.ncbi.nlm.nih.gov/pubmed/6036524
220. Madsen K, Verlander J, Tisher C. Relationship between structure and function in distal tubule and collecting duct. J Electron Microsc Tech. 1988;9:187–208.
http://www.ncbi.nlm.nih.gov/pubmed/3058890
221. Kone B, Madsen K, Tisher C. Ultrastructure of the thick ascending limb of Henle in the rat kidney. Am J Anat. 1984;171:217–226.
http://www.ncbi.nlm.nih.gov/pubmed/6496376
222. Hebert S, Culpepper R, Andreoli T. ADH-stimulated NaCl transport in mouse medullary thick ascending limbs. I. Evidence for ADH-stimulated neutral NaCl co-transport and functional nephron heterogeneity. Am J Physiol. 1981;241:F412–F431.
223. Schiller A, Taugner R, Roesinger B. Vergleichende Morphologie der Zonulae occludentes am Nierentubulus. Verh Anat Ges. 1978;72:229–234.
http://www.ncbi.nlm.nih.gov/pubmed/746705
224. Bouby N, Bankir L, Trinh-Trang-Tan M, et al. Selective ADH-induced hypertrophy of the medullary thick ascending limb in Brattleboro rats. Kidney Int. 1985;28:456–466.
http://www.ncbi.nlm.nih.gov/pubmed/4068480
225. Bankir L, Fischer C, Fischer S, et al. Adaptation of the rat kidney to altered water intake and urine concentration. Pfugers Arch. 1988;412:42–53.
http://www.ncbi.nlm.nih.gov/pubmed/3174386
226. Bouby N, Trinh-Trang-Tan M, Laouari D, et al. Role of the urinary concentrating process in the renal effects of high protein intake. Kidney Int. 1988;34:4–12.
227. Bankir L, Kriz W. Adaptation of the kidney to protein intake and to urine concentrating activity: Similar consequences in health and CFR. Kidney Int. 1995;47:7–24.
228. Welling L, Welling D, Hill J. Shape of cells and intercellular channals in rabbit thick ascending limb of Henle. Kidney Int. 1978;13:144–151.
http://www.ncbi.nlm.nih.gov/pubmed/362035
229. Hoyer J, Sisson S, Vernier R. Tamm-Horsfall glycoprotein. Ultrastructural immunoperoxidase localization in rat kidney. Lab Invest. 1979;41:168–173.
http://www.ncbi.nlm.nih.gov/pubmed/379435
230. Sikri K, Foster C, MacHugh N, et al. Localization of Tamm-Horsfall glycoprotein in the human kidney using immunofluorescence and immuno-electron microscopical techniques. J Anat. 1981;132:597–605.
http://www.ncbi.nlm.nih.gov/pubmed/7028707
231. Chabardes D, Imbert-Teboul M, Gagnan-Brunette M, et al. Different hormonal target sites along the mouse and rabbit nephrons. Curr Probl Clin Biochem. 1977;8:447–454.
http://www.ncbi.nlm.nih.gov/pubmed/616378
232. Morel F, Imbert-Teboul M, Chabardes D. Receptors to vasopressin and other hormones in the mammalian kidney. Kidney Int. 1987;31:512–520.
http://www.ncbi.nlm.nih.gov/pubmed/3031358
233. El-Mernissi G, Doucet A. Quantitation of [3H]ouabain binding and turnover of Na+-K-ATPase along the rabbit nephron. Am J Physiol. 1984;247:F158–F167.
234. Greger R, Schlatter E. Presence of luminal K+, a prerequisite for active NaCl transport in the cortical thick ascending limb of Henle's loop of rabbit kidney. Pfugers Arch. 1981;392:92–94.
http://www.ncbi.nlm.nih.gov/pubmed/7322839
235. Greger R, Schlatter E, Lang F. Evidence for electroneutral sodium chloride cotransport in the cortical thick ascending limb of Henle's loop of rabbit kidney. Pfugers Arch. 1983;396:308–314.
236. Nielsen S, Maunsbach A, Ecelbarger C, et al. Ultrastructural localization of Na-K-2Cl cotransporter in thick ascending limb and macula densa of rat kidney. Am J Physiol Renal Physiol. 1998;275:F885–F893.
237. Obermüller N, Kunchaparty S, Ellison D, et al. Expression of the Na-K-2Cl cotransporter by macula densa and thick ascending limb cells of rat and rabbit nephron. J Clin Invest. 1996;98:635–640.
238. Burg M, Green N. Function of the thick ascending limb of Henle's loop. Am J Physiol. 1973;224:659–668.
http://www.ncbi.nlm.nih.gov/pubmed/4691283
239. Burg M. Thick ascending limb of Henle's loop. Kidney Int. 1982;22:454.
http://www.ncbi.nlm.nih.gov/pubmed/6296522
240. Spanidis A, Wunsch H, Kaissling B, et al. Three-dimensional shape of a Goormaghtigh cell and its contact with a granular cell in the rabbit kidney. Anat Embryol. 1982;165:239–252.
http://www.ncbi.nlm.nih.gov/pubmed/7158812
241. Dorup J. Ultrastructure of distal nephron cells in rat renal cortex. J Ultrastruct Res. 1985;92:101–118.
242. Kaissling B, Stanton B. Adaptation of distal tubule and collecting duct to increased sodium delivery. I. Ultrastructure. Am J Physiol. 1988;255:F1256–F1268.
243. Stanton B, Kaissling B. Adaptation of distal tubule and and collecting duct to increased Na delivery. II. Na+ and K+ transport. Am J Physiol. 1988;255:F1269–F1275.
244. Stanton B, Biemesderfer D, Wade J, et al. Structural and functional study of the rat distal nephron: Effects of potassium adaptation and depletion. Kidney Int. 1981;19:36–48.
http://www.ncbi.nlm.nih.gov/pubmed/7218667
245. Farquhar M, Palade G. Junctional complexes in various epithelia. J Cell Biol. 1963;17:375.
http://www.ncbi.nlm.nih.gov/pubmed/13944428
246. Schmidt U, Dubach U. Activity of (Na+ K+)-stimulated adenosine triphosphatase in the rat nephron. Pfugers Arch. 1969;306:219–226.
http://www.ncbi.nlm.nih.gov/pubmed/4238475
247. Schmidt U, Dubach U. NaK-stimulated adenosinetriphosphatase: Intracellular localisation within the proximal tubule of the rat nephron. Pfugers Arch. 1971;330:265–270.
http://www.ncbi.nlm.nih.gov/pubmed/4258313
248. Kaissling B. Structural aspects of adaptive changes in renal electrolyte excretion. Am J Physiol. 1982;243:F211–F226.
249. Kaissling B, Le Hir M. Distal tubular segments in the rabbit kidney after adaptation to altered Na- and K-intake. I. Structural changes. Cell Tissue Res. 1982;224:469–492.
http://www.ncbi.nlm.nih.gov/pubmed/7116409
250. Kaissling B, Bachmann S, Kriz W. Structural adaptation of the distal convoluted tubule to prolonged furosemide treatment. Am J Physiol. 1985;248:F374–F381.
http://www.ncbi.nlm.nih.gov/pubmed/3976898
251. Biner H, Arpin-Bott M, Loffng J, et al. Human cortical distal nephron; Distribution of electrolyte and water transport pathways. J Am Soc Nephrol. 2002;13:836–847.
http://www.ncbi.nlm.nih.gov/pubmed/11912242

252. Loffing J, Cueni-Loffin D, Valderrabano V et al. Distribution of transcellular calcium and sodium transport pathways along mouse distal nephron. Am J Physiol Renal Physiol. 2001;281:F1019–F1020.
253. Bachmann S, Bostanjoglo M, Schmitt R, et al. Sodium transport-related proteins in the mammalian distal nephron - distribution, ontogeny and functional aspects. Anat Embryol. 1999;200:447–468.
http://www.ncbi.nlm.nih.gov/pubmed/10526014
254. Potter E. Normal and Abnormal Development of the Kidney. Chicago: Year Book; 1972.
255. Howie A, Schmithson N, Rollason T. Reconsideration of the development of the distal tubule of the human kidney. J Anat. 1993;183:141–147.
http://www.ncbi.nlm.nih.gov/pubmed/7505779
256. Kim J, Tisher C, Madsen K. Differentiation of intercalated cells in developing rat kidney: An immunohistochemical study. Am J Physiol. 1994;266: F977–F990.
257. Stanton B. Renal potassium transport: morphological and functional adaptations. Am J Physiol. 1989;257:R989–R997.
258. Loffing J, Kaissling B. Sodium and calcium transport pathways along the mammalian distal nephron from rabbit to human. Am J Physiol Renal Physiol. 2003;284:F628–F643.
259. Fridt G, Palmer L. Na channels in the rat connecting tubule. Am J Physiol Renal Physiol. 2004;286:F669–F674.
260. Coleman R, Wu D, Liu J, Wade J. Expression of aquaporin in the renal connecting tubule. Am J Physiol Renal Physiol. 2000;279:F874–F883.
261. Le Hir M, Kaissling B, Dubach U. Distal tubular segments of the rabbit kidney after adaptation to altered Na- and K-intake. II. Changes in Na-K-ATPase activity. Cell Tissue Res. 1982;224:493–504.
http://www.ncbi.nlm.nih.gov/pubmed/6288247
262. Muto S, Yasoshima K, Yoshitomi K, et al. Electrophysiological identification of a- and b-intercalated cells and their distribution along the rabbit distal nephron segments. J Clin Invest. 1990;86:1829–1839.
263. Meneton P, Loffing J, Warnock D. Sodium and potassium handling by the aldosterone-sensitive distal nephron: the pivotal role of the distal and connecting tubule. Am J Physiol. 2004;287:F593–F601.
264. Kim J, Kim Y, Cha J, et al. Intercalated cell subtypes in connecting tubule and cortical collecting duct of rat and mouse. J Am Soc Nephrol. 1999;10:1–12.
http://www.ncbi.nlm.nih.gov/pubmed/9890303
265. Hansen G, Tisher C, Robinson R. Response of the collecting duct to disturbances of acid-base and potassium balance. Kidney Int. 1980;17:326–337.
http://www.ncbi.nlm.nih.gov/pubmed/7401452
266. Pricam C, Humbert F, Perrelet A, et al. A freeze-etch study of the tight junctions of the rat kidney tubules. Lab Invest. 1974;30:286–291.
http://www.ncbi.nlm.nih.gov/pubmed/4817823
267. Griffth L, Bulger R, Trump B. Structure and staining of mucosubstance on "intercalated cells" from the rat distal tubule and collecting duct. Anat Rec. 1968;160:643–662.
http://www.ncbi.nlm.nih.gov/pubmed/4174122
268. Rastegar A, Biemesderfer D, Kashgarian M, et al. Changes in membrane surfaces of collecting duct cells in potassium adaptation. Kidney Int. 1980;18:293–301.
http://www.ncbi.nlm.nih.gov/pubmed/6257963
269. Wade J, O'Neil R, Pryor J, et al. Modulation of cell membrane area in renal collecting tubules by corticosteroid hormones. J Cell Biol. 1979;81:439–445.
http://www.ncbi.nlm.nih.gov/pubmed/468913
270. Stanton B, Janzen A, Klein-Robbenhaar G, et al. Ultastucture of rat initial collecting tubule. Effect of adrenal corticosteroid treatment. J Clin Invest. 1985;75:1327–1334.
http://www.ncbi.nlm.nih.gov/pubmed/2985657
271. Sun T, Hoek W, Huang Y, et al. Aquaporin-2 localization in clathrin-coated pits: inhibition of endocytosis by dominant-negative dynamin. Am J Physiol. 2002;282:F998–F1011.
272. Loffing J, Cueni-Loffin D, Macher A, et al. Localization of epithelial sodium channel and aquaporin-2 in rabbit cortex. Am J Physiol Renal Physiol. 2000;272:530.
273. Marver D. Evidence of corticosteroid action along the nephron. Am J Physiol. 1984;246:F111–F123.
274. Madsen K, Clapp W, Verlander J. Structure and function of the inner medullary-collecting duct. Kidney Int. 1988;34:441–454.
http://www.ncbi.nlm.nih.gov/pubmed/3059025
275. Bankir L, Trinh-Trang-Tan M. Urea and the kidney. In: Brenner B, ed. The Kidney. Philadelphia: Saunders; 2000:637–679.
276. Alper S, Natale J, Gluck S, et al. Subtypes of intercalated cells in rat kidney collecting duct defned by antibodies against erythroid band 3 and renal vascular H+ -ATPase. Proc Natl Acad Sci USA. 1989;80:5429–5433.
http://www.ncbi.nlm.nih.gov/pubmed/2526338
277. Brown D, Hirsch S, Gluck S. Localization of a proton-pumping ATPase in rat kidney. J Clin Invest. 1988;82:2114–2126.
278. Verlander J, Madsen K, Tisher C. Effect of acute respiratory acidosis on two populations of intercalated cells in rat cortical collecting duct. Am J Physiol Renal Fluid Electrolyte Physiol. 1987;253:F1142–F1156.
279. Verlander J, Madsen K, Tisher C. Two populations of intercalated cells exist in cortical collecting ducts in the rat. Clin Res. 1985;33:501A.
280. Teng-Umnuay P, Verlander J, Yuan W et al. Identifcation of distinct subpopulations of intercalated cells in the mouse collecting duct. J Am Soc Nephrol. 1996;7:260–274.
http://www.ncbi.nlm.nih.gov/pubmed/8785396
281. Schuster V, Bonsib S, Jennings M. Two types of collecting duct mitochondria-rich (intercalated) cells: Lectin and band 3 cytochemistry. Am J Physiol Cell Physiol. 1986;251:C347–C355.
282. Verlander J, Madsen K, Tisher C. Axial distribution of band 3-positive intercalated cells in the collecting duct of control and ammonium chloride-loaded rabbits. Kidney Int. 1996;57:S137–S147.
283. LaFurgey A, Tisher C. Morphology of rabbit collecting duct. Am J Anat. 1979;155:111–124.
http://www.ncbi.nlm.nih.gov/pubmed/463786
284. O'Neil R, Hayhurst R. Functional differentiation of cell types of cortical collecting duct. Am J Physiol. 1985;248:F449–F453.
285. Weiner I, Hamm L. Use of fluorescent dye BCECF to measure intracellular pH in cortical collecting tubule. Am J Physiol. 1989;256:F957–F964.
286. Kim J, Tisher C, Linser P, et al. Ultrastructural localization of carbonic anhydrase ll in subpopulations of intercalated cells of the rat kidney. J Am Soc Nephrol. 1990;1:245–256.
http://www.ncbi.nlm.nih.gov/pubmed/2129509
287. Humbert F, Pricam C, Perrelet A, et al. Specifc plasma membrane differentiations in the cells of the kidney collecting tubule. J Ultrastruct Res. 1975;52:13–20.
http://www.ncbi.nlm.nih.gov/pubmed/1152104
288. Verlander J, Madsen K, Galla J, et al. Response of intercalated cells to chloride depletion metabolic alkalosis. Am J Physiol. 1992;262:F309–F319.
289. Wagner C, Finberg K, Breton S, et al. Renal vacuolar H+ -ATPase. Physiol Rev. 2004;84:1263–1314.
290. Brown D, Orci L. The "coat" of kidney intercalated cell tubulovesicles does not contain clathrin. Am J Physiol. 1986;250:C605–C608.
291. Brown D, Gluck S, Hartwig J. Structure of the novel membrane-coating material in proton-secreting epithelial cells and identifcation as an H+ATPase. J Cell Biol. 1987;105:1637–1648.
292. Stetson D, Wade J, Giebisch G. Morphologic alterations in the rat medullary collecting duct following potassium depletion. Kidney Int. 1980;17:45–56.
http://www.ncbi.nlm.nih.gov/pubmed/7374020
293. Brown D, Sabolic I. Endosomal pathways for water channel and proton pump recycling in kidney epithelial cells. J Cell Sci. 1993;Suppl. 17:49–59.
http://www.ncbi.nlm.nih.gov/pubmed/8144705
294. Kriz W, Kaissling B. Structural organization of the mammalian kidney. In: Seldin D, Giebisch G, eds. The Kidney. Philadelphia: Lippincott Williams & Wilkins; 2000:587–654.
295. Brown D, Kumpulainen T, Roth J, et al. Immunohistochemical localization of carbonic anhydrase in postnatal and adult rat kidney. Am J Physiol. 1983;245:F110–F118.
296. Dobyan D, Magill L, Friedman P, et al. Carbonic anhydrase histochemistry in rabbit and mouse kidneys. Anat Rec. 1982;204:185–197.
http://www.ncbi.nlm.nih.gov/pubmed/6818876
297. Dobyan D, Bulger R. Renal carbonic anhydrase. Am J Physiol. 1982; 243:F311–F324.
298. Madsen K, Tisher C. Response of intercalated cells of rat outer medullary collecting duct to chronic metabolic acidosis. Lab Invest. 1984;51:268–276.
http://www.ncbi.nlm.nih.gov/pubmed/6471808
299. Madsen K, Tisher C. Cellular response to acute respiratory acidosis in rat medullary collecting duct. Am J Physiol. 1983;14:F670–F679.
300. Brown D, Orci L. Junctional complexes and cell polarity in the urinary tubule. J Electron Microsc Tech. 1988;9:145–170.
http://www.ncbi.nlm.nih.gov/pubmed/3058889
301. Weiner I, Hamm L. Regulation of intercellular pH in the rabbit cortical collecting tubule. J Clin Invest. 1990;85:274–281.
http://www.ncbi.nlm.nih.gov/pubmed/2153152
302. Verlander J, Madsen K, Stone D, et al. Ultrastructural localization of H+ ATPase in rabbit cortical collecting duct. J Am Soc Nephrol. 1994;44: 1546–1557.
http://www.ncbi.nlm.nih.gov/pubmed/8025228
303. Emmons C, Kurtz I. Functional characterization of three intercalated cell subtypes in the rabbit outer cortical collecting duct. J Clin Invest. 1994;93: 417–423.

304. Milton A, Weiner I. Regulation of B-type intercalated cell apical anion exchange activity by CO2/HCO3. Am J Physiol. 1998;275:F1086–F1094.
305. Schwartz G, Al-Awqati Q. Carbon dioxide causes exocytosis of vesicles containing H+ pumps in isolated perfused proximal and collecting tubules. J Clin Invest. 1985;75:1638–1644.
306. Quentin F, Chambrey R, Trinh-Trang-Tan M, et al. The Cl/HCO3 exchanger pendrin in rat kidney is regulated in response to chronic alteration in chloride balance. Am J Physiol Renal Physiol. 2004;287:1179–1188.
307. Wall S, Hassell K, Royaux I, et al. Localization of pendrin in mouse kidney. Am J Physiol Renal Physiol. 2003;284:F229–F241.
308. Kim Y, Kwon T, Frische S, et al. Immunocytochemical localization of pendrin in intercalated cell subtypes in rat and mouse kidney. Am J Physiol Renal Physiol. 2002;283:F744–F754.
309. Madsen K, Verlander J, Kim J, Tisher C. Morphological adaptation of the collecting duct to acid-base disturbances. Kidney Int. 1991;40, Suppl.33: S57–S63.
310. Barajas L. The ultrastructure of the juxtaglomerular apparatus as disclosed by three-dimensional reconstrucion from serial sections: The anatomical relationship between the tubular and vascular components. J Ultrastruct Res. 1970;33:116–147.
http://www.ncbi.nlm.nih.gov/pubmed/4922486
311. Barajas L, Latta H. Structure of the juxtaglomerular apparatus. Circ Res. 1967;20–21 Suppl. 2:15.
http://www.ncbi.nlm.nih.gov/pubmed/4970997
312. Kaissling B, Kriz W. Variability of intercellular spaces between macula densa cells: A transmission electron microscopic study in rabbits and rats. Kidney Int. 1982;22:9–17.
http://www.ncbi.nlm.nih.gov/pubmed/6957682
313. Bachmann S, Mundel P. Nitric oxide in the kidney: synthesis, localization and function. Am J Kidney Dis. 1994;24:112–129.
http://www.ncbi.nlm.nih.gov/pubmed/7517625
314. Wilcox C, Welch W, Murad F, et al. Nitric oxide synthase in macula densa regulates glomerular capillary pressure. Proc Natl Acad Sci USA. 1992;89: 11993–11997.
http://www.ncbi.nlm.nih.gov/pubmed/1281548
315. Harris R, McKanna J, Akai Y, et al. Cyclooxygenase-2 is associated with the macula densa of rat kidney and increases with salt restriction. J Clin Invest. 1994;94:2504–2510.
316. Bachmann S, Peters J, Engler E, et al. Transgenic rats carrying the mouse renin gene - Morphological characterization of a low-renin hypertension model. Kidney Int. 1992;41:24.
http://www.ncbi.nlm.nih.gov/pubmed/1593860
317. Taugner R, Hackenthal E, Rix E, et al. Immunocytochemistry of the renin-angiotensin system: Renin, angiotensinogen, angiotensin I, angiotensin II, and converting enzyme in the kidneys of mice, rats, and tree shrews. Kidney Int.1982;22 (Suppl 12):S33–S43.
318. Barajas L. The development and ultrastructure of the juxtaglomerular cell granule. J Ultrastruct Res. 1966;15:400–413.
http://www.ncbi.nlm.nih.gov/pubmed/4957359
319. Peter S. Ultrastructural studies on the secretory process in the epitheloid cells of the juxtaglomerular apparatus. Cell Tissue Res. 1976;168:45–53.
http://www.ncbi.nlm.nih.gov/pubmed/1268928
320. Ryan G, Alcorn D, Coghlan J, et al. Ultrastructural morphology of granule release from juxtaglomerular myoepithelioid and peripolar cells. Kidney Int. 1982;22 (Suppl.12):3–8.
http://www.ncbi.nlm.nih.gov/pubmed/6752537
321. Gorgas K. Structure and innervation of the juxtaglomerular apparatus of the rat. Adv Anat Embryol Cell Biol. 1978;54:5–84.
http://www.ncbi.nlm.nih.gov/pubmed/358773
322. Biava C, West M. Fine structures of normal human juxtaglomerular cells. I. General structure and intercellular relationship. Am J Pathol. 1966;49: 697–721.
323. Taugner R, Schiller A, Kaissling B, et al. Gap junctional coupling between the JGA and the glomerular tuft. Cell Tissue Res. 1978;186:279–285.
http://www.ncbi.nlm.nih.gov/pubmed/627020
324. Goormaghtigh N. Facts in favour of an endocrine function of the renal arterioles. J Pathol Bacteriol. 1945;57:392.
325. Schnermann J, Levine D. Paracrine factors in tubuloglomerular feedback: adenosine, ATP, and nitric oxide. Annu Rev Physiol. 2003;65:501–529.
http://www.ncbi.nlm.nih.gov/pubmed/12208992
326. Kurtz A. Renin release: sites, mechanisms, and control. Annu Rev Physiol. 2011;73:377–399.
http://www.ncbi.nlm.nih.gov/pubmed/20936939
327. Peti-Peterdi J, Komlosi P, Fuson A, et al. Luminal NaCl delivery regulates basolateral PGE_2 release from macla densa cells. J Clin Invest. 2003;112:76–82.
http://www.ncbi.nlm.nih.gov/pubmed/12840061
328. Schweda F, Kurtz A. Cellular mechanism of renin release. Acta Physiol Scand. 2004;181:383–390.
http://www.ncbi.nlm.nih.gov/pubmed/15283749
329. Osswald H, Nabakowski G, Hermes H. Adenosine as a possible mediator of metabolic control of glomerular filtration rate. Int J Biochem. 1980;12:263–267.
http://www.ncbi.nlm.nih.gov/pubmed/7399032
330. Castrop H, Huang Y, Hashimoto S, et al. Impairment of tubuloglomerular feedback regulation of GFR in ecto-5'-nucleotidase/CD73-deficient mice. J Clin Invest. 2004;114:634–642.
http://www.ncbi.nlm.nih.gov/pubmed/15343381
331. Thomson S, Bao D, Deng A, et al. Adenosine formed by 5'-nucleotidase mediates tubuloglomerular feedback. J Clin Invest. 2000;106:289–298.
http://www.ncbi.nlm.nih.gov/pubmed/10903345
332. Persson A, Ollerstam A, Liu R, et al. Mechanism for macula densa cell release of renin. Acta Physiol Scand. 2004;181:471–474.
333. Komlosi P, Fintha A, Bell P. Current mechanisms of macula densa cell signaling. Acta Physiol Scand. 2004;181:463–469.
http://www.ncbi.nlm.nih.gov/pubmed/15283759
334. Moffat D, Fourman J. The vascular pattern of the rat kidney. J Anat. 1963;97:543–553.
http://www.ncbi.nlm.nih.gov/pubmed/14064096
335. Aikens B, Eenboom A, Bohle A. Untersuchungen zur Struktur des Glomerulum. Virchows Arch A Pathol Anat Histopathol. 1979;381:283–293.
http://www.ncbi.nlm.nih.gov/pubmed/155927
336. Murakami T. Glomerular vessels of the rat kidney. A scanning electron microscope study of corrosion casts. Arch Histol Jpn. 1972;34:87.
http://www.ncbi.nlm.nih.gov/pubmed/5062282
337. Winkler D, Elger M, Sakai T, et al. Branching and confluence pattern of glomerular arterioles in the rat. Kidney Int. 1991;39:S-2–S-8.
338. Yamamoto K, Wilson D, Baumal R. Blood supply and drainage of the outer medulla of the rat kidney. Scanning electron microscopy of microvascular casts. Anat Rec. 1984;210:273.
http://www.ncbi.nlm.nih.gov/pubmed/6507893
339. Bulger R, Trump B. Fine structure of the rat renal papilla. Am J Anat. 1966;118:685–722.
http://www.ncbi.nlm.nih.gov/pubmed/5956103
340. Schwartz M, Karnovsky M, Venkatachalam M. Ultrastructural differences between rat inner medullary descending and ascending vasa recta. Lab Invest. 1976;35:161–170.
http://www.ncbi.nlm.nih.gov/pubmed/957604
341. Kriz W, Dieterich H. Das Lymphgefäbsystem der Niere bei einigen Säugetieren. Licht- und elektronenmikroskopische Untersuchungen. Z Anat Entwicklungsgesch. 1970;131:111–147.
http://www.ncbi.nlm.nih.gov/pubmed/5507220
342. Lemley K, Kriz W. Anatomy of the renal interstitium. Kidney Int. 1991; 39:370–381.
http://www.ncbi.nlm.nih.gov/pubmed/2062030
343. Kaissling B, Le Hir M. The renal cortical interstitium: morphological and functional aspects. Histochem Cell Biol. 2008;130:247–262.
http://www.ncbi.nlm.nih.gov/pubmed/18575881
344. Larson M, Sjoquist M, Wolgast M. Renal interstitial volume of the rat kidney. Acta Physiol Scand. 1984;120:297–304.
http://www.ncbi.nlm.nih.gov/pubmed/6369886
345. Pfaller W Rittinger M. Quantitative morphology of the rat kidney. Jnt J Biochem. 1980;12:17–22.
346. Pinter G, Gärtner K. Peritubular capillary, interstitium, and lymph of the renal cortex. Rev Physiol Biochem Pharmacol. 1984;99:184–202.
http://www.ncbi.nlm.nih.gov/pubmed/6695128
347. Swann H, Norman R. The periarterial spaces of the kidney. Tex Rep Biol Med. 1970;28:317–334.
http://www.ncbi.nlm.nih.gov/pubmed/5521884
348. Pedersen J, Persson A, Maunsbach A. Ultrastructure and quantitative characterization of the cortical interstitium in the rat kidney. In: Maunsbach A, Olsen T, Christensen E, eds. Functional Ultrastructure of the Kidney. London: Academic Press; 1980:443–457.
349. Kriz W, Napiwotzky P. Structural and functional aspects of the renal interstitium. Contr. Nephrol. 1979;16:104–108.
350. Kriz W. A periarterial pathway for intrarenal distribution of renin. Kidney Int. 1987;31:S-51–S-56.
351. Albertine K, O'Morchoe C. Distribution and density of the canine renal cortical lymphatic system. Kidney Int. 1979;16:470–480.
http://www.ncbi.nlm.nih.gov/pubmed/548593
352. Knepper M, Danielson R, Saidel G, et al. Quantitative analysis of renal medullary anatomy in rats and rabbits. Kidney Int. 1977;12:313–323.
http://www.ncbi.nlm.nih.gov/pubmed/604620

353. Bohman S. The ultrastructure of the rat renal medulla as observed after improved fixation methods. J Ultrastruct Res. 1974;47:329–360.
354. Bulger R, Nagle R. Ultrastructure of the interstitium in the rabbit kidney. Am J Anat. 1973;136:183–204.
http://www.ncbi.nlm.nih.gov/pubmed/4734341
355. Osvaldo L, Latta H. Interstitial cells of the renal medulla. J Ultrastruct Res. 1966;15:589–613.
http://www.ncbi.nlm.nih.gov/pubmed/5911654
356. Kaissling B, Hegyi I, Loffing J, et al. Morphology of interstitial cells in the healthy kidney. Anat Embryol. 1996;193:303–318.
http://www.ncbi.nlm.nih.gov/pubmed/8694267
357. Kaissling B, Le Hir M. Characterization and distribution of interstitial cell types in the renal cortex of rat. Kidney Int. 1994;45:709–720.
http://www.ncbi.nlm.nih.gov/pubmed/8196273
358. Takahashi-Iwanaga H. The three-dimensional spaces of the kidney. Cell Tissue Res. 1991;264:269–281.
http://www.ncbi.nlm.nih.gov/pubmed/1878946
359. Dawson T, Gandhi R, Le Hir M, et al. Ecto-5'-nucleotidase: Localization in rat kidney by light microscopic histochemical methods. J Histochem Cytochem. 1989;37:39–47.
http://www.ncbi.nlm.nih.gov/pubmed/2535703
360. Humphreys B, Lin SL, Kobayashi A, et al. Fate tracing reveals the pericyte and not epithelial origin of myofibroblasts in kidney fibrosis. Am J Pathol. 2010;176:85–97.
http://www.ncbi.nlm.nih.gov/pubmed/20008127
361. Lin SL, Kisseleva T, Brenner D, et al. Pericytes and perivascular fibroblasts are the primary source of collagen-producing cells in obstructive fibrosis of the kidney. Am J Pathol. 2009;173:1617–1627.
362. Gandhi R, Le Hir M, Kaissling B. Immunolocalization of ecto-5'-nucleotidase in the kidney by a monoclonal antibody. Histochemie. 1990;95: 165–174.
http://www.ncbi.nlm.nih.gov/pubmed/2081690
363. Le Hir M, Kaissling B. Distribution of 5'-nucleotidase in the renal interstitium of the rat. Cell Tissue Res. 1989;258:177–182.
http://www.ncbi.nlm.nih.gov/pubmed/2553262
364. Koury S, Koury M, Bondurant M, et al. Quantitation of erythropoietin-producing cells in kidneys of mice by in situ hybridization: Correlation with hematocrit, renal erythropoietin mRNA, and serum erythropoietin concentration. Blood. 1989;74:645–651.
http://www.ncbi.nlm.nih.gov/pubmed/2752138
365. Lacombe C, Da Silva J, Bruneval P, et al. Peritubular cells are the site of erythropoietin synthesis in the murine hypoxic kidney. J Clin Invest. 1988; 81:620–623.
http://www.ncbi.nlm.nih.gov/pubmed/3339134
366. Bachmann S, Le Hir M, Eckardt K. Co-localization of erythropoietin mRNA and ecto-5' -nucleotidase immunoreactivity in peritubular cells of rat renal cortex indicates that fibroblasts produce erythropoietin. J Histochem Cytochem. 1993;41:335–341.
http://www.ncbi.nlm.nih.gov/pubmed/8429197
367. Bulger R, Griffith L, Trump B. Endoplasmic reticulum in rat renal interstitial cells: Molecular rearrangement after water deprivation. Science. 1966; 151:83–86.
http://www.ncbi.nlm.nih.gov/pubmed/5908968
368. Brown C, Zusman R, Haber E. Identification of an angiotensin receptor in rabbit renomedullary interstitial cells in tissue culture. Circ Res. 1980;46: 802–807.
http://www.ncbi.nlm.nih.gov/pubmed/6247080
369. Kuroda M, Ueno H, Sakato S, et al. A unique affinity and adaptation of renomedullary interstitial cells for hypertonic medium. Prostaglandins. 1979;18:209–220.
http://www.ncbi.nlm.nih.gov/pubmed/523679
370. Pitcock J, Lyons H, Brown P, et al. Glycosaminoglycans of the rat renomedullary interstitium: Ultrastructural and biochemical observations. Exp Mol Pathol. 1988;49:373–387.
http://www.ncbi.nlm.nih.gov/pubmed/2461872
371. Muirhead E. The renomedullary system of blood pressure control. Am J Med Sci. 1988;29531:231–251.
http://www.ncbi.nlm.nih.gov/pubmed/3284345
372. Gothberg G. Physiology of the renomedullary depressor system. J Hypertens. 1994;12:S57–S64.
373. Steinman R. The dendritic cell system and its role in immunogenicity. Annu Rev Immunol. 1991;9:271–296.
http://www.ncbi.nlm.nih.gov/pubmed/1910679
374. Diamond J, van Goor H, Ding G, et al. Myofibroblasts in experimental hydronephrosis. Am J Pathol. 1995;146:121–129.
http://www.ncbi.nlm.nih.gov/pubmed/7856721
375. Desmouliere A, Darby I, Gabbiani G. Normal and pathologic soft tissue remodeling: role of the myofibroblast, with special emphasis on liver and kidney fibrosis. Lab Invest. 2003;83:1689–1707.
376. Iwano M, Neilson E. Mechanisms of tubulointerstitial fibrosis. Curr Opin Nephrol Hypertens. 2004;13:279–284.
http://www.ncbi.nlm.nih.gov/pubmed/15073485
377. Barnes J, Glass W Renal interstitial fibrosis: A critical evaluation of the origin of myofibroblasts. Contrib Nephrol. 2011;169:97–123.
378. Smith H. The Kidney: Structure and Function in Health and Disease. New York: Oxford University Press; 1951.
379. Stephenson J. Concentration of urine in a central core model of the renal counterflow system. Kidney Int. 1972;2:85–94.
http://www.ncbi.nlm.nih.gov/pubmed/4671532
380. Kokko J, Rector F Jr. Countercurrent multiplication system without active transport in inner medulla. Kidney Int. 1972;2:214–223.
381. Becker B. Quantitative Beschreibung der Innenzone der Rattenniere. Muenster: Inaugural dissertation; 1978.
382. Han J, Thompson K, Chou C, et al. Experimental tests of three-dimensional model of urinary concentrating mechanism. J Am Soc Nephrol. 1992;2: 1677–1688.
383. Kriz W. Structural organization of renal medullary circulation. Nephron. 1982;31:290–295.
http://www.ncbi.nlm.nih.gov/pubmed/7177264
384. Layton H. Distribution of Henle's loops may enhance urine concentrating capability. Biophys J. 1986;49:1033–1040.
http://www.ncbi.nlm.nih.gov/pubmed/3708088
385. Lemley K, Kriz W. Cycles and separations: The histotopography of the urinary concentrating process. Kidney Int. 1987;31:538–548.
http://www.ncbi.nlm.nih.gov/pubmed/3550222
386. Trinh-Trang-Tan M, Lasbennes F, Gane P, et al. UT-B1 proteins in rat: tissue distribution and regulation by antidiuretic hormone in kidney. Am J Physiol Renal Physiol. 2002;283:F912–F922.